



University  
of Glasgow

Oxburgh, Stephen B. (2016) *Transforming transformation optics via generalised refraction*. PhD thesis.

<http://theses.gla.ac.uk/7539/>

Copyright and moral rights for this thesis are retained by the author

A copy can be downloaded for personal non-commercial research or study

This thesis cannot be reproduced or quoted extensively from without first obtaining permission in writing from the Author

The content must not be changed in any way or sold commercially in any format or medium without the formal permission of the Author

When referring to this work, full bibliographic details including the author, title, awarding institution and date of the thesis must be given

# Transforming Transformation Optics via Generalised Refraction

Stephen B. Oxburgh

A thesis submitted in fulfilment of the requirements for the degree of  
Doctor of Philosophy

School of Physics and Astronomy  
College of Science and Engineering  
University of Glasgow

August 2016

# Abstract

Generalised refraction is a topic which has, thus far, garnered far less attention than it deserves. The purpose of this thesis is to highlight the potential that generalised refraction has to offer with regards to imaging and its application to designing new passive optical devices. Specifically in this thesis we will explore two types of generalised refraction which takes place across a planar interface: refraction by generalised confocal lenslet arrays (gCLAs), and refraction by ray-rotation sheets. We will show that the corresponding laws of refraction for these interfaces produce, in general, light-ray fields with non-zero curl, and as such do not have a corresponding outgoing waveform. We will then show that gCLAs perform integral, geometrical imaging, and that this enables them to be considered as approximate realisations of metric tensor interfaces. The concept of piecewise transformation optics will be introduced and we will show that it is possible to use gCLAs along with other optical elements such as lenses to design simple piecewise transformation-optics devices such as invisibility cloaks and insulation windows. Finally, we shall show that ray-rotation sheets can be interpreted as performing geometrical imaging into complex space, and that as a consequence, ray-rotation sheets and gCLAs may in fact be more closely related than first realised. We conclude with a summary of potential future projects which lead naturally from the results of this thesis.

# Contents

<b>Abstract</b>	<b>i</b>
<b>Contents</b>	<b>ii</b>
<b>List of Figures</b>	<b>v</b>
<b>Acknowledgements</b>	<b>xi</b>
<b>Declaration of Authorship</b>	<b>xii</b>
<b>Publications</b>	<b>xiii</b>
<b>1 Introduction</b>	<b>1</b>
<b>2 Background</b>	<b>4</b>
2.1 Introduction . . . . .	4
2.2 Optical path length . . . . .	4
2.2.1 Fermat’s principle . . . . .	5
2.2.2 Absolute optical instruments . . . . .	6
2.3 Transformation optics . . . . .	7
2.4 Metamaterials and microstructured metasheets . . . . .	9
2.4.1 Metamaterials . . . . .	9
2.4.2 Microstructured sheets exhibiting generalised refraction . . . . .	10
<b>3 Light-ray fields with non-zero curl</b>	<b>14</b>
3.1 Introduction . . . . .	14
3.1.1 Contributions . . . . .	15
3.2 The curl of a light-ray field . . . . .	15
3.3 Simplifying the z-component of the curl of the outgoing light-ray field	20
3.4 Generalised laws of refraction generated by microstructured metasheets	21
3.4.1 Refraction by generalised confocal lenslet arrays . . . . .	22
3.4.2 The curl of the light-ray field produced by generalised confocal lenslet array refraction . . . . .	25
3.4.3 The curl of the light-ray field produced by ray-rotation refraction	25
3.4.4 The light-ray field of a point light source produced by a ray-rotation sheet, as viewed by an observer . . . . .	28

3.5	Wave-optically forbidden parallax . . . . .	30
3.6	Experimental confirmation . . . . .	30
3.6.1	Forbidden light-ray fields produced by ray-rotation . . . . .	31
3.7	Conclusion . . . . .	33
<b>4</b>	<b>Integral imaging using planar and curved interfaces</b>	<b>34</b>
4.1	Introduction . . . . .	34
4.1.1	Contributions . . . . .	35
4.2	Derivation of the homogeneous imaging equation for a planar interface	36
4.2.1	Homogeneous generalised confocal lenslet arrays as integrally imaging interfaces . . . . .	39
4.3	Perfect imaging with curved interfaces . . . . .	40
4.4	Conclusion . . . . .	43
<b>5</b>	<b>Metarefracting sheets as metric interfaces</b>	<b>44</b>
5.1	Introduction . . . . .	44
5.1.1	Contributions . . . . .	45
5.2	Fermat's principle at the interface between different Riemannian spaces	45
5.3	Generalised confocal lenslet arrays as metric interfaces . . . . .	48
5.4	Metric interfaces and perfect imaging . . . . .	54
5.5	When does a coordinate system not correspond to imaging? . . . . .	56
5.6	Conclusion . . . . .	56
<b>6</b>	<b>Transformation optics with CLAs</b>	<b>58</b>
6.1	Introduction . . . . .	58
6.1.1	Contributions . . . . .	60
6.2	Piecewise transformation optics using gCLAs . . . . .	60
6.2.1	Transformation properties around a closed loop in transforma- tion optics . . . . .	60
6.2.2	Insulation window . . . . .	63
6.3	Piecewise cloaking using CLAs . . . . .	66
6.3.1	Initial cloaking design . . . . .	66
6.3.2	Subsequent cloaking designs . . . . .	68
6.3.3	Carpet Cloak . . . . .	73
6.4	Recent developments . . . . .	76
6.4.1	Omnidirectional cloak constructed from lenses . . . . .	77
6.5	Conclusion . . . . .	80
<b>7</b>	<b>Geometrical imaging into abstract spaces</b>	<b>82</b>
7.1	Introduction . . . . .	82
7.1.1	Contributions . . . . .	83
7.2	Definition of a complex position and the light rays which pass through it	83
7.2.1	Uniqueness of complex positions . . . . .	85
7.2.2	Choosing light rays which pass through two complex positions	86
7.2.3	Finding the intersection point of two light rays in complex space	88

---

7.2.4	Finding the intersection point of three light rays in complex space . . . . .	89
7.3	Applications of complex imaging . . . . .	91
7.3.1	Complex imaging calculation . . . . .	91
7.3.1.1	Consistency Rays . . . . .	93
7.3.1.2	Primary Rays . . . . .	93
7.3.2	Reflection in a planar mirror . . . . .	94
7.4	On the equivalence between ray-rotation sheets and CLAs . . . . .	96
7.4.1	The equivalence between confocal lenslet array imaging and ray-rotation imaging . . . . .	96
7.4.2	The non-equivalence between confocal lenslet array refraction and ray-rotation . . . . .	97
7.5	An analysis of the structure of complex space . . . . .	99
7.6	Conclusion . . . . .	101
<b>8</b>	<b>Future work</b>	<b>102</b>
8.1	Introduction . . . . .	102
8.2	Continued exploration of imaging into abstract spaces . . . . .	102
8.3	Investigating metarefraction as a means of achieving a classical optical analogue of a black hole . . . . .	103
8.4	Improving pixellated refraction . . . . .	104
8.5	Designing wave-optically perfect refracting interfaces . . . . .	105
<b>9</b>	<b>Appendix</b>	<b>107</b>
9.1	Sheet parameters for cubic gCLA cloak . . . . .	108
9.2	Glens parameters for cubic glens cloak . . . . .	109
9.3	Lens parameters for lens tetrahedron . . . . .	110

# List of Figures

2.1	Fermat’s principle states that light rays will travel along the path which requires the least action, or optical path length. In isotropic media like air, this corresponds to the shortest geometrical path length. In this figure the light ray would therefore travel from <b>A</b> to <b>B</b> along a straight trajectory (red) as opposed to a longer curved trajectory (black).	5
2.2	An three-dimensional array of concentric split-ring resonators. Such elements are frequently studied in metamaterial research and have applications in transformation optics. In the microwave regime they can be configured to produce different effective permeabilities and permittivities.	10
2.3	The microwave cloak from [13]. The diamond inner region (black) is where the object being shielded is placed. The material surrounding the inner region is constructed using split-ring resonators and ensures microwave radiation flows around the central region and remains in phase.	11
2.4	Confocal lenslet arrays are comprised of two lenslet arrays which share a common focal plane. Each lenslet pair can be thought of as a mini telescope (or pixel). Due to the fact that light has to pass through an array of telescopes, the outgoing image is pixellated and blurring can also appear between pixels when different parts of the image are inverted inconsistently across different telescopes.	12
2.5	Figure taken from [14]. A dove-prism array ( <b>a</b> ) is described by a mirror plane and a prism axis. Light rays enter each individual dove prism and through a process of internal reflection and refraction ( <b>b</b> ) re-emerge on the other side of the dove prism as though they have been reflected off of the prisms mirror plane. Tilting each dove prism in the array simply has the effect of altering the angle of the mirror plane ( <b>c</b> ). When a light ray is reflected off of two mirror planes which are at an angle to one another, the light ray is rotated by twice the angle of separation. As such, when two dove-prism arrays whose mirror planes are at an angle $\theta'$ to one another share a plane, ( <b>d</b> ), light rays entering the combined interface are rotated by an angle $2\theta'$ on leaving the interface. Hence a combination of two rotated dove-prism arrays form a ray-rotation sheet.	13

- 3.1 Images **a-c**: the real part of the local phase gradient for the superposition of two plane waves as described in Eq.(3.7) with  $a_1 = 1$ ,  $a_2 = -2$ ,  $k_1 = (\sin \theta, \cos \theta)$  and  $k_2 = (\cos \theta, \sin \theta)$ , with  $\theta = \pi$ ,  $\theta = \pi/2$  and  $\theta = \pi/3$  respectively. It is clear that the local phase gradient is changing length and direction from point to point, unlike for a plane wave, where the direction and length are constant as seen in **d**. . . . . 17
- 3.2 On traversing a closed loop (red line) we see that a light-ray vector, **d** (blue vector) returns to its original position on the phase surface (blue plane). If a phase singularity occurs within the loop, such as at an optical vortex, then the light-ray vector will have acquired a height on circumnavigating the loop, and so will not return to its original position. 19
- 3.3 A schematic of how pairs of orthogonal cylindrical lens pairs can be used to make a generalised confocal lenslet array without lenslet rotation. The cylindrical lenses in each pair have their cylinder axes orthogonal to one another. The total distance between the two cylindrical lens pairs is the sum of the focal lengths for each of the two orthogonal cylinder axes, i.e.  $k = f_{1_u} + f_{2_u} = f_{1_v} + f_{2_v}$ . The cylindrical lens pairs can be offset relative to one another as shown. . . . . 23
- 3.4 Two lenslets (blue lines) separated by the sum of their focal lengths. Constructing light rays (red), such that the ingoing ray passes through the central point of lenslet 1, **C**<sub>1</sub>, and a point on the common focal plane **P** and the outgoing light ray passes through **P** and the central point of lenslet 2, **C**<sub>2</sub>, it is straight forward to derive the law of refraction for generalised confocal lenslet arrays on a component by component basis. . . . . 24
- 3.5 Contour plots of the transverse phase profiles in the  $z = 0$  plane of an ingoing and outgoing waveform. The ingoing transverse phase profile is given by solid lines, whereas the outgoing transverse phase profile is given by dashed lines. As can be seen, the outgoing transverse phase profile is at every point a local rotation of the ingoing transverse phase profile, specifically by  $\pi/3$ . . . . . 27
- 3.6 Top: an incident light ray emitted from **L** intersects the interface at position **P** before being refracted towards an observer at position **E**. Bottom: projecting the points **L**, **P** and **E** into the plane of the sheet and constructing a complex coordinate system enables the point **P** to be written in terms of basis vectors which are functions of the components of **L** and **E**. The outgoing light-ray direction can then be calculated as the normalised vector between **P** and **E**, and as such, must also be a function of the source position **L**. . . . . 29
- 3.7 As the observer moves to the left, i.e. the negative  $x$  direction, the green sphere appears to move in the positive  $y$ -direction. This means that  $\partial d_y / \partial x > 0$ . . . . . 31
- 3.8 As the observer moves up, i.e. the positive  $y$  direction, the green sphere appears to move in the positive  $x$ -direction. This means that  $\partial d_x / \partial y < 0$ . 31

3.9	A schematic of the experimental set up to study the parallax of a forbidden light-ray field. A rubiks cube is placed behind a ray rotation sheet which is comprised of two dove prism arrays rotated relative to one another by an angle of $\pi/4$ . This causes outgoing light-rays to be rotated by an angle twice this, $\pi/2$ around the surface normal to the ray rotation sheet, $\mathbf{n}$ . The camera is then moved either horizontally or vertically to observe the effect this has on the image, and therefore the outgoing light-ray field. . . . .	32
3.10	Experimental confirmation of the effect of wave-optical illegality for a $\pi/2$ ray-rotation sheet. a) As the observer moves vertically by 25mm in the $y$ -axis, the Rubik's cube, as seen through the sheet, moves in the negative direction of the $x$ -axis. b) As the observer moves horizontally by -25mm in the $x$ -axis, the Rubik's cube, as seen through the sheet, moves in the negative direction of the $y$ -axis. . . . .	33
4.1	Upper image: the effect that a generalised imaging interface has on light rays. This type of interface can be thought of as a lens with different object- and image-sided focal lengths. As can be seen, a ray at normal incidence to the interface coming in from the object side will be refracted and intersect the image sided focal point $G$ , while a ray coming in parallel from the image side will be refracted such that it intersects the object sided focal point $F$ . Lower image: the effect that a homogeneous generalised confocal lenslet array has on light rays. As can be seen, parallel light rays no longer intersect on focal planes, but instead are redirected and continue to remain parallel. . . . .	37
4.2	Upper image: a flat interface images such that the planes containing the object points and image points intersect. The object plane and the image plane need not lie in the same plane. Lower image: a curved interface images such that the planes containing the object and image points lie in the same plane. This is due to the fact that the points where the light rays intersect the sheet are noncolinear, and we only consider rays which intersect the interface once. . . . .	42
5.1	Construction for applying Fermat's principle to a metric interface. An interface is positioned in the $z = 0$ plane with a metric $g$ in the region $z < 0$ and a metric $h$ in the region $z > 0$ . The ingoing and outgoing light-ray directions, $\mathbf{d}$ and $\mathbf{e}$ , are constructed such that their $z$ components are equal to unity. The points $\mathbf{A}$ and $\mathbf{B}$ , which lie on the light ray before and after the interface respectively, can therefore be written such that $\mathbf{A} = -\mathbf{d}$ and $\mathbf{B} = \mathbf{e}$ . . . . .	46
5.2	Simulated view through (a) gCLAs and (b) through an equivalent metric interface. The parameters of the gCLAs are $\eta = 0.5$ , $\delta_x = 0.2$ , $\delta_y = 0$ . Refraction at the gCLAs is calculated according to Eqns (5.13); refraction at the metric interface is calculated according to equations derived from Fermat's principle [27]. The images were calculated with the custom ray tracer Dr TIM [27, 28]. . . . .	52

5.3	Left: a curved space causes a light-ray (red line) to follow a curved trajectory. Right: a lattice constructed of discrete metric interfaces (represented by black lines) could, in principle, mimic the behaviour of a light-ray passing through curved space. . . . .	54
5.4	Left: a two dimensional cartesian coordinate system. Right: the same cartesian coordinate system after it has been transformed by the gCLA imaging equation where, specifically, $\delta_x = 0.2$ , $\delta_y = 0$ and $\eta = 1.2$ . . .	55
5.5	The coordinate system produced by an imaging interface <b>a</b> and a non-imaging interface <b>b</b> . As we see, in the imaging case, <b>a</b> , the coordinate system in object space and image space align on the surface of the interface. In the non-imaging case, this does not happen and so the system will not image, as in order to image, ingoing light rays would have to jump along the interface to leave from the correct position in the new coordinate system. Clearly this is not possible. . . . .	57
6.1	Three glenses arranged such that they share a common edge. If the intersection behaves like a transformation optics device, the point <b>P</b> will be mapped back to itself on being imaged through each of the glenses in order. . . . .	62
6.2	The same procedure as shown in Fig. 6.8 is applied to calculate the gCLA parameters in the insulation window shown in Fig. 6.3. . . . .	64
6.3	Left: View of a light ray (red) passing through a rectangle of empty space. Right: The same space after a piecewise coordinate transformation using gCLA interfaces. The point <b>E</b> has been mapped to the point <b>E'</b> . A new region spanning <b>A'E'D'F'</b> has been created. This region can in principle be used to conceal an object. For architectural purposes this could hide insulation, thus rendering the above device into an insulation window. . . . .	65
6.4	The simulated view through an insulation window when the viewing direction is orthogonal to the normal of the plane of the window. . . . .	66
6.5	When viewed from an angle the thickness of the window becomes an issue. When the insulation window is thick (top) the view through the window is heavily distorted at certain regions. When the insulation window is thin (bottom), the distortion is reduced, however at the expense of the volume of insulation which can be housed. . . . .	67
6.6	Top: A bird's eye view of our first attempt at a cylindrical cloak. A green ball is what is being cloaked. The red lines represent light rays which are being refracted at each of the gCLAs, which are represented by grey lines. Bottom: The view through the cloak when viewed from one of the correct viewing angles. . . . .	69
6.7	Graphical representation of a cylindrical coordinate transformation. Left: before the cylindrical transformation. Right: after the cylindrical transformation, light rays are directed around the central region and then redirected along their original trajectories. . . . .	70

- 
- 6.8 gCLA equivalent transformation for square prismatic cloaks. In this case, instead of a point being blown up to a circle, a smaller square is blown up to a larger one. This is an example of piecewise transformation optics. . . . . 70
- 6.9 View through the square prismatic cloak from a view orthogonal to one of the outer faces (top) and a view looking directly at one of the edges (bottom). . . . . 73
- 6.10 View through the cubic cloak from a view orthogonal to one of the outer faces (top) and a view looking directly at one of the edges (bottom). 74
- 6.11 A carpet cloak could in principle be built using gCLAs and exotic mirrors. If the gCLAs have the same properties as they do for an insulation window, then the mirrors have to have inhomogenous reflection properties. . . . . 75
- 6.12 A cloak designed using glenses and lenses. The cloak is constructed from two concentric cubes joined together by diagonal interfaces (top left). The faces of the inner and outer cube are spanned by glenses, while the diagonal faces are traditional lenses. For sample glens parameters see Table 9.2 in the Appendix. The cloak suffers the same flaw that all cloaks have; the object can never be completely cloaked, only shrunk. . . . . 76
- 6.13 A ray tracing simulation of a transformation optics device constructed entirely from lenses. The upper image shows the view through the device, whilst the lower image shows, using red lines, the lines where the constituent lenses intersect. . . . . 78
- 6.14 A raytracing simulation of a green ball set inside a tetrahedral transformation-optics device made entirely from lenses. In comparison to the green ball positioned outside the device, we see that the green ball positioned within the smallest internal pyramid of the device has been compressed significantly in the vertical direction. . . . . 79
- 6.15 One possible configuration to achieve cloaking using two transformation-optics tetrahedra. Upper image: using red lines to show where the lenses intersect, we can outline the structure of a possible omnidirectional cloak. In this case we have positioned a smaller transformation-optics tetrahedron inside the smallest internal pyramid of a larger transformation-optics such that the bases of the two tetrahedra are at right angles. Lower image: The simulated view through such a device. As can be seen the ball placed inside the composite device has been compressed in both the vertical and horizontal directions. . . . . 81
- 7.1 A ray-rotation sheet which rotates light rays by  $140^\circ$ . A cone of light rays is transformed into a hyperboloid of light rays. Before rotation, the light rays share a common intersection point whilst after rotation the light rays share a common hyperboloid waist. We can think of the ray-rotation sheet as mapping the intersection point before the sheet to a complex position after the sheet, which is physically manifested as a hyperboloid, via our definition of the contact point defined in Eq.(7.2). 84

- 
- 7.2 A visual representation of a light ray passes between two complex positions in real space. The light ray with direction  $\hat{\mathbf{a}}$  passes between the two contact points  $|\mathbf{P}_i \times \hat{\mathbf{a}}|$  and  $|\mathbf{Q}_i \times \hat{\mathbf{a}}|$ . For the case of the complex position  $\mathbf{P}$ , the contact point lies on a disc of radius  $|\mathbf{P}_i|$  and is a distance  $|\mathbf{P}_i \times \hat{\mathbf{a}}|$  from  $\mathbf{P}_r$ , the centre of the disc. Similarly expressions hold for the complex position  $\mathbf{Q}$ . . . . . 85
- 7.3 A two-dimensional representation of our complex imaging system. Primary rays (green) emanate from the object point  $\mathbf{P}$  and refract across the real sheet situated in the  $z = 0$  plane before intersecting again at the image point  $\mathbf{P}'$ . Consistency rays (red) intersect the primary rays before the sheet and on refraction intersect the refracted primary rays. 92
- 8.1 An array of Luneburg lenses in contact with one another. We see that light rays entering the array at normal incidence (red rays) are refracted in a uniform way as they pass through the point where the lenses touch. Ray bundles going in at any other angle (green rays) get redirected in different ways directions. By transforming the Luneburg lenses such that their surfaces on the interior of the array are touching at all points, one could in effect create a gCLA whilst removing field of view issues. . . . . 104

# Acknowledgements

This research would not have been made possible without the help and guidance of others. In particular I would like to thank my supervisor Dr Johannes Courtial for being a good natured, fun and patient PhD supervisor - I realise my stupidity must be have been frustrating at times! I would also like to thank Dr Chris White for many an interesting conversation on mathematical ideas relating to coordinate transformations and metrics. I would also like to thank Ms Lena Mertens and Dr Neal Radwell for being around to bounce mathematical ideas off of.

Finally, this work was supported by the Engineering and Physical Sciences Research Council [grant number EP/K503058/1].

# Declaration of Authorship

I hereby declare that this thesis is the result of my own work, except where explicit reference is made to the work of others, and has not been presented in any previous application for a degree at this or any other institution.

Stephen B. Oxburgh

# Publications

What follows is a list of papers written during my PhD which have either been published, or are currently in preparation.

1. S. Oxburgh, C. D. White, G. Antoniou and J. Courtial, “Law of refraction for generalised confocal lenslet arrays”. *Optics Communications* **313**, 118-122, 2014.
2. S. Oxburgh and J. Courtial, “Perfect imaging with planar interfaces”. *Journal of the Optical Society of America A* **30**, 2334-2338, 2013
3. J. Courtial, S. Oxburgh and T. Tyc, “Direct stigmatic imaging with curved surfaces”. *Journal of the Optical Society of America A* **32**, 478-481, 2015
4. S. Oxburgh, C. D. White, G. Antoniou, E. Orife, T. Sharpe and J. Courtial, “Large-scale, white-light, transformation optics using integral imaging”. *Journal of Optics* **18**, 2016.
5. T. Tyc, S. Oxburgh, E. Cowie, G. Chaplain, G. Macauley, C. D. White and J. Courtial, “Omni-directional transformation-optics cloak made from lenses and glenses”. *Journal of the Optical Society of America A* **33**, 1032-1040, 2016
6. T. Tyc, S. Oxburgh, C. D. White, E. Cowie and J. Courtial, “The loop imaging theorem of transformation optics”. In preparation.
7. J. Courtial, S. Oxburgh, E. Cowie, C. D. White and T. Tyc, “Omni-directional transformation-optics device made from lenses”. In preparation.

8. C. D. White, L. Mertens, C. Mullen, S. Oxburgh, G. Antoniou, J. Ramsay, D. McCall and J. Courtial, “Windows into non-Euclidean spaces”. In preparation.
9. A. Strathearn, S. Oxburgh, J. Moncreiff, M. Alonso and J. Courtial, “Imaging between complex object and image positions”. In preparation.

# Chapter 1

## Introduction

Attempting to harness and manipulate light is one of the oldest scientific endeavours in history. For thousands of years, man has been designing and refining optical devices for such purposes, the most famous example being of course the lens which exploits Snell's law. Snell's law tells us how light propagates when it passes between materials with different refractive indices and is a direct result of applying Maxwell's equations when studying the electric field across a material interface. Other refraction can occur when the optical properties of the medium are no longer isotropic, for example in optical crystals.

In recent years, a new class of materials, known as anisotropic optical metamaterials, has emerged which employs spatially anisotropic material parameters so that light can be directed in unprecedented ways. These exotic materials are clearly still governed by Maxwell's equations. The only difference between conventional optical materials and optical metamaterials is that the optical parameters inside a conventional optical material emerge primarily from its substance (i.e its atomic or molecular structure), whereas the optical parameters in an optical metamaterial emerge from its internal composition. With a conventional optical material such as a homogenous material, graded index material or an optical crystal, because the optical parameters arise from the atomic or molecular structure of the medium, they cannot be chosen easily. For example in a semiconductor, one can dope a crystal, but the positioning of the dopant within the semiconductor will be fixed when the system reaches equilibrium and hence the optical properties of the system are bound by the laws of thermodynamics. Likewise in a graded index material the optical properties can be structured, but current technology does not allow us to change individual atoms or molecules to

give us complete control. In an anisotropic optical metamaterial however, because the material derives its optical properties from large-scale structure, rather than individual atoms or molecules, far greater control of the optical properties of the material can be achieved.

So, far from being done and dusted, thanks to the birth of optical metamaterials, the interest in refraction is as popular as ever, however very little research has been carried out with regards to new laws of refraction. As mentioned, Snell's law is a direct consequence of analysing the electric field locally across an optical interface. However Snell's law is not the only law of refraction across an interface. One avenue to creating new laws of refraction is by utilising metasurfaces [1, 2]. Metasurfaces make it possible to generalise Snell's law and to produce out of plane refraction. Nevertheless, these laws of refraction are still Snell-like and are quite difficult to achieve requiring metamaterials to manufacture; hence it is prudent to try and come up with new ideas to broaden refraction. In this thesis we will explore and develop the geometry of a new kind of refraction called *metarefraction*.

The appropriate question to ask at this point is 'in what sense does metarefraction differ from conventional refraction?'. We state the answer formally now in order to motivate the reader:

*A metarefracted light-ray field has, in general, no underlying global phase structure, and therefore its geometrical description cannot be reconciled with wave-optics.*

Further to this, metarefracted light-ray fields (as considered in this thesis) are produced by refraction across planar interfaces and as such cannot be created easily with solid materials.

This thesis will be structured as follows: Chapter 2 will briefly introduce the ideas and theories relevant to the research which is to follow - i.e. theorems on classical optical imaging, transformation optics and finally metamaterials and micro-structured metasheets. Chapter 3 will explore in detail the wave-optical properties of light-ray fields produced by metarefracting sheets and will show how metarefracted light-ray fields exhibit different parallax to conventional light-ray fields. Chapter 4 will show that a subset of a certain class of metarefracting sheet, called generalised confocal lenslet arrays, perform integral imaging, and that curved interfaces can never perform

---

perfect stigmatic imaging. Chapter 5 reinterprets the refraction performed by generalised confocal lenslet arrays and shows that generalised confocal lenslet arrays can be considered as metric tensor interfaces. Chapter 6 utilises the results of Chapter 4 to show that pixellated, piecewise transformation optics devices can be designed using special configurations of confocal lenslet arrays. Chapter 7 presents a set of results that aim to show that ray-rotation sheets can be considered as imaging into complex space, and that up to a point, ray-rotation and confocal lenslet array refraction can be considered as conjugates of one another. Finally in Chapter 8 we summarise the results of this thesis and briefly describe future work that could be undertaken to advance the research already presented.

# Chapter 2

## Background

### 2.1 Introduction

Before proceeding to the main chapters of this thesis, we must first introduce relevant background theory and ideas.

### 2.2 Optical path length

When considering matters of geometry one is frequently concerned with calculating distances. In optics – specifically geometrical optics – one is also often concerned with optical distance, or optical path length as it is more commonly known. The optical path length is a construction which gives an intuitive picture as to why a wave experiences a phase shift after travelling through a material when compared to another wave which starts from the same source but travels through vacuum. For example, if two monochromatic waves emanate from the same source, but one passes through a sheet of glass while the other passes through air, the wave which passes through glass will arrive at the same geometrical distance from the source slightly later than the wave which travelled through air. This is because the wave which passes through the glass propagates more slowly. As such a phase shift occurs when the phase of each of the two waves is measured. A more intuitive picture of this is as follows: the geometrical distance between the source and the point where the phase of each wave is measured is identical, however from the perspective of the light which travels through the glass, it has actually travelled further than the wave which did not

pass through the glass. In other words the “optical distance” the wave experiences as it travels inside the glass is greater than the distance the wave which does not pass through the glass experiences. In a material of constant refractive index the optical path length is given by

$$O = nl, \quad (2.1)$$

where  $n$  is the refractive index of the material and  $l$  is the geometrical path length. One can see that for a typical piece of glass, a wave passing through it will, from its perspective, have travelled approximately 1.5 times further than if the glass was not there.

### 2.2.1 Fermat’s principle

It is well known that in isotropic media such as air or glass, light rays travel along straight lines. Mathematically this is explained via Fermat’s principle, which states that the trajectory which light rays will travel between two points will be the one which has the stationary optical path length [3]. Fermat’s principle is a specific example found in optics of the more general principle of least action which arises in variational calculus. In classical mechanics extremising the action allows the equations of motion of a system to be found.

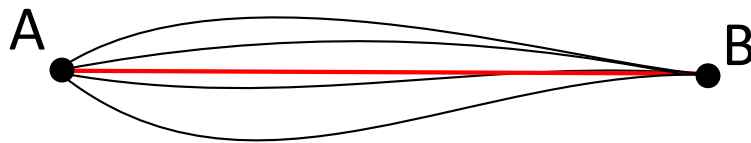


FIGURE 2.1: Fermat’s principle states that light rays will travel along the path which requires the least action, or optical path length. In isotropic media like air, this corresponds to the shortest geometrical path length. In this figure the light ray would therefore travel from **A** to **B** along a straight trajectory (red) as opposed to a longer curved trajectory (black).

In the context of optics, extremising the optical path length, which plays the role of the action, allows the trajectory of light rays to be calculated. In full variational calculus, we must perturb the action by infinitesimally varying the path along the trajectory. The difference between the perturbed action and the original action is then set to zero, and after mathematical manipulations taken in the limit of small variations, the equations of motion can be found. In this thesis we need not concern

ourselves with the full variational calculus version of Fermat's principle, as we will only be applying it across optical interfaces placed in air, and hence only varying the optical path length with respect to one plane intersecting the trajectory. As such extremising the optical path length simply corresponds to taking its derivatives with respect to the interface coordinates and setting them to zero. We now elaborate in slightly more detail. The optical path length between two points,  $\mathbf{A}$  and  $\mathbf{B}$  is given by

$$O(\mathbf{x}) = \int_{\mathbf{A}}^{\mathbf{B}} n(\mathbf{x}) dl, \quad (2.2)$$

where  $n$  is the refractive index profile of the medium and  $dl$  is the infinitesimal increment along the geometric path and  $\mathbf{x} = (x, y, z)$ . We now look at a path which deviates slightly from the original (a perturbation) between  $\mathbf{A}$  and  $\mathbf{B}$ . The optical path length for this path is

$$O(\mathbf{x} + \delta\mathbf{x}) = \int_{\mathbf{A}}^{\mathbf{B}} n(\mathbf{x} + \delta\mathbf{x}) dl. \quad (2.3)$$

Fermat's principle states that light rays will travel along paths for which the optical path length is stationary. Recall that when one finds the stationary point for a curve, one takes the derivative and sets it to zero. The same applies here when finding the stationary optical path. Hence one must solve

$$\delta O = O(\mathbf{x} + \delta\mathbf{x}) - O(\mathbf{x}) = \int_{\mathbf{A}}^{\mathbf{B}} (n(\mathbf{x} + \delta\mathbf{x}) - n(\mathbf{x})) dl = 0. \quad (2.4)$$

This expression is then perturbed, where necessary, about  $\delta\mathbf{x}$  and after suitable manipulation produces the "equations of motion" of the system. If the refractive index profile is known, the equations of motion can be used to find the trajectory of any light ray passing through the medium between the two points  $\mathbf{A}$  and  $\mathbf{B}$ . For example, in anisotropic materials such as photonic crystals and exotic graded index materials where the optical parameters are spatially varying, the trajectories can be curved. On the other hand, if the material parameters are not known, but the trajectory is, one can use the trajectory to solve for the material parameters.

### 2.2.2 Absolute optical instruments

A key requirement of many optical systems is that they perform imaging. A point  $\mathbf{P}$  is said to be stigmatically imaged when all rays passing through it are later found

to pass through a new point  $\mathbf{P}'$ . If all points in the region before the system are imaged stigmatically, the system is said to be an absolute optical instrument [4], and the image points make up what is called image space, while those points which generate them make up what is called object space. In this sense, an absolute optical instrument images all of object space to all of image space. It can be shown that absolute optical instruments image points in such a way as to ensure that the optical path length between any two object points is the same as the optical path length between their two corresponding image points [4].

## 2.3 Transformation optics

Transformation optics utilises the mathematics of differential geometry to design dielectrics with spatially varying optical properties. The result is an optical material which mimics the effects of curved space for light. As such, light travels along predetermined curved trajectories inside the material. The archetypal transformation optics device is the invisibility cloak.

Theoretically, transformation optics is achieved by placing Maxwell's equations in empty space on a curved background and reinterpreting the results. Written using Einsteins convention Maxwells equations on a curved background are

$$\begin{aligned}
 (\sqrt{g}g^{ij}E_j)_{,i} &= \frac{\sqrt{g}\rho}{\epsilon_0}, \\
 (\sqrt{g}g^{ij}H_j)_{,i} &= 0, \\
 [ijk]E_{k,j} &= -\mu_0 \frac{\partial(\pm\sqrt{g}g^{ij}H_j)}{\partial t}, \\
 [ijk]H_{k,j} &= \frac{\partial(\pm\sqrt{g}g^{ij}E_j)}{\partial t} + \sqrt{g}j^i,
 \end{aligned} \tag{2.5}$$

where subscript  $i$  denotes the  $i$ th component of a vector, subscript  $,i$  denotes the derivative with respect to the  $i$ th coordinate,  $g^{ij}$  is the metric tensor of the curved background and  $[ijk]$  is the Levi Civita symbol. Treating the charge and current densities,  $\rho$ , and  $j^i$ , and the electric permittivity and magnetic permeability,  $\epsilon_0$  and

$\mu_0$ , as having been transformed as follows:

$$\begin{aligned}
\varrho &= \pm \sqrt{g}\rho, \\
J^i &= \pm \sqrt{g}j^i, \\
\epsilon &= \epsilon_0 \epsilon^{ij} = \pm \epsilon_0 \sqrt{g}g^{ij}, \\
\mu &= \mu_0 \mu^{ij} = \pm \mu_0 \sqrt{g}g^{ij},
\end{aligned} \tag{2.6}$$

these new transformed quantities can then be used to reinterpret Maxwell's equations as being on a flat background in a dielectric with spatially varying optical parameters:

$$\begin{aligned}
D_{,i}^i &= \varrho, \\
B_{,i}^i &= 0, \\
[ijk]E_{k,j} &= -\frac{\partial B^i}{\partial t}, \\
[ijk]H_{k,j} &= \frac{\partial D^i}{\partial t} + J^i,
\end{aligned} \tag{2.7}$$

where  $D^i = \epsilon E_j$  and  $B^i = \mu H_j$ . Hence we have designed a dielectric with spatially varying optical properties. Because  $\epsilon^{ij} = \mu^{ij}$  the resulting impedance,  $Z$ , of the dielectric is everywhere unity as  $Z = \sqrt{\mu/\epsilon}$ . This means that the dielectric is impedance matched with the surrounding vacuum where the impedance is also unity. The optical properties are clearly functions of the metric tensor of the geometry used, and the metric itself is constructed using the Jacobian matrix  $\Lambda_J$  for some underlying coordinate transformation

$$\mathbf{g} = \Lambda_J^T \boldsymbol{\eta} \Lambda_J, \tag{2.8}$$

where  $\boldsymbol{\eta}$  is the euclidean metric. Dielectrics designed using transformation optics are almost always spatially varying and complicated - if not impossible - to achieve using natural materials. For example, consider the archetypal device created using transformation optics - the invisibility cloak. The coordinate transformation which produces the cylindrical cloak is (in cartesian coordinates) given by the following equations

$$\begin{aligned}
x' &= \frac{r'(r)x}{\sqrt{x^2 + y^2}}, \\
y' &= \frac{r'(r)y}{\sqrt{x^2 + y^2}}, \\
z' &= z,
\end{aligned} \tag{2.9}$$

where  $r'$  is the new radius of the cylinder we are creating and  $r$  is the radius of

the original cylinder which we assume to be infinitesimal. This coordinate system is clearly radially dependent, and so a naturally occurring mineral or crystal will not provide the required optical properties. As such, transformation optics devices such as cloaks have to be designed using synthetic (i.e. not naturally occurring) materials, especially when their optical parameters are dependent on three spatial dimensions.

Beyond cloaking, transformation optics is being applied in several areas. In the field of plasmonics it is being utilised to design transformation-plasmonic devices [5, 6]. In conventional plasmonic systems, an isotropic dielectric is placed on a conductor and surface plasmons are excited using electromagnetic radiation. Transformation optics allows the dielectric parameters to be carefully designed such that more complicated plasmonic behaviour can be achieved. Transformation optics is also being used in conjunction with ultrashort laser pulses to attempt to create optical black holes in optical fibres [7]. The hope is that by doing this, an optical analogue of Hawking radiation [8] may be observed. More complicated transformation optics devices which implement complex coordinate transformations [9, 10] have been suggested as a way of modulating loss and gain at different regions in the device.

## 2.4 Metamaterials and microstructured metasheets

### 2.4.1 Metamaterials

As mentioned previously, the cylindrical cloak, and by extension its three-dimensional generalisation, the spherical cloak, rely on optical parameters which vary spatially in a very complicated way. The natural world, as far as we know, offers no such miracle material with optical properties that vary in such a unique way, hence it will require synthetic materials to achieve the required effects. To avoid diffraction, the constituent components of the material must be significantly smaller than the wavelength which is to be redirected. One's first thought might therefore be to turn to chemistry and utilise properties of atoms and molecules; however to create a device which is spatially varying in a very precise way at the molecular or atomic level is beyond current technology. Fortunately, if we restrict ourselves to larger wavelengths, then it is possible to create such materials using metamaterials. Metamaterials are constructed from arrays of subwavelength electromagnetic elements such as split-ring resonators and metal rods among others. The effect of such arrays is to create a

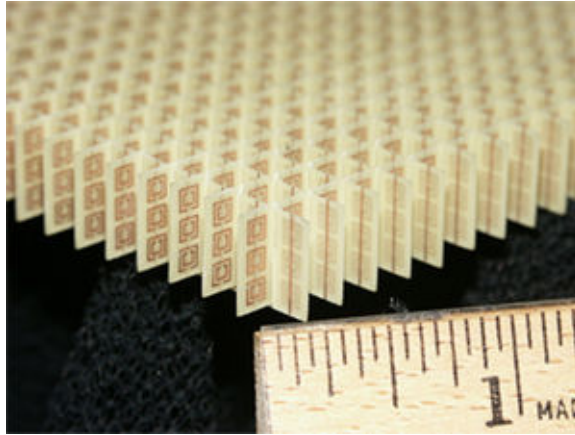


FIGURE 2.2: An three-dimensional array of concentric split-ring resonators. Such elements are frequently studied in metamaterial research and have applications in transformation optics. In the microwave regime they can be configured to produce different effective permeabilities and permittivities.

smoothly varying effective permeability and permittivity throughout the material [11]. Indeed such metamaterials have been used to build cloaks designed using transformation optics [12] [13].

### 2.4.2 Microstructured sheets exhibiting generalised refraction

Metarefraction and its applications are at the heart of this thesis. Specifically we will study metarefraction generated by two different types of microstructured metasheets. The first are called generalised confocal lenslet arrays (gCLAs) and the second are called ray-rotation sheets. CLAs are comprised of two lenslet arrays separated by the sum of their focal lengths. The lenslets are aligned with each other and as such the sheet can be thought of as an array of telescopes. Because the sheet is comprised of an array of telescopes, the image produced by a CLA is pixellated and the ordering of the light rays after passing through each telescope can be inverted. Because of this the image will also be slightly blurred, as from telescope to telescope, the ordering of light rays will be mixed up to an extent. This is shown in Fig. 2.4 where we see that if all the light rays entering one telescope with the same direction are the same colour then the outgoing light rays are inverted but are indistinguishable as they are all of the same colour. However, if the light rays entering the telescope are of different colours, we see that the outgoing image will have its light rays visibly in a different order. As a consequence of this, blurring can occur between regions of

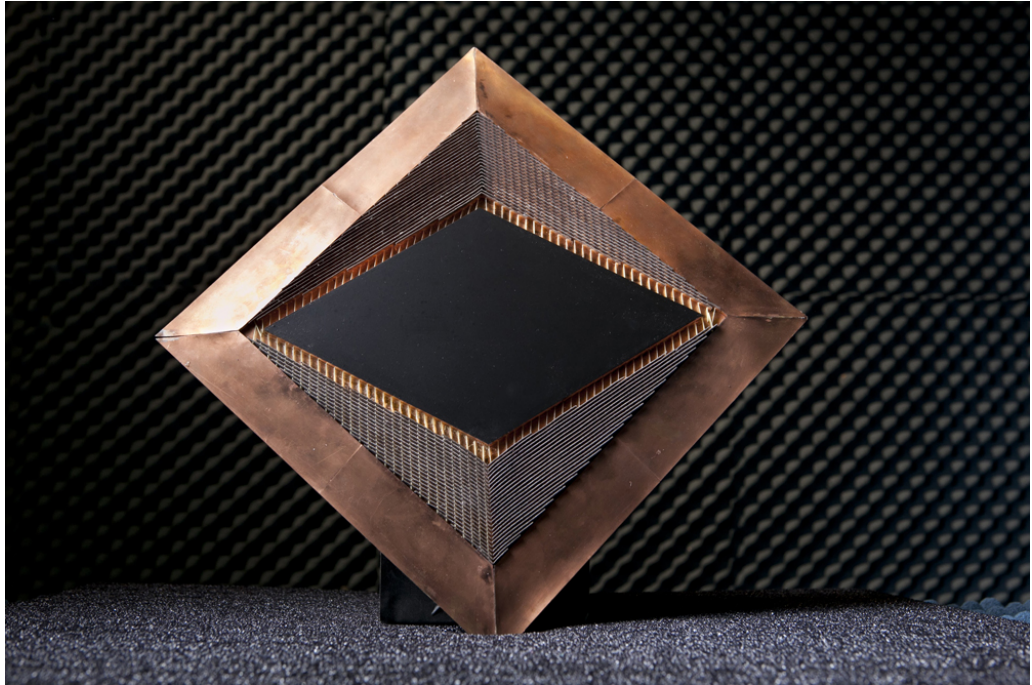


FIGURE 2.3: The microwave cloak from [13]. The diamond inner region (black) is where the object being shielded is placed. The material surrounding the inner region is constructed using split-ring resonators and ensures microwave radiation flows around the central region and remains in phase.

different colours across different telescopes. However, in general, the overall image will remain intact as such changes are minimal if the telescopes are small.

The other type of metasheet we will be studying is the ray-rotation sheet. Ray-rotation sheets are comprised of two dove-prism arrays which are parallel but have their mirror planes rotated relative to one another [15]. The effect this has is that light rays crossing the interface are rotated by twice the angle between the mirror planes of the individual dove-prism arrays, as shown in Fig. 2.5. Ray-rotation sheets also pixellate the outgoing light-ray field as it is each individual light ray which is rotated, and not the image as a whole.

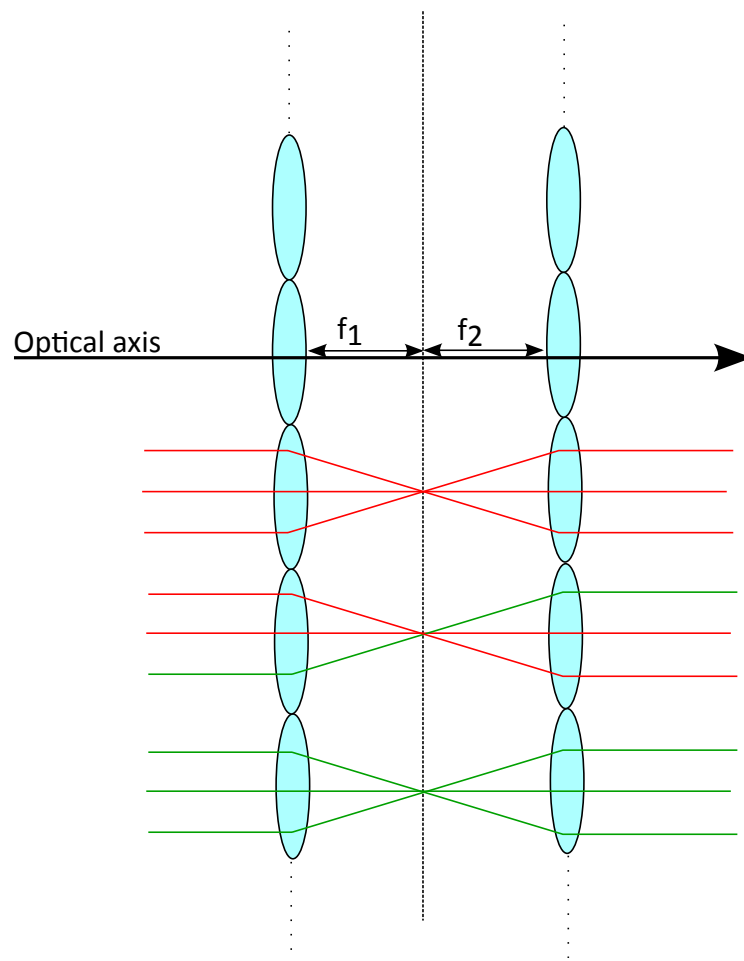


FIGURE 2.4: Confocal lenslet arrays are comprised of two lenslet arrays which share a common focal plane. Each lenslet pair can be thought of as a mini telescope (or pixel). Due to the fact that light has to pass through an array of telescopes, the outgoing image is pixellated and blurring can also appear between pixels when different parts of the image are inverted inconsistently across different telescopes.

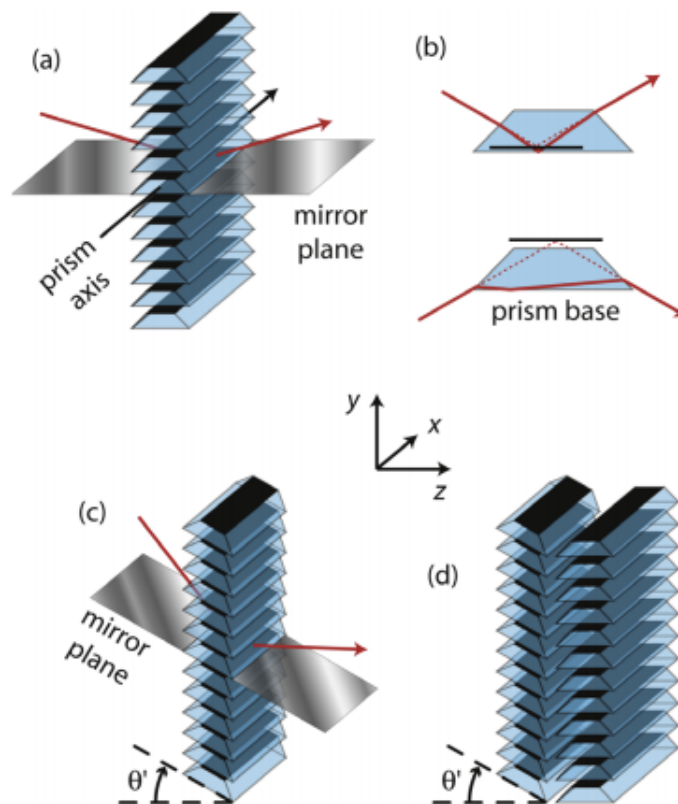


FIGURE 2.5: Figure taken from [14]. A dove-prism array **(a)** is described by a mirror plane and a prism axis. Light rays enter each individual dove prism and through a process of internal reflection and refraction **(b)** re-emerge on the other side of the dove prism as though they have been reflected off of the prisms mirror plane. Tilting each dove prism in the array simply has the effect of altering the angle of the mirror plane **(c)**. When a light ray is reflected off of two mirror planes which are at an angle to one another, the light ray is rotated by twice the angle of separation. As such, when two dove-prism arrays whose mirror planes are at an angle  $\theta'$  to one another share a plane, **(d)**, light rays entering the combined interface are rotated by an angle  $2\theta'$  on leaving the interface. Hence a combination of two rotated dove-prism arrays form a ray-rotation sheet.

# Chapter 3

## Light-ray fields with non-zero curl

### 3.1 Introduction

Conventional optical systems are, fundamentally, described by equations which can always be reconciled with wave optics. For example, when a wave passes through a phase hologram, the phase structure of the wave is altered across a plane which causes the field to evolve in a new, useful way. The only way to understand a phase hologram is through wave optics. Snell's law is geometrical, however it emerges from Maxwell's equations and thus can be re-cast in terms of wave optics. Transformation optics is another example; here in essence we just reinterpret the wave equation on a curved background metric and see what effect this has on light rays. In all of the examples mentioned, the properties that the outgoing light-ray fields have are a direct consequence of the underlying wave theory which underpins them. In other words, conventional optical systems must reflect the wave-optical nature of light, even if one only studies them ray-optically. Thus conventional optical systems are bound by wave optics and hence limited to what they can do. If an optical manipulation could be found which was not bound by wave optics, this would be an interesting advance in optics. Metarefraction has the ability to perform such manipulations. In this chapter we will show that light-ray fields produced by metarefraction have non-zero curl which means that they cannot be described using wave optics.

### 3.1.1 Contributions

The work that follows was undertaken by myself with help from Simon Horsley and Tom Philbin.

## 3.2 The curl of a light-ray field

It is a basic result of vector calculus that the curl of any gradient is zero almost everywhere:

$$\nabla \times \nabla\phi = \mathbf{0}. \quad (3.1)$$

It is well known that in the ray-optics limit of wave optics, the direction of a light ray is directly proportional to the phase gradient of the underlying waveform. Hence it is true that

$$\nabla \times \mathbf{d} = \nabla \times \frac{\nabla\phi}{|\nabla\phi|} = \frac{1}{|\nabla\phi|} \nabla \times \nabla\phi = \mathbf{0}, \quad (3.2)$$

where  $\mathbf{d}$  is the normalised light-ray direction,  $\phi$  is the phase of the wave and  $|\nabla\phi| = 2\pi/\lambda$ . The phase,  $\phi$ , is a continuous function which spans all of space and as such can be described as a “global” function (however this does not mean the phase cannot be locally varying). If a function is not continuous it cannot be described as global as different positions in space will be described using different “local” functions. Beyond the ray-optics limit where the phase gradient is free to change from one point to the next in direction and magnitude, one has to be more careful. For example consider a scalar field given by

$$u = \sqrt{I} \exp(i\phi), \quad (3.3)$$

where  $I$  is the intensity, and  $\phi$  is the phase. The gradient of the scalar field is given by

$$\nabla u = i\nabla\phi u + \frac{\nabla I}{2I} u, \quad (3.4)$$

and so we see that the gradient of the phase (assuming the change in intensity from one point to the next is negligible) is given by

$$\nabla\phi = \frac{\nabla u}{iu} = \operatorname{Re} \left( -i \frac{\nabla u}{u} \right). \quad (3.5)$$

Using complex analysis, this can be re-written in the more familiar [16] way

$$\nabla\phi = -i\frac{1}{2}\left(\frac{\nabla u}{u} - \left(\frac{\nabla u}{u}\right)^*\right) = \frac{-i}{2I}(u^*\nabla u - u\nabla u^*), \quad (3.6)$$

where  $I = u^*u$ . The above expression was derived from a wave form with arbitrary phase  $\phi$ , however the final expression can clearly be applied to calculate the local phase gradient for arbitrary wave-forms. Indeed consider a superposition of two plane waves where we have ignored the temporal part of each phase for simplicity:

$$\psi(x, y) = a_1 \exp(i(k_{1x}x + k_{1y}y)) + a_2 \exp(i(k_{2x}x + k_{2y}y)). \quad (3.7)$$

When the local phase gradient for this field is calculated using the expression defined above, we see that the length and direction of the local phase gradient can change from point to point, as seen in Fig. 3.1. In analogy with the phase gradient of a plane wave, the local phase gradient is used to define the local light-ray direction. In general the field of local phase gradients and light-ray directions are continuous, the only exception being where phase singularities occur, as at phase singularities the phase gradient diverges. Indeed, when phase singularities arise in the field this leads to the curl of the phase-gradient being non-zero:

$$\nabla \times \nabla\phi \neq \mathbf{0}. \quad (3.8)$$

Phase singularities are always dark, so while they can occur at specific positions in a field, they cannot occur everywhere, otherwise the field would not exist. We will show that when analysed, metarefracted fields appear to have phase singularities everywhere, however this is not the case. This is an important point which we must explore in detail, hence we proceed now to explain mathematically the foundations of metarefraction.

The Kelvin-Stokes theorem tells us that the integral of the curl of the phase gradient over an area  $A$  equals the line integral of the phase gradient around the closed loop  $S$  bounding  $A$ :

$$\int_A (\nabla \times \nabla\phi) \cdot dA = \oint_S \nabla\phi \cdot dS. \quad (3.9)$$

Calculating the line integral of the phase gradient around a closed loop allows us to calculate how much phase the field picks up when going round a closed loop. Clearly in order to be curl-free, the phase must be continuous and therefore unchanged after circumnavigating the loop, the only exception being where phase discontinuities arise

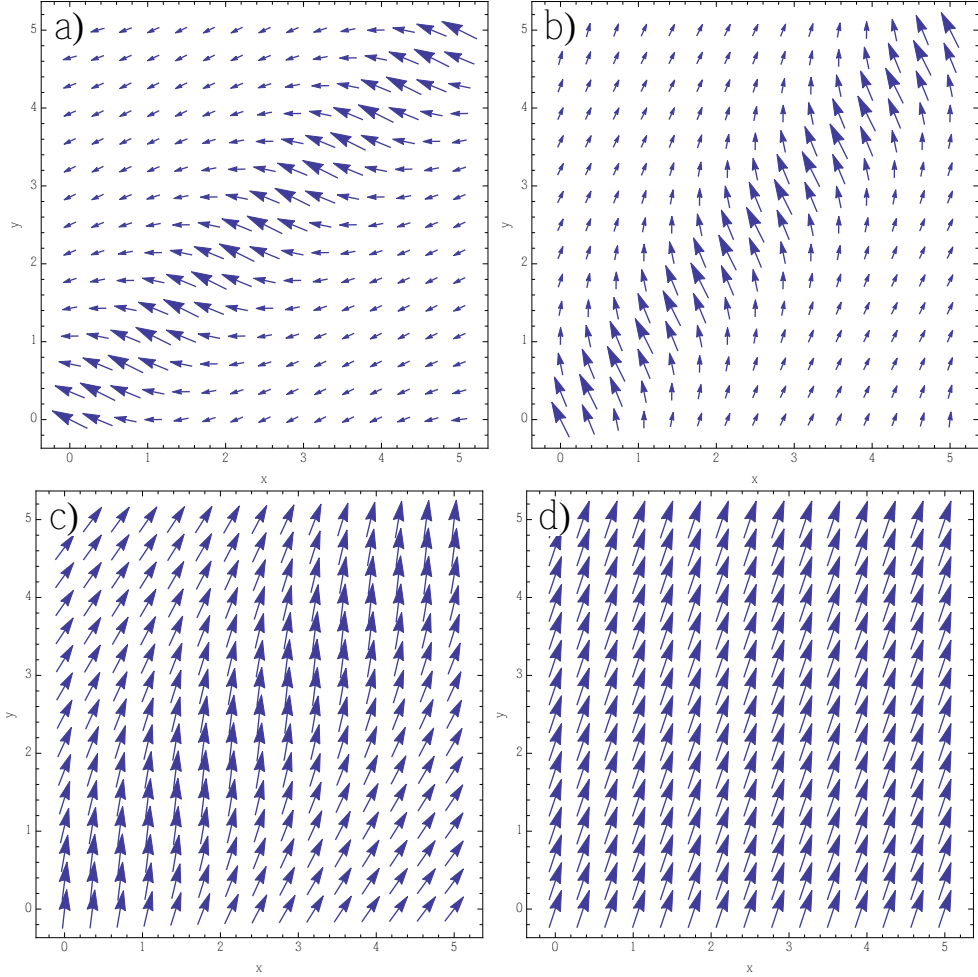


FIGURE 3.1: Images **a-c**: the real part of the local phase gradient for the superposition of two plane waves as described in Eq.(3.7) with  $a_1 = 1$ ,  $a_2 = -2$ ,  $k_1 = (\sin \theta, \cos \theta)$  and  $k_2 = (\cos \theta, \sin \theta)$ , with  $\theta = \pi$ ,  $\theta = \pi/2$  and  $\theta = \pi/3$  respectively. It is clear that the local phase gradient is changing length and direction from point to point, unlike for a plane wave, where the direction and length are constant as seen in **d**.

as here the local phase gradient diverges. If the phase gradient has non-zero curl everywhere, this implies that the underlying phase surface is discontinuous at all points in space, which in turn implies that the light-ray field does not exist.

We see that the curl of the phase gradient and the curl of the light-ray field are intimately linked, however what does the curl of the light-ray vector actually tell us? Consider a vector,  $\boldsymbol{\nu}$ , that lies in a plane which is orthogonal to the normalised phase gradient,  $\mathbf{s}$ , i.e.  $\boldsymbol{\nu}$  is tangential to the local phase surface of the field. The scalar product of  $\boldsymbol{\nu}$  and a vector aligned with the normalised phase gradient,  $\mathbf{d}$ , must be zero:

$$(d_x, d_y, d_z) \cdot (\nu_x, \nu_y, \nu_z) = 0. \quad (3.10)$$

Expanding and rearranging for  $\nu_z$ , we get

$$\frac{d_x \nu_x + d_y \nu_y}{d_z} = -\nu_z. \quad (3.11)$$

If we are located somewhere on the phase surface and “carry” the vector  $\mathbf{d}$  (which we recall is aligned with the local phase gradient) with us as we move a distance  $\nu_x$  along the  $x$ -axis and  $\nu_y$  along the  $y$ -axis, then Eq.(3.11) can be used to find out how much height we must gain in the  $z$ -axis in order for the vector  $\mathbf{d}$  to still be located on the phase surface. We can apply this result to our calculation for the curl of  $\mathbf{d}$ . Assuming that the non-normalised vector field is constructed such that  $d_z = 1$  at all points in space, we see that Eq.(3.11) gives the same expression as half of the line integral around a closed, square loop whose sides are of length  $\nu_x = \nu_y = \nu$  in the  $xy$ -plane. That is to say, when  $d_z = 1$ , in the limit of small  $\nu$ , two copies of Eq.(3.11), one for each half of the loop, will produce a calculation which is equivalent to a discrete application of the right hand side of Eq.(3.9). Fig. 3.2 illustrates this visually, for one half of the loop. Explicitly we calculate the following for the full loop:

$$\begin{aligned} \nu_{z_1} + \nu_{z_2} &= -\nu \left( d_x(x, y - \nu/2) + d_y(x + \nu/2, y) \right) + \nu \left( d_x(x, y + \nu/2) + d_y(x - \nu/2, y) \right) \\ &= -\nu^2 \left( \frac{\partial d_y(x, y)}{\partial x} - \frac{\partial d_x(x, y)}{\partial y} \right) \\ &= -\nu^2 (\nabla \times \mathbf{d})_z, \end{aligned} \quad (3.12)$$

where  $\nu_{z_1}$  and  $\nu_{z_2}$  are the first and second halves of the loop respectively. Thus we can state that the  $z$ -component of the curl of  $\mathbf{d}$  can be used to tell us the height gained in the  $z$ -direction when taking a step of size  $\nu_x$  in the  $x$ -direction and  $\nu_y$  in the  $y$ -direction on the phase front. Hence we see that if we construct our light-ray vector such that  $d_z = 1$ , Eq.(3.12) must equal zero if we are to stay on the phase surface and return to our original position on it. In the case where an optical vortex arises, we would not return to our original position on the phase surface and so clearly the above calculation will therefore give the distance between two parts of a helical phase surface.

Note that Eq.(3.12) will not work for any other ray construction. We can see this directly when we attempt to use a different ray normalisation. Clearly if Eq.(3.12) is equal to zero we see that

$$\frac{\partial d_y}{\partial x} = \frac{\partial d_x}{\partial y}. \quad (3.13)$$

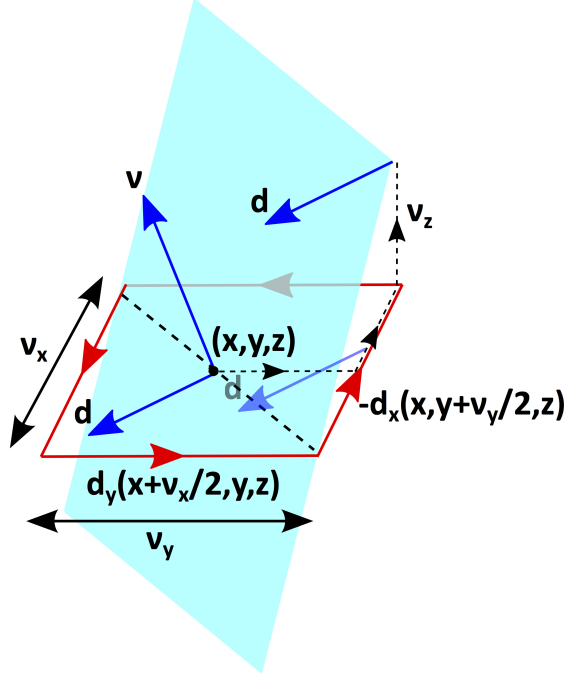


FIGURE 3.2: On traversing a closed loop (red line) we see that a light-ray vector,  $\mathbf{d}$  (blue vector) returns to its original position on the phase surface (blue plane). If a phase singularity occurs within the loop, such as at an optical vortex, then the light-ray vector will have acquired a height on circumnavigating the loop, and so will not return to its original position.

Now consider a case where the ray vector is normalised differently, for example consider the field  $\mathbf{e}$  where

$$\mathbf{e} = x\mathbf{d}. \quad (3.14)$$

It follows that

$$\frac{\partial e_x}{\partial y} = x \frac{\partial d_x}{\partial y} \quad (3.15)$$

$$\frac{\partial e_y}{\partial x} = d_y + x \frac{\partial d_y}{\partial x}. \quad (3.16)$$

Substituting Eq.(3.13) into Eq.(3.16) we see that it can be re-written

$$\frac{\partial e_y}{\partial x} = d_y + x \frac{\partial d_x}{\partial y} = d_y + \frac{\partial e_x}{\partial y}, \quad (3.17)$$

which shows that  $\partial e_y / \partial x \neq \partial e_x / \partial y$  unless  $d_y = 0$  which in general will not be the case. Hence we see that calculating the curl of the light-ray field depends on how one normalises the light-ray field in the first place. One size does not fit all.

### 3.3 Simplifying the $z$ -component of the curl of the outgoing light-ray field

The calculation in the previous section was orchestrated such that we calculated the  $z$ -component of the curl for a light-ray field constructed where  $d_z = 1$ . We could have calculated any of the other components of the curl in the same way, however we chose the  $z$ -component for good reason. In the following sections it will be our aim to determine whether or not an outgoing meta-refracted light-ray field has zero curl. In all the examples we will consider, we will assume that refraction takes place across the  $z = 0$  plane. If we knew how the outgoing field evolved on propagation along the  $z$ -axis, we would not have to perform our initial calculation in the first place as it would only be possible to know how the light-ray field evolves if it is in fact curl free. Hence we look at the  $z$ -component of the curl because it contains no derivatives with respect to  $z$  of the outgoing light-ray vector components, unlike the  $x$  and  $y$  components of the curl, which do. Indeed, due to their dependence on  $z$  derivatives, it would be difficult (if not impossible) to calculate the  $x$  and  $y$  components of the curl. Note however that if the  $z$ -component of the curl is zero this does not necessarily mean that the field in question can be described wave-optically as the  $x$  and  $y$  components of the curl may still be non-zero. However, in the refraction we shall consider in this thesis, the  $z$ -component of the curl is (in most cases) non-zero, and so we need not concern ourselves with the  $x$  and  $y$  components.

Previously when examining zero-curl-preserving laws of refraction, that is laws of refraction which take light-ray fields with zero curl and refract them again into light-ray fields with zero curl, it was shown that the  $z$ -component of the curl of the normalised outgoing light ray direction field was given by [17]

$$0 = \frac{\partial s'_y}{\partial s_x} \frac{\partial s_x}{\partial x} + \frac{\partial s'_y}{\partial s_y} \frac{\partial s_y}{\partial x} + \frac{\partial s'_y}{\partial s_z} \frac{\partial s_z}{\partial x} - \frac{\partial s'_x}{\partial s_x} \frac{\partial s_x}{\partial y} - \frac{\partial s'_x}{\partial s_y} \frac{\partial s_y}{\partial y} - \frac{\partial s'_x}{\partial s_z} \frac{\partial s_z}{\partial y}, \quad (3.18)$$

where  $s_i$  and  $s'_i$  are the spatially dependent components (for  $i = x, y, z$ ) of the ingoing and outgoing light-ray directions respectively. As the ingoing light-ray direction vector is normalised assuming  $s_z > 0$ , it must be possible to write the light-ray direction vector such that  $s_z$  is a function of  $s_x$  and  $s_y$  (i.e.  $s_z = \sqrt{1 - s_x^2 - s_y^2}$ ). This then means that we can eliminate the terms involving derivatives of  $s_z$  from Eq.(3.18), as the terms involving derivatives of  $s_x$  and  $s_y$  now contain all the information we require. Recalling that for an incident field to be curl free  $\partial s_x / \partial y = \partial s_y / \partial x$ , Eq.(3.18)

reduces to

$$0 = \frac{\partial s'_y}{\partial s_x} \frac{\partial s_x}{\partial x} + \left( \frac{\partial s'_y}{\partial s_y} - \frac{\partial s'_x}{\partial s_x} \right) \frac{\partial s_x}{\partial y} - \frac{\partial s'_x}{\partial s_y} \frac{\partial s_y}{\partial y}, \quad (3.19)$$

which is much simpler.

Of course we can arrive at Eq.(3.19) simply by applying the chain rule, as the ingoing and outgoing light-ray fields can be written in the form  $s_x(x, y)$  and  $s'_x(s_x, s_y)$  respectively.

Equation (3.19) must hold for all combinations of the “field derivatives”, that is the derivatives of the ingoing light-ray field [17] and so it must therefore be true that the coefficients of these terms must be individually zero. Hence we can re-write the constraints for the law derivatives in our simpler form to get

$$\frac{\partial s'_x}{\partial s_y} = 0, \quad (3.20)$$

$$\frac{\partial s'_y}{\partial s_x} = 0, \quad (3.21)$$

$$\frac{\partial s'_y}{\partial s_y} - \frac{\partial s'_x}{\partial s_x} = 0. \quad (3.22)$$

We see that we now have three conditions as opposed to the five that were previously found. In the following subsections we shall show that in general, light-ray fields produced by generalised confocal lenslet arrays and ray-rotation sheets will have non-zero curl. We shall also show that there are cases where these laws of refraction produce light-ray fields which do have zero curl.

### 3.4 Generalised laws of refraction generated by microstructured metasheets

Now that the relationship between the curl of a light-ray field and the curl of the local phase gradient has been explained, we will proceed to introduce the laws of refraction for generalised confocal lenslet arrays and ray-rotation sheets. We will show that in general, these laws of refraction lead to light-ray fields with non-zero curl.

### 3.4.1 Refraction by generalised confocal lenslet arrays

We now look at the first of our two wave-optically “forbidden” light-ray fields, those produced by generalised confocal lenslet arrays (gCLAs). We shall derive the ray-optical law of refraction for gCLAs and then show that it does indeed produce, in general, fields with non-zero curl. We start by considering confocal lenslet arrays which have been generalised in the following way:

1. The centres of the two lenses are shifted relative to one another in directions orthogonal to the optical axis of the system.
2. Each lens is replaced by two cylindrical lenses whose cylinder axes are orthogonal and whose focal lengths can be different. One pair of cylindrical lenses must still be confocally arranged with their counterparts in the other cylindrical lens pair. That is to say, the lenses are aligned and the sum of their focal lengths must still add up to the separation of the lenses.
3. Each lenslet pair can be rotated around the axis which is tangent to the sheet.

We now define the geometry of the system. We shall define the optical axis, to point in the direction  $\hat{\mathbf{a}}$ . We have stated that in our generalisation, we replace our lenses by cylindrical lens pairs. In this case the cylinder axes of the first and second cylindrical lenses in each pair lie along  $\hat{\mathbf{u}}$  and  $\hat{\mathbf{v}}$  respectively where  $\hat{\mathbf{u}}$  and  $\hat{\mathbf{v}}$  are orthogonal to  $\hat{\mathbf{a}}$ . A schematic of this system is shown in Fig.3.3.

Now that the system is set, we can begin our derivation. We initially model the refraction for the first cylindrical lens axis,  $\hat{\mathbf{u}}$ , hence we will be working in the  $(a, u)$  plane. Consider a light-ray vector  $\mathbf{d}$  which is defined such that  $d_a = 1$  and which passes through the centre of the first cylindrical lens  $\mathbf{C}_1$  whose cylinder axis points along  $\hat{\mathbf{u}}$ . This ray will pass through the point  $\mathbf{P}$  on the focal plane of the lens. The components of  $\mathbf{P}$  in the  $(a, u)$  plane are therefore given by

$$P_u = C_{1u} + \frac{d_u}{d_a} f_{1u}, \quad P_a = C_{1a} + f_{1u}. \quad (3.23)$$

The outgoing light-ray will leave with a direction  $\mathbf{d}'$ . If we take a parallel outgoing ray, we can always choose one which passes through both  $\mathbf{P}$  and the centre of the second lens  $\mathbf{C}_2$ . In that case, the outgoing light-ray vector is given by

$$\mathbf{d}' = \frac{1}{f_{2u}} (\mathbf{C}_2 - \mathbf{P}), \quad (3.24)$$

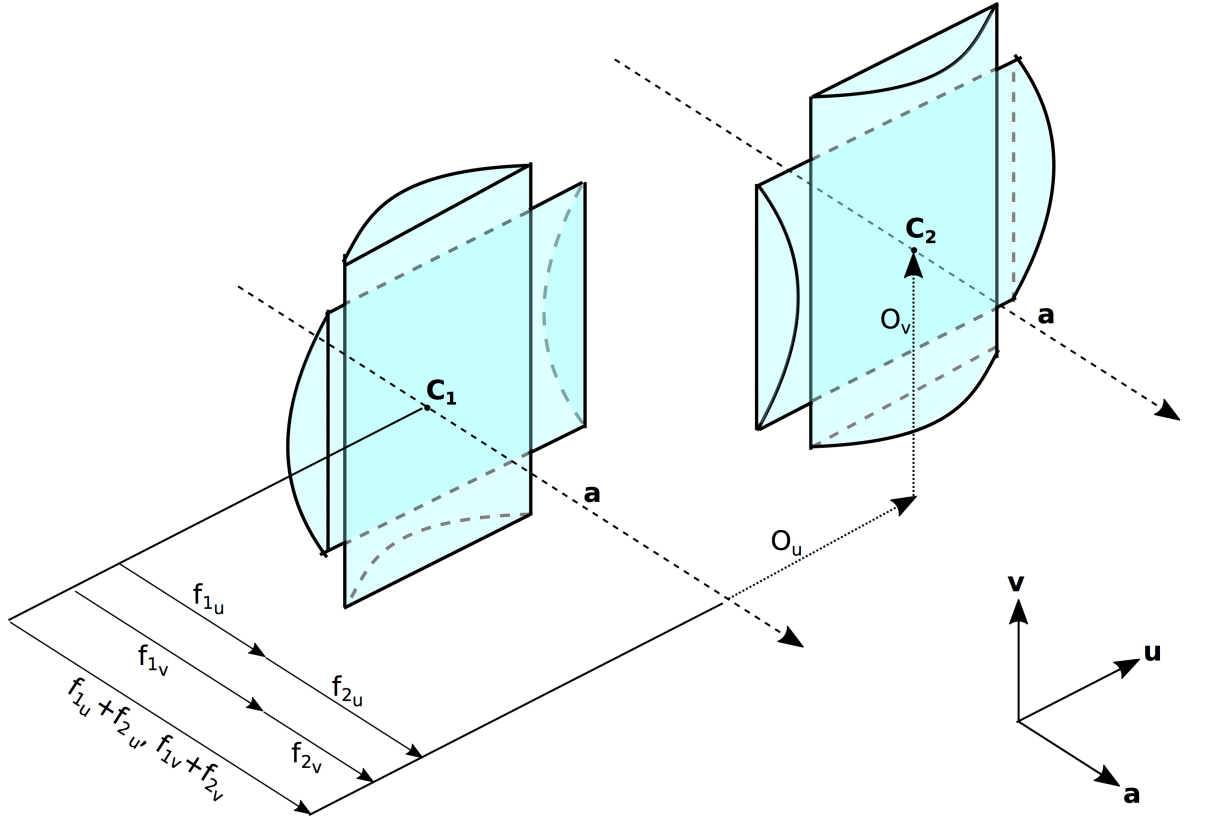


FIGURE 3.3: A schematic of how pairs of orthogonal cylindrical lens pairs can be used to make a generalised confocal lenslet array without lenslet rotation. The cylindrical lenses in each pair have their cylinder axes orthogonal to one another. The total distance between the two cylindrical lens pairs is the sum of the focal lengths for each of the two orthogonal cylinder axes, i.e.  $k = f_{1u} + f_{2u} = f_{1v} + f_{2v}$ . The cylindrical lens pairs can be offset relative to one another as shown.

where we have divided by  $f_{2u}$  so that  $d'_a = 1$ . Hence the components of the outgoing light-ray vector in the  $(a, u)$  plane are given by

$$d'_u = \frac{C_{2u} - (C_{1u} + (d_u/d_a)f_{1u})}{f_{2u}}, \quad d'_a = \frac{C_{2a} - (C_{1a} + f_{1u})}{f_{2u}}. \quad (3.25)$$

However we know that  $C_{2u} = C_{1u} + o_u$  and  $C_{2a} = C_{1a} + f_{1u} + f_{2u}$ , so we can re-write the components of  $\mathbf{d}'$  as

$$d'_u = \frac{o_u - (d_u/d_a)f_{1u}}{f_{2u}}, \quad d'_a = 1, \quad (3.26)$$

or more tidily as

$$d'_u = \frac{d_u - \delta_u}{\eta_u}, \quad d'_a = 1, \quad (3.27)$$

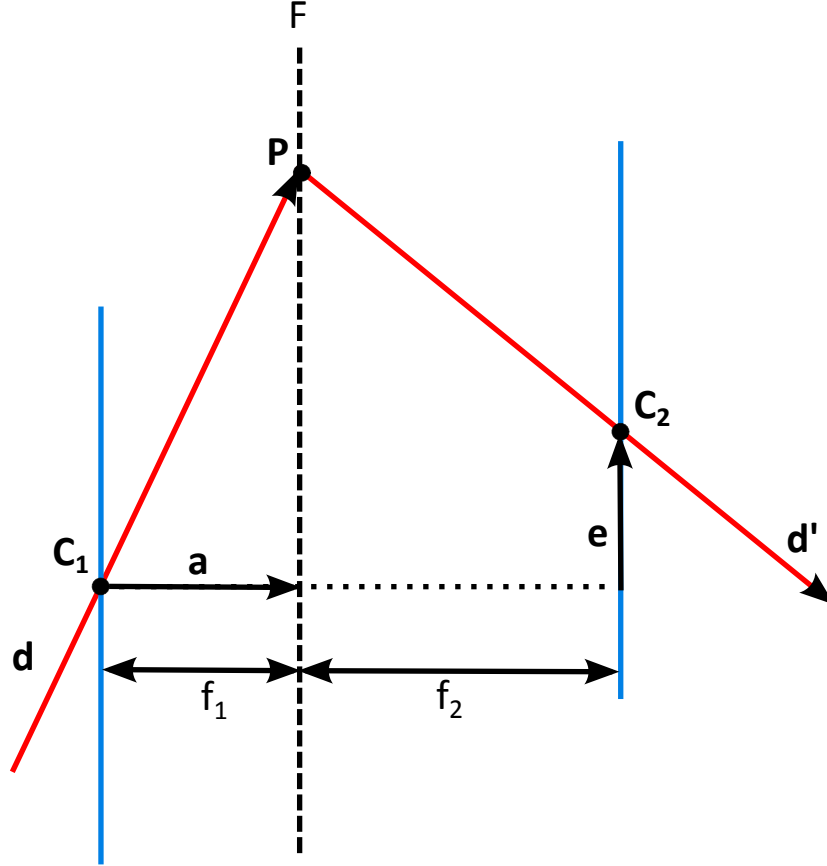


FIGURE 3.4: Two lenslets (blue lines) separated by the sum of their focal lengths. Constructing light rays (red), such that the ingoing ray passes through the central point of lenslet 1,  $C_1$ , and a point on the common focal plane  $\mathbf{P}$  and the outgoing light ray passes through  $\mathbf{P}$  and the central point of lenslet 2,  $C_2$ , it is straight forward to derive the law of refraction for generalised confocal lenslet arrays on a component by component basis.

where  $\delta_u = o_u/f_{1_u}$  and  $\eta_u = -f_{2_u}/f_{1_u}$  and we have used the fact that  $d_a = 1$ . These are the final expressions for the outgoing light-ray components in the  $(a, u)$  plane. The process can be repeated for the  $(a, v)$  plane and analogous expressions derived. The complete light-ray vector is thus defined by

$$\mathbf{d}' = \frac{d_u - \delta_u}{\eta_u} \hat{\mathbf{u}} + \frac{d_v - \delta_v}{\eta_v} \hat{\mathbf{v}} + \hat{\mathbf{a}}. \quad (3.28)$$

In the special case where  $\eta_u = \eta_v = \eta$ , the equation can be simplified further to give

$$\mathbf{d}' = \frac{\mathbf{d} - \boldsymbol{\delta}}{\eta}. \quad (3.29)$$

### 3.4.2 The curl of the light-ray field produced by generalised confocal lenslet array refraction

We now show that light-ray fields produced by generalised confocal lenslet arrays have, in general, non-zero curl. Consider the normalised light-ray vector  $\mathbf{d}$  for a system where  $\hat{\mathbf{a}} = \hat{\mathbf{z}}$

$$\mathbf{d} = \left( d_x, d_y, \sqrt{1 - d_x^2 - d_y^2} \right). \quad (3.30)$$

After refraction through a gCLA, the outgoing light-ray vector is given by

$$\mathbf{d}' = \left( \frac{d_x / \sqrt{1 - d_x^2 - d_y^2} - \delta_x}{\eta_x}, \frac{d_y / \sqrt{1 - d_x^2 - d_y^2} - \delta_y}{\eta_y}, 1 \right). \quad (3.31)$$

On taking the curl of  $\mathbf{d}'$ , very complicated and lengthy expressions are found. Setting  $\eta_x = \eta_y = \eta$  and  $\delta_x = \delta_y = 0$  simplifies the expressions and allows us to arrive at the following expression for the  $z$ -component:

$$\eta \left( (-1 + d_y^2) \frac{\partial d_x}{\partial y} + d_x d_y \left( -\frac{\partial d_y}{\partial y} + \frac{\partial d_x}{\partial x} \right) - (-1 + d_x^2) \frac{\partial d_y}{\partial x} \right) \quad (3.32)$$

Recall that for the outgoing light-ray field to be curl free, this must be equal to zero. We see that if the derivatives of the ingoing light-ray field equal zero, i.e. if the ingoing field is a plane-wave, the expression is satisfied. More generally the field will have non-zero curl. For the more general case where  $\eta_x$  and  $\eta_y$  are different, we expect that in general the outgoing light-ray fields will have non-zero curl, but that there will be specific ingoing wave forms and special configurations of the gCLA parameters which will produce curl-free fields.

### 3.4.3 The curl of the light-ray field produced by ray-rotation refraction

As with the previous example, when we consider refraction performed by a ray rotation sheet placed in the  $z = 0$  plane, if the ingoing light-ray direction is given by Eq.(3.30), the outgoing light-ray direction is simply a rotation of  $\mathbf{d}$  by an angle  $\theta$  around the  $z$ -axis:

$$\mathbf{d}' = \left( d_x \cos \theta - d_y \sin \theta, d_y \cos \theta + d_x \sin \theta, \sqrt{1 - d_x^2 - d_y^2} \right). \quad (3.33)$$

The expression for the curl of the light ray field produced by ray rotation is far simpler than that of its gCLA counterpart, and so we can examine it directly. The  $z$ -component of the curl, once set to zero, is given by

$$\sin \theta \left( \frac{\partial d_y}{\partial y} + \frac{\partial d_x}{\partial x} \right) = 0. \quad (3.34)$$

Clearly then to produce an outgoing field with zero curl we can have any incident field but must rotate by zero or  $180^\circ$ , as this will ensure that  $\sin \theta$ , and hence the  $z$ -component of the curl, are zero. Or we can have an ingoing light-ray field which satisfies

$$\frac{\partial d_y}{\partial y} = -\frac{\partial d_x}{\partial x}. \quad (3.35)$$

Plane waves will satisfy this expression, but are there any other solutions? We know that the curl of the light-ray field and the curl of the phase gradient are closely related. If an ingoing waveform is to be ray-rotated and leave still with zero-curl, then the outgoing waveform must simply be a local rotation of the ingoing transverse phase profile at the plane  $z = 0$  (as this is where the sheet sits), by the angle which the sheets rotates light rays by around the local sheet normal. Hence, to find possible solutions for ingoing waveforms which will produce outgoing light-ray fields with zero curl, we need only find pairs of transverse waveforms which are, at every point in the plane  $z = 0$ , rotated by an angle  $\theta$  to one another. Fortunately, such a class of waveforms exists. Consider a complex analytic function

$$f(w) = aw^n + bw^{n-1} + cw^{n-2} + \dots d \quad (3.36)$$

where  $w$  is a complex number of the form  $w = x + iy$  and  $a, b, c$  etc are constants. If  $f$  is a complex analytic function, then it is true that the real and imaginary parts

$$\begin{aligned} u &= \text{Re}[f(x + iy)] \\ v &= \text{Im}[f(x + iy)], \end{aligned} \quad (3.37)$$

define surfaces which are orthogonal to one another. That is to say

$$\nabla u \cdot \nabla v = 0. \quad (3.38)$$

In this framework, our ingoing transverse phase profile is described by  $u$  and our outgoing transverse profile is described by  $v$ . Clearly though, with this approach, no matter what function  $f$  we start with, we will only find sets of ingoing and outgoing

fields which are rotated by  $\pi/2$  to one another. However we can expand this class of functions for any angle of rotation by redefining  $v$ . For arbitrary angles of rotation, our transverse phase profiles are now given by

$$\begin{aligned} u &= \operatorname{Re}[f(x + iy)] \\ v &= \operatorname{Re}[f(x + iy)] \cos \theta + \operatorname{Im}[f(x + iy)] \sin \theta. \end{aligned} \quad (3.39)$$

For example, consider the complex analytic function

$$f(w) = -w + 2w^2 - \frac{1}{2}z^4, \quad (3.40)$$

where  $w = x + iy$ . Using the expressions in Eq.(3.39), and an angle of rotation of  $\pi/3$ , we can plot contour plots of the ingoing and outgoing transverse phase profiles,  $u$  and  $v$  in the  $z = 0$  plane as in Fig.3.5. We see in Fig.3.5 that the outgoing transverse phase profile, given by dashed lines, is always at an angle of  $\pi/3$  to the contour lines of the ingoing transverse phase profile, shown by solid lines.

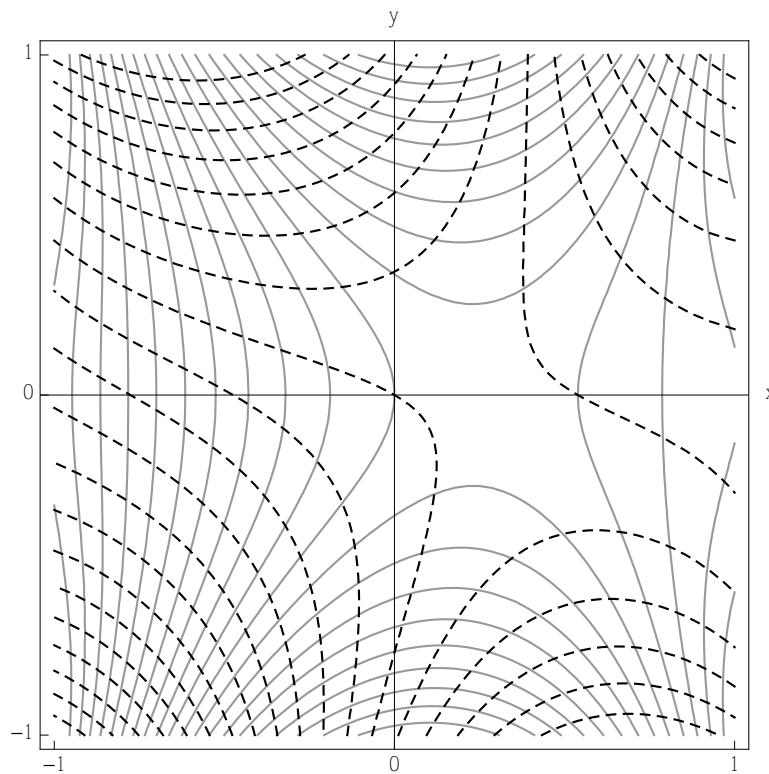


FIGURE 3.5: Contour plots of the transverse phase profiles in the  $z = 0$  plane of an ingoing and outgoing waveform. The ingoing transverse phase profile is given by solid lines, whereas the outgoing transverse phase profile is given by dashed lines. As can be seen, the outgoing transverse phase profile is at every point a local rotation of the ingoing transverse phase profile, specifically by  $\pi/3$ .

### 3.4.4 The light-ray field of a point light source produced by a ray-rotation sheet, as viewed by an observer

Previously it was shown that the refraction performed by ray-rotation sheets can effectively be modelled as refraction across an interface which has a complex refractive index ratio [18].

An integral step in this mathematical interpretation involves orthographically projecting the point where a light ray strikes the sheet into a complex plane which spans the plane in which the sheet lies. Specifically the orthographic projection of the point  $\mathbf{P}$  where the light ray from a particular point light source that then goes to the eye strikes the sheet, into the complex plane spanning the sheet (in this case the  $z = 0$  plane), is given by [15]

$$P = \frac{1}{1 + \frac{z_1}{z_2} e^{i\alpha}}, \quad (3.41)$$

where  $z_1$  is the distance between the point light source and the sheet,  $z_2$  is the distance between the sheet and the observer and  $\alpha$  is the angle of rotation around the  $z$ -axis. If we orthographically project the position of the point light source,  $\mathbf{L} = (L_x, L_y, -z_1)$  and the position of the observer,  $\mathbf{E} = (E_x, E_y, z_2)$  into the plane of the window ( $z = 0$ ) as in Fig.3.6, we can define basis vectors to span the plane. We define the first basis vector to be

$$\mathbf{b}_1 = \frac{1}{\sqrt{(E_x - L_x)^2 + (E_y - L_y)^2}} \begin{pmatrix} E_x - L_x \\ E_y - L_y \\ 0 \end{pmatrix}, \quad (3.42)$$

and the second to be at right angles to this

$$\mathbf{b}_2 = \frac{1}{\sqrt{(-E_y + L_y)^2 + (E_x - L_x)^2}} \begin{pmatrix} -E_y + L_y \\ E_x - L_x \\ 0 \end{pmatrix}, \quad (3.43)$$

We now re-cast the orthographic projection of  $\mathbf{P}$  in the complex plane into this new coordinate system. It can be shown that in this new basis, which is centered on the orthographic projection of  $\mathbf{L}$  the orthographic projection of  $\mathbf{P}$  is now given by

$$\mathbf{P}_{real} = \begin{pmatrix} L_x \\ L_y \\ 0 \end{pmatrix} + \text{Re}(\mathbf{P})\mathbf{b}_1 + \text{Im}(\mathbf{P})\mathbf{b}_2, \quad (3.44)$$

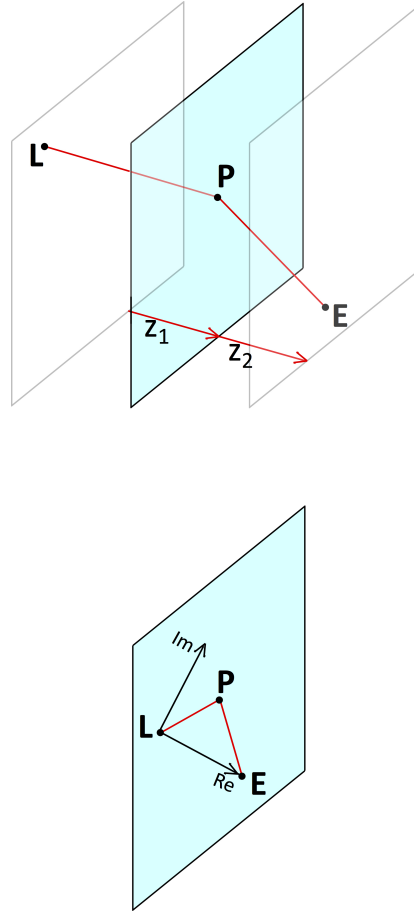


FIGURE 3.6: Top: an incident light ray emitted from  $\mathbf{L}$  intersects the interface at position  $\mathbf{P}$  before being refracted towards an observer at position  $\mathbf{E}$ . Bottom: projecting the points  $\mathbf{L}$ ,  $\mathbf{P}$  and  $\mathbf{E}$  into the plane of the sheet and constructing a complex coordinate system enables the point  $\mathbf{P}$  to be written in terms of basis vectors which are functions of the components of  $\mathbf{L}$  and  $\mathbf{E}$ . The outgoing light-ray direction can then be calculated as the normalised vector between  $\mathbf{P}$  and  $\mathbf{E}$ , and as such, must also be a function of the source position  $\mathbf{L}$ .

or more explicitly,

$$\mathbf{P}_{real} = \begin{pmatrix} L_x \\ L_y \\ 0 \end{pmatrix} + \frac{z_2(z_2 - z_1 \cos \alpha)}{z_2^2 + z_1^2 - 2z_2z_1 \cos \alpha} \mathbf{b}_1 + \frac{z_2z_1 \sin \alpha}{z_2^2 + z_1^2 - 2z_2z_1 \cos \alpha} \mathbf{b}_2. \quad (3.45)$$

The outgoing light-ray direction vector is then given by

$$\mathbf{d} = \frac{\mathbf{E} - \mathbf{P}_{real}}{\sqrt{(\mathbf{E} - \mathbf{P}_{real}) \cdot (\mathbf{E} - \mathbf{P}_{real})}}. \quad (3.46)$$

Clearly the light-ray direction changes depending on the position of the observer. By letting  $(E_x, E_y, z_2) = (x, y, z)$  the curl of the light-ray field can be calculated. The curl of the light-ray direction vector is too long to reproduce here, however it shows that the curl is always non-zero for angles other than 0 or  $\pi$ . In the following sections we will show ray-tracing simulations and experimental observations which corroborate this.

### 3.5 Wave-optically forbidden parallax

We have thus far described laws of refraction which produce light-ray fields with non-zero curl. This description has been purely mathematical and it is prudent to ask, *how do these light-ray fields actually behave when we observe them?* We will show that light-ray fields with non-zero curl exhibit a different type of parallax to conventional fields. Parallax is commonly observed when looking at distant objects whilst moving. Using a coordinate system centred on the observer's position, objects close to the observer will appear to change positions more quickly than objects further away. This is obvious when driving in the country side and one can see that the distant hills barely move, while the nearby hedges flash past. This holds true for light-ray fields with non-zero curl. However something else happens as well. Recall that light-ray fields with non-zero curl do not satisfy Eq.(3.13). That is to say

$$\frac{\partial d_y}{\partial x} - \frac{\partial d_x}{\partial y} = \delta \neq 0. \quad (3.47)$$

If we can measure the change in the  $y$ -component of the light-ray direction vector with respect to  $x$  and the  $x$ -component of the light-ray direction vector with respect to  $y$ , then we can calculate  $\delta$ . In general, both derivatives will be non-zero, and so we can see that if that is the case, that moving horizontally or vertically will cause the image produced by the interface to move vertically or horizontally. We show this in ray-tracing simulations in Fig.(3.7) and Fig.(3.8).

### 3.6 Experimental confirmation

We show now how forbidden light-ray fields produced by a ray-rotation sheet behave when an observer changes position and compare this with a light-ray field which

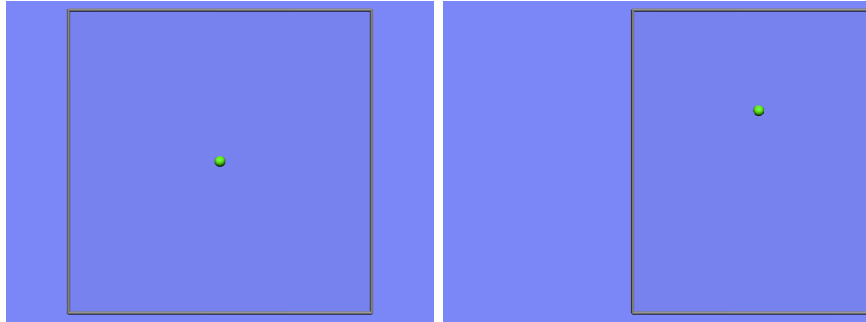


FIGURE 3.7: As the observer moves to the left, i.e. the negative  $x$  direction, the green sphere appears to move in the positive  $y$ -direction. This means that  $\partial d_y / \partial x > 0$ .

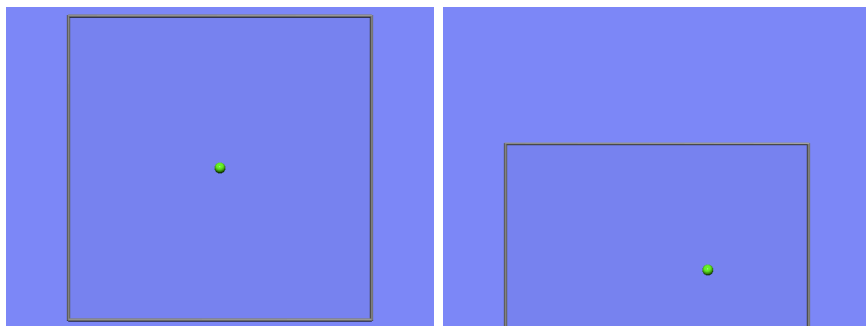


FIGURE 3.8: As the observer moves up, i.e. the positive  $y$  direction, the green sphere appears to move in the positive  $x$ -direction. This means that  $\partial d_x / \partial y < 0$ .

is not forbidden. In the experimental set-up used, a Rubik's cube was positioned 100mm behind a  $\pi/2$  ray-rotation sheet, while the observing camera was positioned 100mm in front. This set up is shown in Fig. 3.9. The camera was then moved in 5mm increments either vertically or horizontally and the image recorded for each increment.

### 3.6.1 Forbidden light-ray fields produced by ray-rotation

On measuring the change in light-ray direction for both the horizontal shifts and vertical shifts it was found that the rate of change of the  $y$ -component of the light-ray vector with respect to the  $x$ -axis and the rate of change of the  $x$ -component of the light-ray vector with respect to the  $y$ -axis were respectively

$$\frac{\partial d_y}{\partial x} = -4.4 \times 10^{-3} \quad (3.48)$$

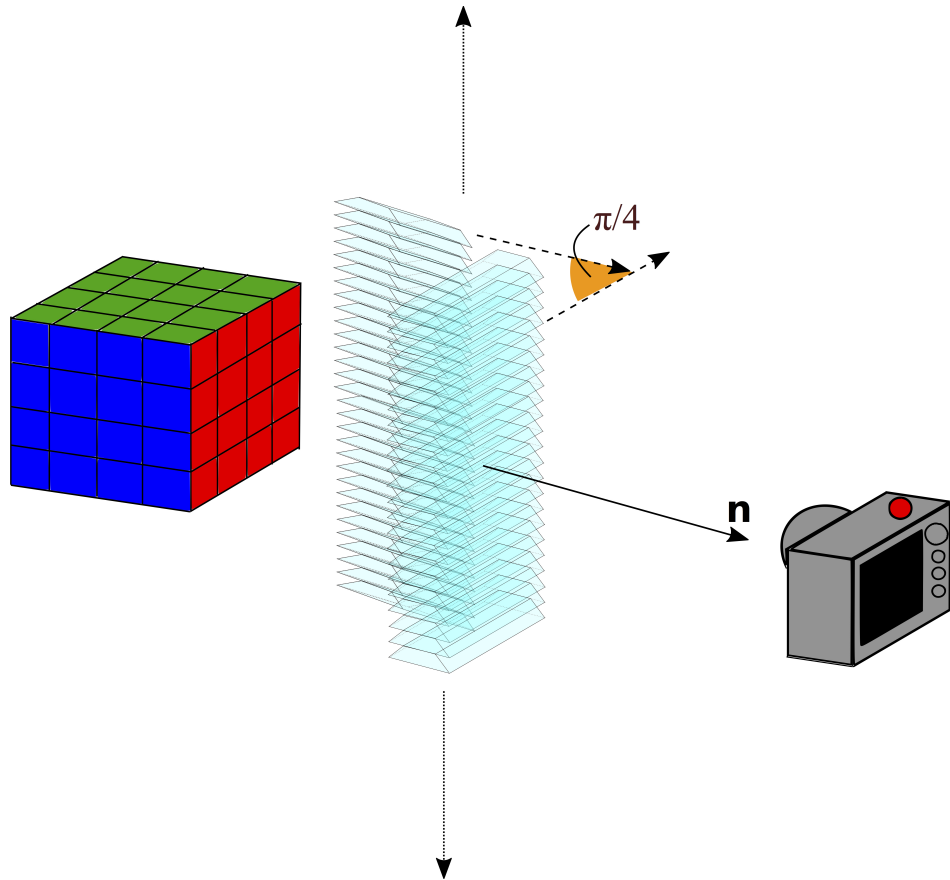


FIGURE 3.9: A schematic of the experimental set up to study the parallax of a forbidden light-ray field. A rubiks cube is placed behind a ray rotation sheet which is comprised of two dove prism arrays rotated relative to one another by an angle of  $\pi/4$ . This causes outgoing light-rays to be rotated by an angle twice this,  $\pi/2$  around the surface normal to the ray rotation sheet,  $\mathbf{n}$ . The camera is then moved either horizontally or vertically to observe the effect this has on the image, and therefore the outgoing light-ray field.

$$\frac{\partial d_x}{\partial y} = 4.5 \times 10^{-3}. \quad (3.49)$$

Hence the  $z$ -component of the curl of the light-ray vector is

$$\frac{\partial d_y}{\partial x} - \frac{\partial d_x}{\partial y} = -4.4 \times 10^{-3} - 4.5 \times 10^{-3} = -8.9 \times 10^{-3}, \quad (3.50)$$

which is clearly non-zero. We see in Fig.3.10 that the results of Eq.(3.48) and Eq.(3.49) do indeed manifest themselves in the unusual parallax predicted in Figures 3.7 and 3.8.

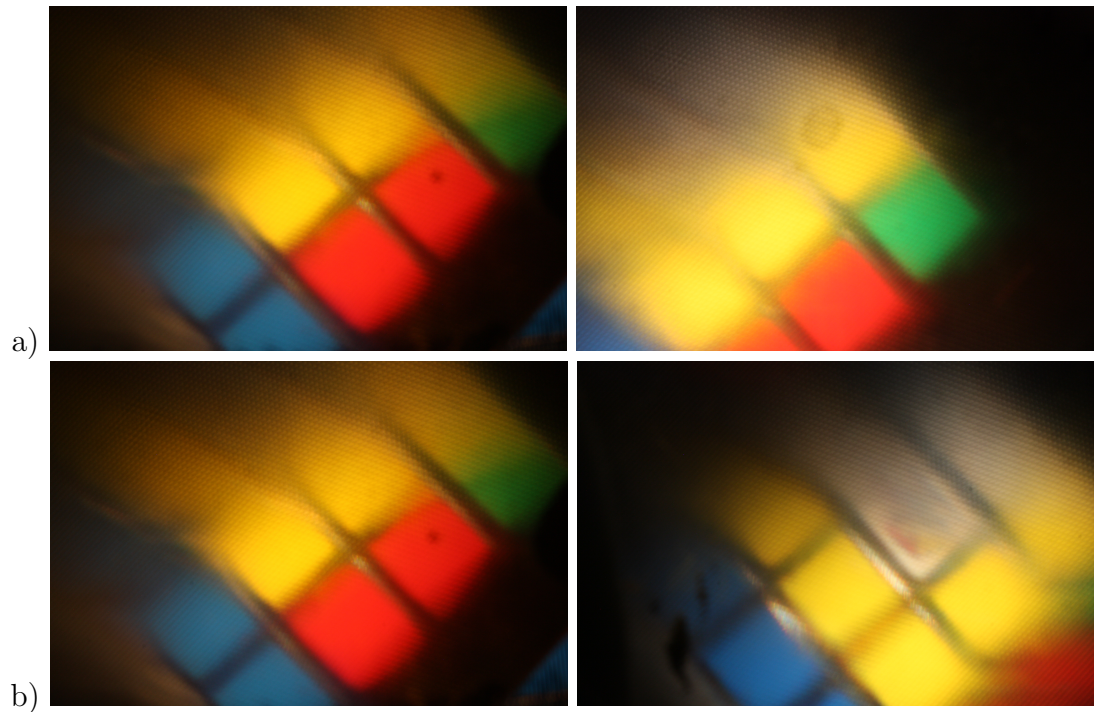


FIGURE 3.10: Experimental confirmation of the effect of wave-optical illegality for a  $\pi/2$  ray-rotation sheet. a) As the observer moves vertically by 25mm in the  $y$ -axis, the Rubik's cube, as seen through the sheet, moves in the negative direction of the  $x$ -axis. b) As the observer moves horizontally by -25mm in the  $x$ -axis, the Rubik's cube, as seen through the sheet, moves in the negative direction of the  $y$ -axis.

### 3.7 Conclusion

We have theoretically described how the curl of a light-ray field is related to the curl of its underlying phase gradient and have stated that in order for a field to be described properly by wave optics, the curl of the light-ray vector has to be zero. We then introduced generalised confocal lenslet arrays and ray-rotation sheets and showed that they refract light in such a way that the outgoing light-ray field has, in general, non-zero curl. We then proceeded to show how a light-ray field with non-zero curl behaves when an observer changes position by providing ray-tracing simulations and experimental images. In the following chapters we will see that the ability to create light-ray fields with non-zero curl offers the potential to design and create exotic optical devices which otherwise would not be possible.

# Chapter 4

## Integral imaging using planar and curved interfaces

### 4.1 Introduction

One of the most important concepts to emerge from optics is that of imaging. Indeed, the whole purpose of many – possibly most – useful optical systems is to transfer information or power from one point to another in a predictable way. Imaging finds uses in a vast array of different areas, from the Hubble telescope taking photographs of distant galaxies and microscopes zooming in on bacteria, to imaging using entangled photons [19] and of course transformation optics [20, 21]. All of the afore-mentioned applications (with the exception of standard transformation optics) involve designing optical systems involving lenses, mirrors, beams splitters and other optical devices. The ability to reconfigure an imaging system is an advantage when a system is required to operate in a number of ways. However, as a consequence, such systems are typically complicated and in many cases require frequent realignment and calibration to operate effectively. If an imaging system is only to be used in one configuration, then it makes sense to reduce the number of internal components to a minimum and use the simplest components possible to reduce the need for recalibration. The most simple type of imaging device which does not require any significant calibration effort is the lens. The lens has no movable parts and so only its position and direction have to be monitored. However, despite their usefulness, lenses are rather limited in terms of imaging. If new passive optical components can be designed which image and require no more calibration effort than a lens, this could open the way to more

efficient designs for larger, more complicated systems.

Some effort has already been made with regards to this goal. In 1940 Gabor produced a paper outlining a new device, called a superlens, which consisted of two confocally arranged lenslet arrays where the lenslet arrays were of different pitch [22, 23]. The result was a device which exhibited unusual lens-like behaviour in that it behaved like a lens with different object- and image-sided focal lengths. However this is only an illusion as the superlens is not a true lens; it does not perform conventional imaging. It performs integral imaging and as such parallel rays do not converge to a single position after passing through a superlens, but instead parallel ray bundles entering the superlens at different positions will all meet at a common region where their axes intersect. Previous work investigating imaging with planar interfaces was able to show that the most general type of interface capable of imaging all of space corresponded to an infinitesimally thin lens with different object and image sided focal length [24]. Of course, infinitesimally thin lenses do not exist. The imaging equations derived in [24] are for an idealised system which maps each point in object space to a corresponding point in image space, subject to certain assumptions such as there is no offset between the ingoing and outgoing light rays. In practice, however, these conditions are impossible to meet, but a close approximation can be found with the Gabor superlens. We will show now that it is possible to perform perfect imaging (within the limit of ray-optics) using planar interfaces. We will then show that idealised gCLAs exhibiting homogeneous refraction are examples of such interfaces. Finally, we will discuss whether it is possible to perform perfect imaging with curved interfaces.

### 4.1.1 Contributions

The work in this chapter was carried out as part of a collaboration. Specifically the derivation of the gCLA imaging equation in section 4.2 was undertaken by myself and Johannes Courtial. The discussion on perfect imaging using curved interfaces in section 4.3 is a result of collaboration between myself and Johannes Courtial with Tomáš Tyc.

## 4.2 Derivation of the homogeneous imaging equation for a planar interface

In reference [24] the concept of imaging across an interface was explored. One of the assumptions made for studying such a system was that the interface would not offset light-rays along the interface after refraction. This in turn demands that the interface is infinitesimally thin. The medium before and after the interface was also assumed to be homogeneous so that light rays would travel along straight lines. Through geometrical arguments based on the observation that multiple light rays each passing through the same two object positions must be refracted in the same way, and that therefor if the sheet images, the corresponding image points must therefore lie on the refracted trajectory, it was shown that a thin interface can indeed perform geometrical imaging. Further to this, it was noted that the imaging equation which was derived corresponded to the imaging performed by a thin lens with different object and image sided focal lengths. This in turn, it was argued, could be approximately realised by coupling a conventional lens to a confocal lenslet array which would scale the image sided focal length of the lens.

The imaging provided by such an interface is shown in Fig. 4.1. If the sheet is placed in the  $z = 0$  plane and its optic axis is the  $z$ -axis, the imaging is described by the equations

$$\begin{aligned}x' &= \frac{fx}{f+z}, \\y' &= \frac{fy}{f+z}, \\z' &= \frac{gz}{f+z},\end{aligned}\tag{4.1}$$

where  $f$  is the image-sided focal length and  $g = \eta f$  is the object-sided focal length. We see that the object positions  $\mathbf{P} = (x, y, z)$  are imaged to the image positions  $\mathbf{P}' = (x', y', z')$  in such a way that positions at different distances from the interface get imaged differently. This is due to the fact that when parallel light rays pass through a lens, they are redirected along different directions such that they intersect at the focal point. In the case of our sheet, this also happens, only the length of the focal length after the lens is scaled by a fact of  $\eta$ .

Evidently in the limit for which the image sided focal length  $f$  goes to infinity, the outgoing rays will essentially remain parallel, hence it must be true that a thin sheet which performs homogeneous imaging, must be a special case of the earlier result

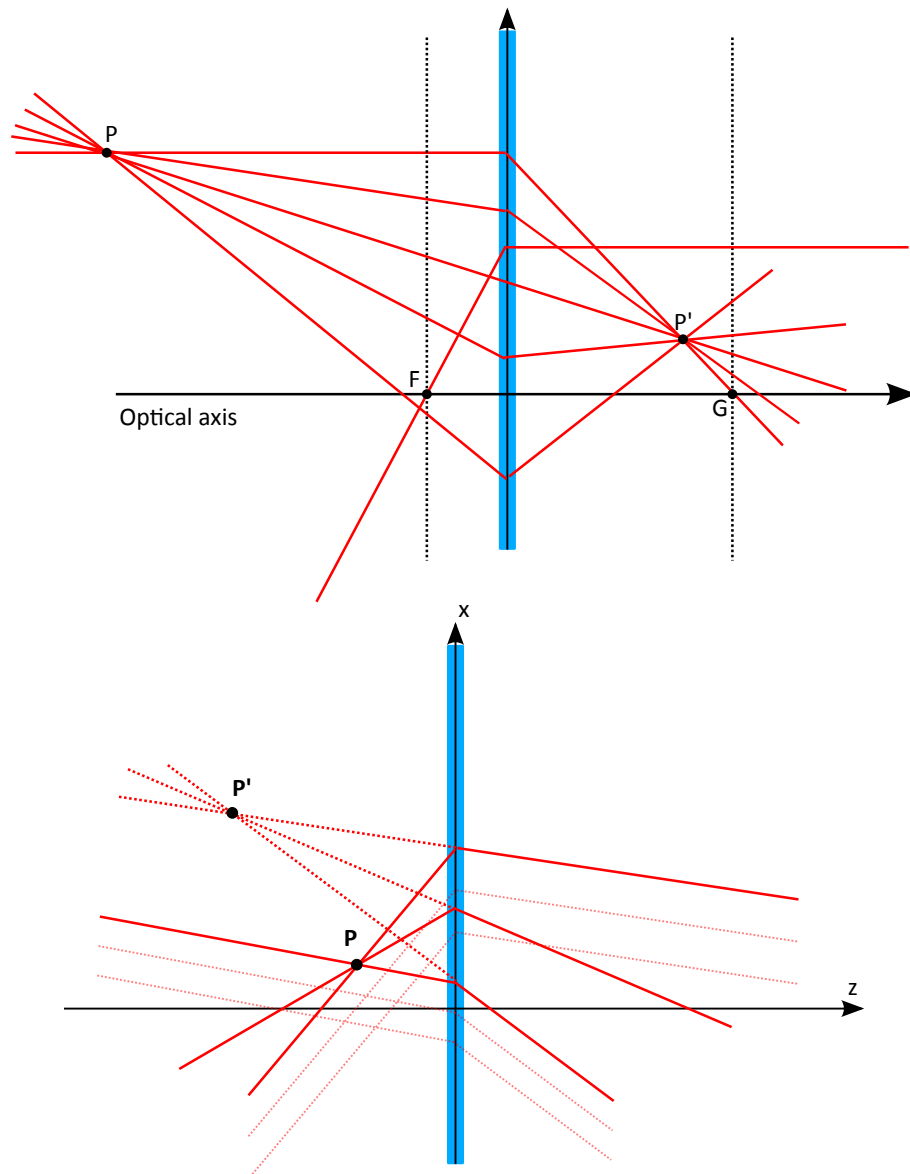


FIGURE 4.1: Upper image: the effect that a generalised imaging interface has on light rays. This type of interface can be thought of as a lens with different object- and image-sided focal lengths. As can be seen, a ray at normal incidence to the interface coming in from the object side will be refracted and intersect the image sided focal point  $G$ , while a ray coming in parallel from the image side will be refracted such that it intersects the object sided focal point  $F$ . Lower image: the effect that a homogeneous generalised confocal lenslet array has on light rays. As can be seen, parallel light rays no longer intersect on focal planes, but instead are redirected and continue to remain parallel.

presented above, namely where the focal length of the thin lens,  $f$ , goes to infinity. We now wish to derive the imaging equation for such a special case. Starting with our inhomogeneous system, consider the point  $\mathbf{R}$  on the sheet (which itself lies in the  $z = 0$  plane). Any point in object or image space can be written as a function of  $\mathbf{R}$ , for example

$$\begin{aligned}x &= R_x + \bar{x}, \\y &= R_y + \bar{y}, \\z &= \bar{z},\end{aligned}\tag{4.2}$$

$$\begin{aligned}x' &= R_x + \bar{x}', \\y' &= R_y + \bar{y}', \\z' &= \bar{z}',\end{aligned}\tag{4.3}$$

where non-primes denote object space and primes denote image space. In this form, the imaging equations become

$$\begin{aligned}R_x + \bar{x}' &= \frac{f(R_x + \bar{x})}{f + \bar{z}}, \\R_y + \bar{y}' &= \frac{f(R_y + \bar{y})}{f + \bar{z}}, \\ \bar{z}' &= \frac{g\bar{z}}{\bar{z} + f}.\end{aligned}\tag{4.4}$$

If we then rearrange for  $\bar{x}'$ ,  $\bar{y}'$  and  $\bar{z}'$  and then define the parameters  $g = \eta f$ ,  $t_x = R_x/f$  and  $t_y = R_y/f$  we get for the first two components

$$\begin{aligned}\bar{x}' &= \frac{f(ft_x + \bar{x})}{f + \bar{z}} - ft_x = \frac{f}{f + \bar{z}}(\bar{x} - \bar{z}t_x), \\ \bar{y}' &= \frac{f(ft_y + \bar{y})}{f + \bar{z}} - ft_y = \frac{f}{f + \bar{z}}(\bar{y} - \bar{z}t_y).\end{aligned}\tag{4.5}$$

In the limit where  $f \rightarrow \infty$  the equations become

$$\begin{aligned}\bar{x}' &= \bar{x} - \bar{z}t_x, \\ \bar{y}' &= \bar{y} - \bar{z}t_y, \\ \bar{z}' &= \eta\bar{z},\end{aligned}\tag{4.6}$$

which on dropping the bars from the components can be written in vector form as

$$\mathbf{P}' = \mathbf{P} - z \begin{pmatrix} t_x \\ t_y \\ 1 - \eta \end{pmatrix}. \quad (4.7)$$

This equation clearly describes the most general mapping between object space and image space for a homogeneous interface that does not offset rays. We are now in a position to show that this is the imaging performed by idealised homogeneous generalised confocal lenslet arrays (gCLAs).

### 4.2.1 Homogeneous generalised confocal lenslet arrays as integrally imaging interfaces

Recall the unnormalised law of refraction for gCLAs (lying in the  $z = 0$  plane) where  $\eta_x = \eta_y = \eta$  [25],

$$\mathbf{d}' = \frac{d_x - d_z \delta_x}{\eta} \hat{\mathbf{x}} + \frac{d_y - d_z \delta_y}{\eta} \hat{\mathbf{y}} + d_z \hat{\mathbf{z}}. \quad (4.8)$$

The vectors  $\mathbf{d} = (d_x, d_y, d_z)$  and  $\mathbf{d}'$  are defined such that they point in the direction that the light rays travel, however they are not normalised. Now consider our perfectly imaging homogeneous sheet where a light ray passes through  $\mathbf{P}$ , intersects the sheet at  $\mathbf{S}$ , is redirected and passes through  $\mathbf{P}'$ . We can define the ingoing light-ray vector  $\mathbf{d}$  and outgoing vector  $\mathbf{d}'$  in terms of our object and image point,  $\mathbf{P}$  and  $\mathbf{P}'$ , and a point on the sheet  $\mathbf{S} = (S_x, S_y, 0)$  as

$$\begin{aligned} \mathbf{d} &= \mathbf{S} - \mathbf{P}, \\ \mathbf{d}' &= \mathbf{P}' - \mathbf{S} = \mathbf{P}' - (\mathbf{d} + \mathbf{P}). \end{aligned} \quad (4.9)$$

Substituting for  $\mathbf{P}$  and  $\mathbf{P}'$  makes the components of the latter

$$\begin{aligned} d'_x &= d_z t_x - d_x, \\ d'_y &= d_z t_y - d_y, \\ d'_z &= -\eta d_z. \end{aligned} \quad (4.10)$$

Dividing through by  $(-\eta)$  gives

$$\begin{aligned} d'_x &\propto \frac{d_x - d_z t_x}{\eta}, \\ d'_y &\propto \frac{d_y - d_z t_y}{\eta}, \\ d'_z &\propto d_z \end{aligned} \tag{4.11}$$

which we see is the exact same form as the law of refraction for gCLAs. Hence if  $t_x = \delta_x$  and  $t_y = \delta_y$ , the imaging equation for homogeneous gCLAs is

$$\mathbf{P}' = \mathbf{P} - z \begin{pmatrix} \delta_x \\ \delta_y \\ 1 - \eta \end{pmatrix}. \tag{4.12}$$

Note that this expression only applies to gCLAs where  $\eta_x = \eta_y = \eta$ ; in the case where  $\eta_x \neq \eta_y$ , gCLAs are non-imaging. So we have shown that idealised gCLAs where  $\eta_x = \eta_y = \eta$  are the only sheets which can perform perfect imaging albeit only in integral form. In practice gCLAs will not perform exactly the perfect imaging we have described. Recall that we used the imaging equations from [24] as our starting point in our derivation. But these equations themselves assume that the interface does not offset light rays as they cross the interface. This is not the case with gCLAs and so in reality gCLAs will perform at best integral imaging.

### 4.3 Perfect imaging with curved interfaces

At the start of this chapter we stated that it was possible to perform perfect imaging with inhomogeneous planar interfaces. We then proceeded to show that it was also possible to perform perfect imaging using homogeneous planar interfaces. We now wish to see if it is possible to perform perfect imaging using curved interfaces. In what follows we will employ the same geometrical arguments as presented in [24].

Consider a curved surface denoted by  $\sigma$ . Initially we shall assume that  $\sigma$  is imaging, that is if we choose some point  $A$  in an open region  $R$  in object space, then any straight line passing through  $A$  which intersects  $\sigma$  will then pass through a corresponding point  $A'$  in image space. If we had chosen points in a closed region, this would mean we would only be concerning ourselves with a subregion of object space, perhaps isolated points or points on a line. Note that in what follows we are only

considering straight lines which intersect the interface once. Now consider three non-collinear points  $A$ ,  $B$  and  $C$  which lie in the region  $R$ . If the points are such that the straight lines  $AB$ ,  $AC$  and  $BC$  intersect  $\sigma$  at the points  $P_{AB}$ ,  $P_{AC}$  and  $P_{BC}$  respectively, then the points  $A$ ,  $B$ ,  $C$ ,  $P_{AB}$ ,  $P_{AC}$  and  $P_{BC}$  must all lie in a common plane. The intersection points of the image-pair lines  $A'B'$ ,  $A'C'$  and  $B'C'$  with  $\sigma$ , are also  $P_{AB}$ ,  $P_{AC}$  and  $P_{BC}$  respectively, as the rays leave  $\sigma$  from the same points at which they intersect it. Hence  $A'$ ,  $B'$ ,  $C'$ ,  $P_{AB}$ ,  $P_{AC}$  and  $P_{BC}$  also lie in a common plane. Indeed the plane in which  $A$ ,  $B$ ,  $C$  lie and the plane in which  $A'$ ,  $B'$ ,  $C'$  lie, are one and the same. As can be seen in Fig. 4.2, this is because the points  $P_{AB}$ ,  $P_{AC}$  and  $P_{BC}$  are noncollinear. If they were collinear, they would lie on a straight line, and the plane in which the object points and the plane in which the image points lie would intersect along this line and would be free to be at non-zero angles to one another like in the case of a planar surface. However because they are noncollinear, and because we have stipulated that rays may only intersect the interface once, the planes must coincide.

Now consider a third point  $D$  which lies in  $R$ , but not in the plane in which  $A$ ,  $B$  and  $C$  do, and assume that the lines which pass through all pairs of the points  $A$ ,  $B$ ,  $C$  and  $D$  intersect  $\sigma$  (namely at the points  $P_{AB}$ ,  $P_{AC}$ ,  $P_{BC}$ ,  $P_{AD}$ ,  $P_{CD}$  and  $P_{BD}$ ). By appropriately choosing  $A$ ,  $B$ ,  $C$  and  $D$ , any set of triple intersection points on  $\sigma$  can all be noncollinear. Hence we can repeat the argument above, in which we said that  $A$ ,  $B$ ,  $C$  and  $A'$ ,  $B'$ ,  $C'$  lie in the same plane, for each triple combination of points containing  $D$ :  $[A, B, D]$ ,  $[A, C, D]$  and  $[B, C, D]$ . Hence we can say that the points  $[A', B', D']$  lie in the same plane as the points  $[A, B, D]$ , the points  $[A', C', D']$  lie in the same plane as the points  $[A, C, D]$  and the points  $[B', C', D']$  lie in the same plane as the points  $[B, C, D]$ . It is clear that the three planes corresponding to the triple of points  $[A, B, D]$ ,  $[A, C, D]$  and  $[B, C, D]$  must intersect at the point  $D$ , while the three planes corresponding to the triple of points  $[A', B', D']$ ,  $[A', C', D']$  and  $[B', C', D']$  must intersect at the point  $D'$ . However as the two sets of three planes are identical, they must intersect at the same position and therefore it must be that  $D' = D$ . This then shows that for a curved interface, where light rays only intersect once, the interface can only perform trivial imaging of a point back into itself. This then means that such a curved interface either has no effect on light rays, or else retroreflects them back along their original trajectory.

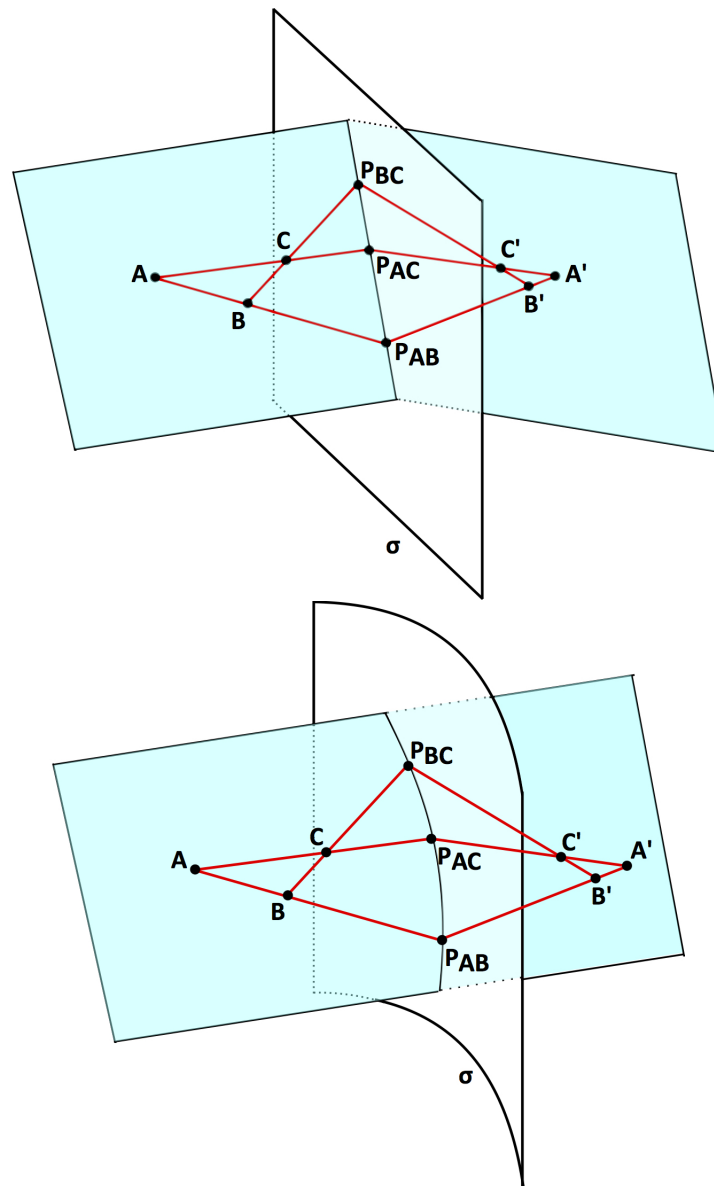


FIGURE 4.2: Upper image: a flat interface images such that the planes containing the object points and image points intersect. The object plane and the image plane need not lie in the same plane. Lower image: a curved interface images such that the planes containing the object and image points lie in the same plane. This is due to the fact that the points where the light rays intersect the sheet are noncolinear, and we only consider rays which intersect the interface once.

## 4.4 Conclusion

We have shown that idealised homogeneous gCLAs can perform imaging, but that in practice, this imaging will not be stigmatic, but integral. We also showed that curved interfaces can only perform the most trivial type of imaging, that of mapping a point back onto itself. In the next chapter we will show how gCLAs, both imaging and non-imaging, can be used to effect metric tensor interfaces, albeit in pixellated form. Such an exploration leads naturally to the question of whether gCLAs can be used to perform pixellated piecewise transformation optics and we will show in the chapters to come that imaging gCLAs can in fact be used to create such devices.

# Chapter 5

## Metarefracting sheets as metric interfaces

### 5.1 Introduction

In chapter two, the concept of transformation optics (TO) was introduced. Recall that transformation optics utilises coordinate transformations to create optical spaces with non-Euclidean metrics. This opens up the possibility of designing devices capable of redirecting light rays in unconventional ways. However in practice it is often the case that in order to create transformation-optics devices one has to use materials which have anisotropic and inhomogeneous optical properties. As a consequence of this metamaterials such as those described in chapter two have to be designed and fabricated. Metamaterials for TO devices are difficult to design and manufacture for the visible spectrum because the components of which they are comprised are spatially varying, and must be smaller than the wavelength of the light the device is to manipulate. As such they are also significantly expensive at the present moment. Hence if we could find some other way of achieving transformation optics that avoided at least some of these drawbacks this would be a useful step forward.

Transformation optics involves creating a spatially varying metric tensor, which, in essence, can be interpreted as defining an effective local refractive index which may or may not be homogeneous and (or) isotropic [20, 21]. Hence in transformation optics the metric tensor defines a non-Euclidean optical space and allows us to measure the

distance in that optical space, i.e. the metric can be used to calculate the optical path length. For example, as we stated in chapter two, in a conventional dielectric material of index  $n$  the squared optical path length is  $ds^2 = n^2 dx^2 + n^2 dy^2 + n^2 dz^2$ .

According to Fermat's principle, light rays travel along paths for which the optical path length is stationary [26]. If the metric used to calculate the optical path length is spatially varying, light rays will, in general, change direction when the metric changes along their trajectory. This result, whilst based on a continuous metric, is also applicable to systems where discrete changes in the metric occur. By this reasoning light should refract when it passes through a plane with different metrics on either side. Indeed this does happen when light passes from air into glass. We aim to show that refraction across a metric interface can be approximately realised by a subset of generalised confocal lenslet arrays (gCLAs), but that while a true metric tensor interfaces behave like an absolute optical instruments, gCLAs do not.

### 5.1.1 Contributions

The work carried out in this chapter stems from a collaboration between Johannes Courtial, Chris White, Georgios Antoniou and Myself.

## 5.2 Fermat's principle at the interface between different Riemannian spaces

In three-dimensional Euclidean space, the squared length of the line element in cartesian coordinates is given by

$$ds^2 = dx^2 + dy^2 + dz^2. \quad (5.1)$$

This is simply Pythagoras' theorem. In three-dimensional Riemannian spaces this definition generalises to include mixed terms and the line element becomes

$$ds^2 = g_{11}dx^2 + g_{22}dy^2 + g_{33}dz^2 + 2g_{12}dxdy + 2g_{13}dxdz + 2g_{23}dydz, \quad (5.2)$$

where the numbers  $g_{ij}$  are the elements of the (symmetric) metric tensor,  $g$ . In a Euclidean space the metric is given by the Kronecker delta,  $g_{ij} = \delta_{ij}$ , for all allowed values of  $i$  and  $j$  (i.e. 1 to  $n$  for  $n$ -dimensional spaces). A Riemannian space where this is not the case is therefore non-Euclidean.

Recall from chapter two that we stated that Fermat's principle dictates that light rays will follow trajectories for which the optical path length is stationary. In what follows we will examine Fermat's principle for a light-ray crossing a metric interface. We proceed by constructing a coordinate system where the interface is in the  $z = 0$  plane as seen in Fig. 5.1. The space before the interface (i.e. when  $z < 0$ ) is characterised by the metric tensor  $g$  and the space after the interface (when  $z > 0$ ) is characterised by the metric tensor  $h$ . Our ingoing light-ray direction (which originates in the region  $z < 0$ ) is described by the unnormalised vector  $\mathbf{d} = (d_x, d_y, 1)$ . The outgoing light-ray

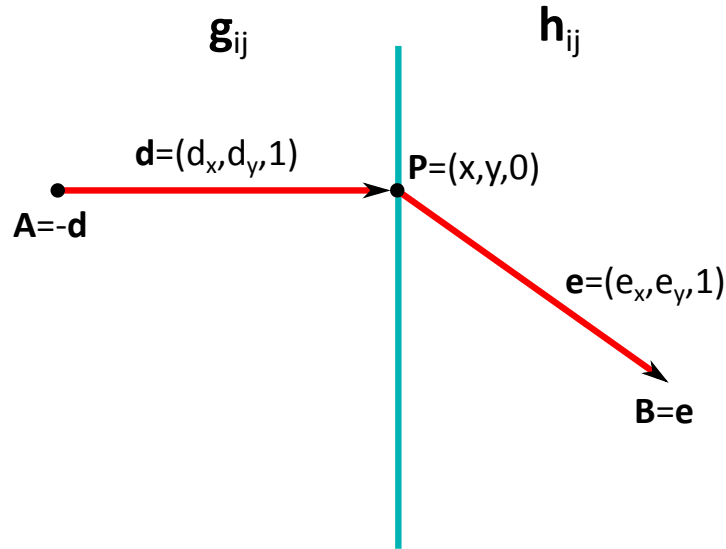


FIGURE 5.1: Construction for applying Fermat's principle to a metric interface. An interface is positioned in the  $z = 0$  plane with a metric  $g$  in the region  $z < 0$  and a metric  $h$  in the region  $z > 0$ . The ingoing and outgoing light-ray directions,  $\mathbf{d}$  and  $\mathbf{e}$ , are constructed such that their  $z$  components are equal to unity. The points  $\mathbf{A}$  and  $\mathbf{B}$ , which lie on the light ray before and after the interface respectively, can therefore be written such that  $\mathbf{A} = -\mathbf{d}$  and  $\mathbf{B} = \mathbf{e}$ .

is given by  $\mathbf{e} = (e_x, e_y, 1)$ . We now pick points on the ingoing and outgoing light ray so that we can calculate the optical path length. For simplicity we choose a point  $\mathbf{A} = -\mathbf{d}$  before the interface and a point  $\mathbf{B} = \mathbf{e}$  after the interface. If the ray intersects the interface at the point  $\mathbf{P} = (x, y, 0)$ , then the optical path length is the

sum of the optical path lengths from  $\mathbf{A}$  to  $\mathbf{P}$ , and from  $\mathbf{P}$  to  $\mathbf{B}$ :

$$\begin{aligned} O &= O_{AP} + O_{PB} \\ &= \sqrt{(\mathbf{d} + \mathbf{P})^T g(\mathbf{d} + \mathbf{P})} + \sqrt{(\mathbf{e} - \mathbf{P})^T h(\mathbf{e} - \mathbf{P})}. \end{aligned} \quad (5.3)$$

If Fermat's principle is to be obeyed, the total optical path length has to be stationary, i.e. its derivatives w.r.t.  $x$  and  $y$  must equal zero. Hence we have

$$\begin{aligned} \frac{\partial \sqrt{(\mathbf{d} + \mathbf{P})^T g(\mathbf{d} + \mathbf{P})}}{\partial x} &= \frac{\partial \sqrt{(\mathbf{e} - \mathbf{P})^T h(\mathbf{e} - \mathbf{P})}}{\partial x}, \\ \frac{\partial \sqrt{(\mathbf{d} + \mathbf{P})^T g(\mathbf{d} + \mathbf{P})}}{\partial y} &= \frac{\partial \sqrt{(\mathbf{e} - \mathbf{P})^T h(\mathbf{e} - \mathbf{P})}}{\partial y}. \end{aligned} \quad (5.4)$$

The terms inside the square roots of either side of Eqs(5.4) are of the same form; they can be re-written using index notation and the Einstein summation convention as follows:

$$(\mathbf{c} \pm \mathbf{P})^T f(\mathbf{c} \pm \mathbf{P}) = (c_k \pm x_k) f_{jk} (c_j \pm x_j). \quad (5.5)$$

If the  $+$  sign is chosen then  $\mathbf{c} = \mathbf{d}$  and  $f = g$ , whilst if the  $-$  sign is chosen,  $\mathbf{c} = \mathbf{e}$  and  $f = h$ . Using this notation, the derivatives with respect to  $x_i$  then become

$$\begin{aligned} \frac{\partial \sqrt{(\mathbf{c} \pm \mathbf{P})^T f(\mathbf{c} \pm \mathbf{P})}}{\partial x_i} &= a \frac{\partial}{\partial x_i} [(c_k \pm x_k) f_{jk} (c_j \pm x_j)] \\ &= a \frac{\partial}{\partial x_i} [c_k f_{jk} c_j \pm c_k f_{jk} x_j \pm x_k f_{jk} c_j + x_k f_{jk} x_j] \\ &= a [\pm c_k f_{jk} \delta_{ij} \pm \delta_{ik} f_{jk} c_j + \delta_{ik} f_{jk} x_j + x_k f_{jk} \delta_{ij}], \end{aligned} \quad (5.6)$$

where

$$a = \frac{1}{2\sqrt{(\mathbf{c} \pm \mathbf{P})^T f(\mathbf{c} \pm \mathbf{P})}}. \quad (5.7)$$

With our choice of  $\mathbf{A}$  and  $\mathbf{B}$ , the light ray passes through the interface at  $\mathbf{P} = (0, 0, 0)$ . We now choose the point where the light-ray strikes the interface. For convenience we shall set  $\mathbf{P} = (0, 0, 0)$ . At this point Eq.(5.6) becomes

$$\left. \frac{\partial \sqrt{(\mathbf{c} \pm \mathbf{P})^T f(\mathbf{c} \pm \mathbf{P})}}{\partial x_i} \right|_{\mathbf{P}=0} = \pm \frac{c_k f_{jk} \delta_{ij} + \delta_{ik} f_{jk} c_j}{2\sqrt{\mathbf{c}^T f \mathbf{c}}} \quad (5.8)$$

$$= \pm \frac{f_{ik} c_k}{\sqrt{\mathbf{c}^T f \mathbf{c}}}, \quad (5.9)$$

where, in the last line, we have used the fact that  $f$  is symmetric, i.e.  $f_{ij} = f_{ji}$  and then re-named the dummy index  $j$  to  $k$  in the second term. Written in vector notation this then becomes a much simpler expression:

$$\left. \frac{\partial \sqrt{(\mathbf{c} \pm \mathbf{P})^T f (\mathbf{c} \pm \mathbf{P})}}{\partial x_i} \right|_{\mathbf{P}=0} = \pm \frac{(f\mathbf{c})_i}{\sqrt{\mathbf{c}^T f \mathbf{c}}}. \quad (5.10)$$

Re-writing this once again in terms of the ingoing and outgoing light-ray direction and substituting into Eq.(5.4) gives

$$\frac{(g\mathbf{d})_i}{\sqrt{\mathbf{d}^T g \mathbf{d}}} = \mp \frac{(h\mathbf{e})_i}{\sqrt{\mathbf{e}^T h \mathbf{e}}}, \quad (5.11)$$

where clearly  $i = 1, 2$  (as these equations are equivalent to the derivatives of the optical path length w.r.t.  $x$  and  $y$ ). Projecting both sides into the  $z = 0$  plane such that Eq.(5.11) becomes satisfied for  $i = 3$  gives the following equation:

$$\frac{g\mathbf{d} - (g\mathbf{d} \cdot \hat{\mathbf{n}})\hat{\mathbf{n}}}{\sqrt{\mathbf{d}^T g \mathbf{d}}} = \mp \frac{h\mathbf{e} - (h\mathbf{e} \cdot \hat{\mathbf{n}})\hat{\mathbf{n}}}{\sqrt{\mathbf{e}^T h \mathbf{e}}}, \quad (5.12)$$

where  $\hat{\mathbf{n}}$  is the normalised surface normal. This then is the expression which must be satisfied if Fermat's principle is to hold across a flat metric interface. We will come back to this equation shortly, first however we revisit the gCLA law of refraction.

### 5.3 Generalised confocal lenslet arrays as metric interfaces

Recall that the gCLA law of refraction [25] for a gCLA situated in the  $z = 0$  plane with optical axes perpendicular to the sheet is given by

$$e_x = \frac{d_x - \delta_x}{\eta_x}, \quad e_y = \frac{d_y - \delta_y}{\eta_y}, \quad e_z = 1, \quad (5.13)$$

where we choose an incident light-ray vector such that  $d_z = 1$ . For our purposes, these equations are best written in the following vector form

$$\mathbf{e} = \mathbf{M} \cdot \mathbf{d}, \quad (5.14)$$

where

$$\mathbf{M} = \begin{pmatrix} 1/\eta_x & 0 & -\delta_x/\eta_x \\ 0 & 1/\eta_y & -\delta_y/\eta_y \\ 0 & 0 & 1 \end{pmatrix}, \quad (5.15)$$

and

$$\mathbf{M}^{-1} = \begin{pmatrix} \eta_x & 0 & \delta_x \\ 0 & \eta_y & \delta_y \\ 0 & 0 & 1 \end{pmatrix}. \quad (5.16)$$

We now proceed to manipulate Eq.(5.12) so that we may, in due course, solve for the elements of the metric  $h$ . The identity matrix  $\mathbf{I} = \mathbf{M}\mathbf{M}^{-1} = (\mathbf{M}^T)^{-1}\mathbf{M}^T$  can be inserted into the RHS of Eq.(5.12) to give

$$\frac{g\mathbf{d} - (g\mathbf{d} \cdot \hat{\mathbf{n}})\hat{\mathbf{n}}}{\sqrt{\mathbf{d}^T g \mathbf{d}}} = \mp \frac{h\mathbf{M}\mathbf{M}^{-1}\mathbf{e} - (h\mathbf{M}\mathbf{M}^{-1}\mathbf{e} \cdot \hat{\mathbf{n}})\hat{\mathbf{n}}}{\sqrt{\mathbf{e}^T (\mathbf{M}^{-1})^T \mathbf{M}^T h \mathbf{M}\mathbf{M}^{-1} \mathbf{e}}} \quad (5.17)$$

$$= \mp \frac{h\mathbf{M}\mathbf{d} - (h\mathbf{M}\mathbf{d} \cdot \hat{\mathbf{n}})\hat{\mathbf{n}}}{\sqrt{\mathbf{d}^T \mathbf{M}^T h \mathbf{M} \mathbf{d}}}, \quad (5.18)$$

where in the second line we have used the fact that  $\mathbf{d} = \mathbf{M}^{-1}\mathbf{e}$ . Now consider a matrix  $\mathbf{N}$  of the form

$$\mathbf{N} = \begin{pmatrix} 1 & 0 & 0 \\ 0 & 1 & 0 \\ N_{13} & N_{23} & N_{33} \end{pmatrix}. \quad (5.19)$$

Because the RHS of Eq.(5.18) is a projection of Eq.(5.11) into the  $z = 0$  plane, all that is left is the transverse components. Hence multiplying by  $\mathbf{N}$  does not alter the transverse components of the vector in Eq.(5.18). If  $\eta_x = \eta_y = \eta$ , the matrix  $\eta\mathbf{M}^T$  has the same form as  $\mathbf{N}$  and thus the RHS of Eq.(5.18) can be written

$$\mp \frac{\eta\mathbf{M}^T h \mathbf{M} \mathbf{d} - (\eta\mathbf{M}^T h \mathbf{M} \mathbf{d} \cdot \hat{\mathbf{n}})\hat{\mathbf{n}}}{\sqrt{\mathbf{d}^T \mathbf{M}^T h \mathbf{M} \mathbf{d}}}. \quad (5.20)$$

Defining

$$h' = \eta^2 \mathbf{M}^T h \mathbf{M}, \quad (5.21)$$

the expression becomes

$$\mp \frac{h'\mathbf{d} - (h'\mathbf{d} \cdot \hat{\mathbf{n}})\hat{\mathbf{n}}}{\sqrt{\mathbf{d}^T h' \mathbf{d}}}. \quad (5.22)$$

Hence Eq.(5.18) can be written

$$\frac{g\mathbf{d} - (g\mathbf{d} \cdot \hat{\mathbf{n}})\hat{\mathbf{n}}}{\sqrt{\mathbf{d}^T g \mathbf{d}}} = \mp \frac{h'\mathbf{d} - (h'\mathbf{d} \cdot \hat{\mathbf{n}})\hat{\mathbf{n}}}{\sqrt{\mathbf{d}^T h' \mathbf{d}}}. \quad (5.23)$$

If this is to hold for any vector  $\mathbf{d}$ , this implies that

$$h' = g, \quad (5.24)$$

and hence from Eq.(5.21)

$$h = \frac{1}{\eta^2}(\mathbf{M}^T)^{-1}g\mathbf{M}^{-1}. \quad (5.25)$$

Thus the elements of the metric  $h$  are

$$\begin{aligned} h_{11} &= g_{11}, & h_{22} &= g_{22}, & h_{12} &= g_{12}, \\ h_{13} &= \frac{g_{13} + g_{12}\delta_y + g_{11}\delta_x}{\eta}, & h_{23} &= \frac{g_{23} + g_{12}\delta_x + g_{22}\delta_y}{\eta}, \\ h_{33} &= \frac{g_{33} + 2\delta_y g_{23} + \delta_y^2 g_{22} + 2\delta_x g_{13} + \delta_x^2 g_{11} + 2\delta_x \delta_y g_{12}}{\eta^2}. \end{aligned} \quad (5.26)$$

We can check that this is in fact correct using ray tracing simulations. Figure 5.2 shows a comparison between a coloured lattice as seen through a gCLA and the same coloured lattice as seen through an interface between spaces with metrics  $g$  and  $h$ . As can be seen, both images are, as expected, identical.

The ray tracing simulations shown in Fig.5.2 and elsewhere in this thesis were performed using Dr TIM, an interactive, open-source custom ray tracer created and developed at the University of Glasgow by my supervisor Johannes Courtial. Dr TIM is purely a geometrical ray tracer: wave-optical considerations such as interference and diffraction are not considered when calculating ray trajectories. Dr TIM was designed specifically for studying generalised refraction across planar interfaces and aims to show what an image might look like if observed in reality. Each planar interface is modelled using a law of refraction or a metric, and is assumed to be perfectly smooth with no structure, this differs to other well known ray-tracers such as POV-ray, which incorporate surface structure. Hence a ray tracing simulation for gCLAs will not show pixellation due to the surface structure of the individual lenslets. Because of this, the renderings performed by Dr TIM will differ from what would actually be seen in reality. The advantage Dr TIM has is that it can simulate images through refracting interfaces quicker than POV-ray can and also has a simple

user interface, making it much easier for other researchers to use and follow our work on generalised refraction. In the case of Fig.5.2 Dr TIM calculated the effect of a metric interface by directly applying Fermat's principle using the two metrics  $g$  and  $h$  whereas the simulation of the gCLA simply applies the gCLA law of refraction directly to the light rays in object space. In both cases the parameters,  $\eta$  and  $\delta$  have to be input manually using an interface.

Now consider two pairs of points  $\mathbf{P}$  and  $\mathbf{Q}$ . In object space the optical path length between  $\mathbf{P}$  and  $\mathbf{Q}$  is simply the geometrical length using the Euclidean metric. That is to say

$$\begin{aligned} O_{PQ} &= \sqrt{(Q - P) \cdot (Q - P)} \\ &= \sqrt{(Q_x - P_x)^2 + (Q_y - P_y)^2 + (Q_z - P_z)^2}. \end{aligned} \quad (5.27)$$

Now consider a metric tensor interface which images like a gCLA. In image space the optical path length is

$$\begin{aligned} O_{P'Q'} &= \sqrt{(Q' - P') \cdot h \cdot (Q' - P')} \\ &= \sqrt{(Q_x - P_x)^2 + (Q_y - P_y)^2 + (Q_z - P_z)^2}, \end{aligned} \quad (5.28)$$

where we have used the metric for imaging gCLAs,  $h$ . So we see that  $O_{PQ} = O_{P'Q'}$ . Hence the metric tensor interface preserves optical path length and can be thought of as an absolute optical instrument. However gCLAs do not actually alter the metric of space - it is an illusion as the space before and after the interface is normal euclidean space. Hence an imaging gCLA might appear like a metric interface, but because it does not actually create a new metric space, the optical path length is

$$\begin{aligned} O_{P'Q'} &= \sqrt{(Q' - P') \cdot (Q' - P')} \\ &= \sqrt{(P_x - Q_x + (Q_z - P_z)\delta_x)^2 + (P_y - Q_y + (Q_z - P_z)\delta_y)^2 + \eta^2(P_z - Q_z)^2}, \end{aligned} \quad (5.29)$$

which is clearly not equal to  $O_{PQ}$ , so gCLAs cannot be classed as absolute optical instruments. The concept of an absolute optical instrument rests upon wave-optical foundations therefore it is not surprising that gCLAs are not absolute optical instruments as gCLAs perform refraction and therefore imaging which cannot be properly represented using wave-optics.

Clearly we have shown that gCLAs with an optical axis perpendicular to the plane in which they lie and for which  $\eta_x = \eta_y = \eta$  can be considered as approximations

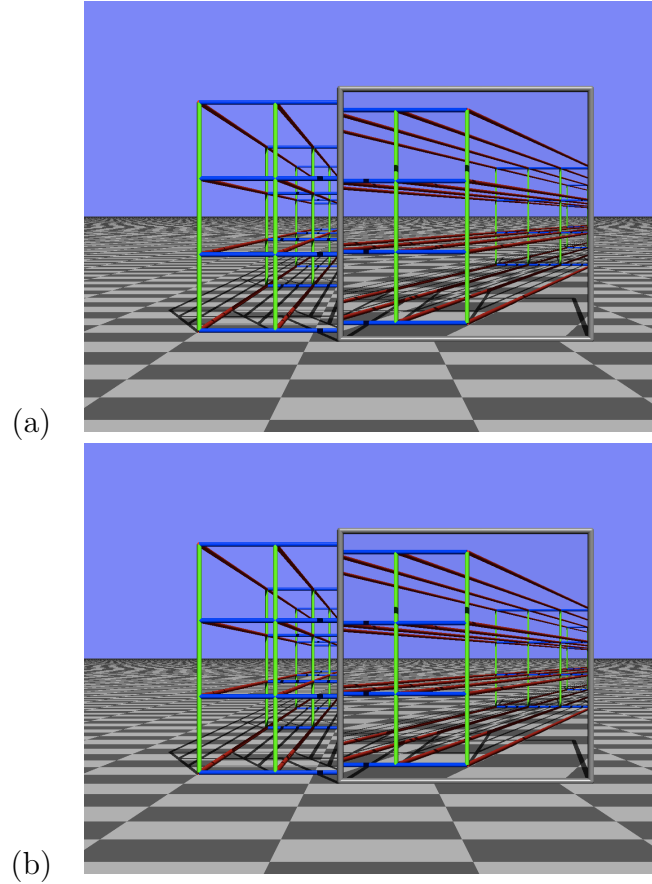


FIGURE 5.2: Simulated view through (a) gCLAs and (b) through an equivalent metric interface. The parameters of the gCLAs are  $\eta = 0.5$ ,  $\delta_x = 0.2$ ,  $\delta_y = 0$ . Refraction at the gCLAs is calculated according to Eqns (5.13); refraction at the metric interface is calculated according to equations derived from Fermat's principle [27]. The images were calculated with the custom ray tracer Dr TIM [27, 28].

to metric interfaces. The above procedure however does not address the question of whether gCLAs with  $\eta_x \neq \eta_y$  can also be described as metric interfaces. Solving Fermat's principle using conventional analytic methods results in a more general solution for gCLAs where  $\eta_x \neq \eta_y$ . If Eq.(5.4) is to be satisfied for all light-ray directions  $\mathbf{d}$ , then every individual term of Eq.(5.4) once multiplied by the denominator must be zero. In other words, after all terms have been brought to the LHS and the expression written as a polynomial in  $d_x$  and  $d_y$ , each coefficient must equal zero. As the light-ray direction vector will always be non-zero, this implies that the coefficients of the terms in Eq.(5.4) must be zero. Hence we end up with a set of equations which must equal zero and which are functions of the elements of the metric  $g$  and the metric  $h$ . By a process of trial and error, one can then attempt to solve for the elements of  $h$  such that all coefficients are zero simultaneously. On doing so one finds that the

elements of  $h$  are given by

$$\begin{aligned}
 h_{11} &= \frac{g_{11}\eta_x}{\eta_y}, & h_{22} &= \frac{g_{22}\eta_y}{\eta_x}, & h_{12} &= g_{12}, \\
 h_{13} &= \frac{g_{13} + g_{11}\delta_x + g_{12}\delta_y}{\eta_y}, & h_{23} &= \frac{g_{23} + g_{12}\delta_x + g_{22}\delta_y}{\eta_x}, \\
 h_{33} &= \frac{g_{11}\delta_x^2 + 2g_{13}\delta_x + 2g_{12}\delta_x\delta_y + g_{22}\delta_y^2 + 2g_{23}\delta_y + g_{33}}{\eta_x\eta_y}.
 \end{aligned} \tag{5.30}$$

This is the most general solution we have been able to achieve thus far and it is obvious that when  $\eta_x = \eta_y = \eta$  this corresponds to the solution shown in Eq.(5.26).

There may still be more solutions which have yet to be uncovered for this configuration of gCLA parameters. Note that all of the above is for gCLAs whose lenslets have optical axes which are orthogonal to the plane in which the array lies. The cases where the optical axes are rotated has not yet been attempted as we prioritised gCLAs with non-rotated lenslets, because these, as we shall show, find application in piecewise homogeneous transformation-optics devices. As such we have focused our attention on these potential applications and we shall look in depth at the results in the chapter to come. So there may be more metric interfaces which can be found to correspond to gCLAs.

It may be reasonable to think that if a significant number of metric interfaces could be found, that one could construct a grid of cells using gCLAs and indeed the inhomogenous imaging sheets from the previous chapter, each with their own unique metric, and hence begin to construct exotic, piecewise transformation optics devices as in Fig. 5.3. However this in general will not be possible, as at the heart of transformation optics lies an underlying coordinate transformation. We will show now that while in principle all gCLAs with non-rotated lenslets can be used to effect a metric interface, only gCLAs which are imaging can be used to effect coordinate transformations.

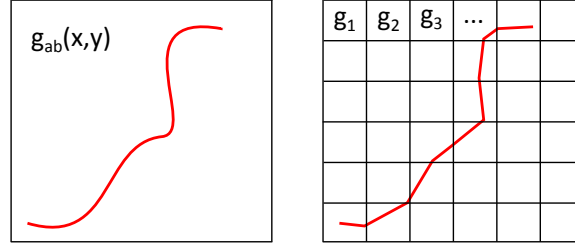


FIGURE 5.3: Left: a curved space causes a light-ray (red line) to follow a curved trajectory. Right: a lattice constructed of discrete metric interfaces (represented by black lines) could, in principle, mimic the behaviour of a light-ray passing through curved space.

## 5.4 Metric interfaces and perfect imaging

In the preceding chapter we showed that idealised gCLAs where  $\eta_x = \eta_y = \eta$  are perfectly imaging. Recall the imaging equation was specifically

$$\mathbf{P}' = \mathbf{P} - z \begin{pmatrix} \delta_x \\ \delta_y \\ 1 - \eta \end{pmatrix}. \quad (5.31)$$

Each point in object space is mapped to one and only one point in image space. This is exactly how a non-singular coordinate transformation behaves when transforming from an original coordinate system to a new one. This is shown clearly in Fig. 5.4.

Hence we can construct the metric effected by imaging gCLAs using the same method one would use if one were creating transformation optics devices. That is to say, when  $\mathbf{P} = (x, y, z)^T$  and  $\mathbf{P}' = (x', y', z')^T$ , the Jacobian matrix for the transformation is

$$\Lambda_J = \begin{pmatrix} \frac{\partial x'}{\partial x} & \frac{\partial x'}{\partial y} & \frac{\partial x'}{\partial z} \\ \frac{\partial y'}{\partial x} & \frac{\partial y'}{\partial y} & \frac{\partial y'}{\partial z} \\ \frac{\partial z'}{\partial x} & \frac{\partial z'}{\partial y} & \frac{\partial z'}{\partial z} \end{pmatrix} = \begin{pmatrix} 1 & 0 & -\delta_x \\ 0 & 1 & -\delta_y \\ 0 & 0 & \eta \end{pmatrix}. \quad (5.32)$$

Standard differential geometry states [29] that the metric  $h$  is then related to the metric  $g$  as follows:

$$h = (\Lambda_J^{-1})^T g (\Lambda_J^{-1}). \quad (5.33)$$

Calculating the metric in this way is far simpler and gives the same result as Eq.(5.26). Similarly for perfectly imaging inhomogenous sheets described in the previous chapter

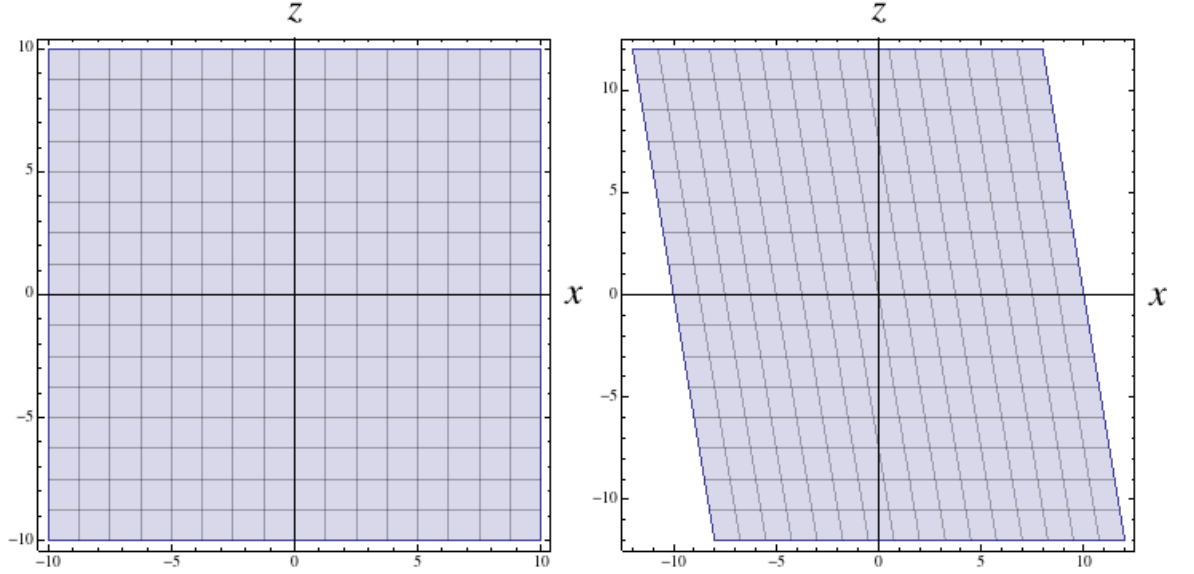


FIGURE 5.4: Left: a two dimensional cartesian coordinate system. Right: the same cartesian coordinate system after it has been transformed by the gCLA imaging equation where, specifically,  $\delta_x = 0.2$ ,  $\delta_y = 0$  and  $\eta = 1.2$ .

the metric, calculated in the same way, is

$$\begin{aligned}
 h'_{11} &= \frac{f^2 g_{11}}{(f+z)^2}, & h_{22} &= \frac{f^2 g_{22}}{(f+z)^2}, & h_{12} &= \frac{f g_{12}}{(f+z)^2}, \\
 h_{13} &= \frac{f^2 (g g_{13} - g_{11} x - g_{12} y)}{(f+z)^3}, & h_{23} &= \frac{f^2 (g g_{23} - g_{12} x - g_{22} y)}{(f+z)^3}, \\
 h_{33} &= \frac{f^2 (g^2 g_{33} + g_{11} x^2 + y(2g_{12} x + g_{22} y) - 2g(g_{13} x + g_{23} y))}{(f+z)^4},
 \end{aligned} \tag{5.34}$$

where  $g = \eta f$  is the object sided focal length for the inhomogenous sheet and is different from the metric tensor  $g_{ij}$ .

If the gCLA is non-imaging, then a coordinate transformation does not exist and while it can be used to effect a metric interface, it cannot be used within a grid of cells to create transformation-optics devices.

## 5.5 When does a coordinate system not correspond to imaging?

There are three types of refracting interfaces. The first kind performs a coordinate transformation and hence has a metric tensor interpretation, but is non-imaging. An example would be Snell's law where the coordinate transformation is simply a scaling of the original coordinate system by the refractive index  $n$ . As we see in Fig.5.5, the coordinate transformation which Snell's law can be described with, results in the new coordinate system and the original coordinate system failing to match up on the surface of the interface. This means that points on the surface in the old coordinate system get mapped to new points further along the interface. Hence, if Snell's law was imaging, when an ingoing light ray strikes one of these positions, it would emerge from the new position further along on the interface. This clearly cannot happen, which is why Snell's law, despite implementing a coordinate transformation cannot image. The object space coordinate system and the image space coordinate system have to coincide on the interface as shown in the top diagram of Fig.5.5. The second kind of refractive interface performs a coordinate transformation and hence has a metric tensor interpretation but also images. As we have seen, an example of this would be gCLAs where  $\eta_x = \eta_y$ . The third and final type of refractive interface does not perform a coordinate transformation, but does have a metric tensor interpretation, but is not imaging. An example of this type of interface would be gCLAs where  $\eta_x \neq \eta_y$ .

## 5.6 Conclusion

In this chapter we have shown that on applying Fermat's principle to gCLA refraction, gCLAs can be reinterpreted as pixellated metric tensor interfaces and have shown ray-tracing simulations which corroborate this interpretation. The case where gCLAs are constructed using rotated lenslets has yet to be looked at, but will be explored in future. We have shown that the metric tensor for imaging gCLAs can be found by using the Jacobian matrix which describes the imaging performed by gCLAs, as when imaging systems image, this corresponds to performing a coordinate transformation on object space. Finally we discussed why some interface systems described in terms of coordinate systems such as Snell's law, are non-imaging, while others such as

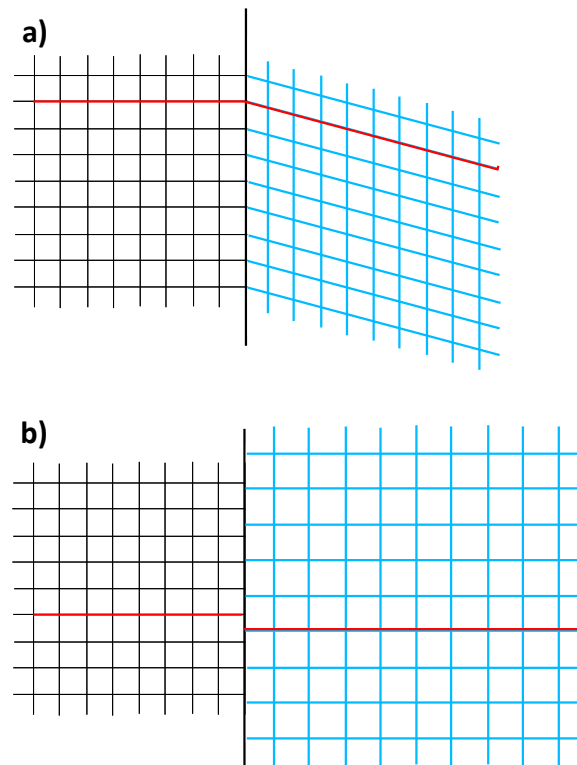


FIGURE 5.5: The coordinate system produced by an imaging interface **a** and a non-imaging interface **b**. As we see, in the imaging case, **a**, the coordinate system in object space and image space align on the surface of the interface. In the non-imaging case, this does not happen and so the system will not image, as in order to image, ingoing light rays would have to jump along the interface to leave from the correct position in the new coordinate system. Clearly this is not possible.

gCLAs are. In the following chapter we will use the fact that gCLAs are imaging to design simple homogeneous piecewise transformation optics devices.

# Chapter 6

## Transformation optics with CLAs

### 6.1 Introduction

Invisibility devices are traditionally the province of science fiction and mythology. Once thought to be impossible, in recent years advancements in optics and material physics have meant that it may be possible, and indeed even likely, that a real, working invisibility device will be created within the not too distant future. But what do we class as an invisibility device? Before proceeding we need to state what we mean when we call something an invisibility device. Optically speaking, an invisibility device is a device which causes light to appear as though it has propagated through a region without having its trajectory or phase altered, when in fact the light is propagating along a curved trajectory around a hidden subregion within the region. That is to say that there is absolutely no distortion to the light whatsoever when it passes through the device.

In 2006 both Pendry et al [21] and Leonhardt [20] independently discovered the theory of transformation optics which allows invisibility devices to be realised. As an example of the power of their design methodology, Pendry used a spherically symmetric coordinate transformation to design a hollow, spherical, spatially varying medium that would cause light to travel along straight lines in the coordinate system and around the hollow interior. The transformation works by taking a point and blowing it up to a finite size. The resulting coordinate system is curved around this inner region. This means that any object inside this interior region would be impossible to see from outside the sphere and as such that the spherical medium would be acting like a cloaking device. This type of cloak is, in principle, completely perfect as it

preserves phase, perfectly images and is spherically symmetric (and as such clearly works from all viewing directions). Despite theoretical advances however, currently such cloaks do not exist at visible wavelengths and macroscopic scales. There are both theoretical issues and practical limitations which hinder their construction. Perhaps the most problematic is that light passing through the original point with the device absent would take an infinitesimally small length of time to do so. After the coordinate transformation however, this point has a finite size, so in order to stay in phase the light has to travel at infinite phase and group velocity on the surface of this area.

Current metamaterials are constructed using subwavelength arrays of resonant, metallic components. These components can be arranged such that they provide an infinite phase velocity for frequencies of light that match the resonant frequency of the metallic resonators. Clearly the problem here is that the phase velocity only reaches infinity for discrete frequencies and does not, as a result, work over a broad band of frequencies. The group velocity also tends to zero at resonance. Leonhardt and Tyc proposed that a way of achieving broadband cloaking would be to use a non-Euclidean coordinate transformation [30]. The advantage here is that the group velocity of the light is always finite. Even this type of cloak is difficult to create as it still requires extreme material parameters. However if the definition of an invisibility device is relaxed such that phase preservation is not required, then the task of creating an invisibility device becomes somewhat easier and indeed we shall see that under this new definition, in certain circumstances, it is possible to create a much simpler cloaking device that does not rely on conventional transformation optics.

A team of researchers led by Chen adopted an altogether different approach to cloaking. Instead of using a continuous transformation as in previous work, they used a piecewise homogeneous transformation. The resulting device was realised using a hexagonal arrangement of prisms to create a “cylindrical” cloak that worked in the visible spectrum [31]. The resulting cloak worked perfectly when viewed from six different directions, however when viewed from any other direction, the view was distorted and the cloak’s presence apparent.

Still more recently, it has been proposed that it may be possible to use conventional refractive index media to perform cloaking [32]. In [32] Horsley et al proposed that devices which redirect surface waves and with refractive index singularities could be realised using a transformation which transformed both the shape of the device and its optical parameters. In doing so, points in the original device with singular

refractive indices could be reshaped to have singular geometry, but finite refractive index contrast, thus making them feasible for production. Whilst this work was confined purely to two dimensional surface devices, they have suggested that the same method could in principle be applied to three dimensional cloaking in transformation optics.

### 6.1.1 Contributions

The work in this chapter was carried out by numerous collaborators. Section 6.2.1 presents work carried out by Myself, Johannes Courtial and Georgios Antoniou. Section 6.2.2 presents work carried out by Myself, Johannes Courtial and Chris White. Section 6.3.1 was conceived by Johannes Courtial and Tim Sharpe. Section 6.3.2 was carried out by myself and section 6.3.3 was a collaboration between Myself, Johannes Courtial and Chris White. Section 6.4 was a collaboration between Myself, Johannes Courtial, Tomáš Tyc and Euan Cowie.

## 6.2 Piecewise transformation optics using gCLAs

### 6.2.1 Transformation properties around a closed loop in transformation optics

Before we examine any piecewise transformation optics devices it is prudent to highlight an important result which applies to all of transformation optics. It is well known that on curved surfaces parallel lines do not remain parallel, as such there is no global concept of parallelism on a curved surface, or more generally on a curved manifold. Consider a sphere, if we parallel transport a vector around a closed loop on the surface of a sphere, then on completely circumnavigating the loop, our vector will be rotated by  $\pi/2$ . Compare this with a closed loop on a flat surface, and the vector returns to its starting position with the same initial direction. It stands to reason that if, in both cases, our vector is pointing along one of the axes which defines the coordinate system on the surface, then on a flat surface the coordinate system must also be mapped back to itself after circumnavigating the loop, whereas on the sphere the coordinate system is rotated as it traverses the loop. This property is a direct consequence of the underlying geometry. We can show that this result also holds

in piecewise geometry - and hence our piecewise, pixellated transformation optics - provided certain conditions are met.

To illustrate that this result is correct we shall perform a loop calculation using three general imaging sheets. Recall that the most general type of imaging one can consider using a planar interface is (for a sheet placed in the  $z = 0$  plane) given by Eq.(4.1):

$$\begin{aligned} x' &= \frac{fx}{f+z}, \\ y' &= \frac{fy}{f+z}, \\ z' &= \frac{gz}{f+z}. \end{aligned} \tag{6.1}$$

We said that the imaging performed by this interface was the same as the imaging performed by a thin lens followed immediately by a confocal lenslet array, which compressed the image-sided focal length. In this sense the sheet can therefore be thought of as an idealised generalised lens (referred to as a glens from now on), with a unique object and image-sided focal length:  $f$  and  $g$ . In a conventional lens, if light passes through the centre of the lens, which we call the nodal point, light is undeviated. In a glens however, because the focal lengths on either side of the glens are different, the nodal point,  $\mathbf{N}$ , no longer lies on the centre of the glens, though it still lies on the optical axis. Indeed the nodal point of a glens is positioned a distance  $n = f + g$  along the optical axis. The nodal point  $\mathbf{N}$  is equivalent to the centre point of a conventional lens, in that any ray passing through  $\mathbf{N}$  will pass through the glens undeviated. Considered in this way, the imaging equations can be recast in the following form:

$$\mathbf{P}' = \mathbf{P} + \frac{(\mathbf{P} - \mathbf{I}) \cdot \hat{\mathbf{a}}}{f - (\mathbf{P} - \mathbf{I}) \cdot \hat{\mathbf{a}}}(\mathbf{P} - \mathbf{N}), \tag{6.2}$$

where  $\mathbf{P}$  and  $\mathbf{P}'$  are the object and image positions,  $\mathbf{I}$  is a point on the glens,  $f$  is the object sided focal length and  $\hat{\mathbf{a}}$  is the direction of the optical axis. Now assume we have three glenses all intersecting a common edge such that they are all rotated about a common axis. Specifically, let glens **1** be situated in the  $z = 0$  plane and let glens **2** and glens **3** be rotated from glens **1** about the  $z$ -axis by angles  $\alpha_2$  and  $\alpha_3$  respectively as in Fig. 6.1. Assuming all the focal lengths are non-zero (which we must, otherwise one or more of the glenses would fail to exist), we can show that on mapping a point through each of the glenses and ensuring that at the end the final image point coincides with the original object point, the following constraints have

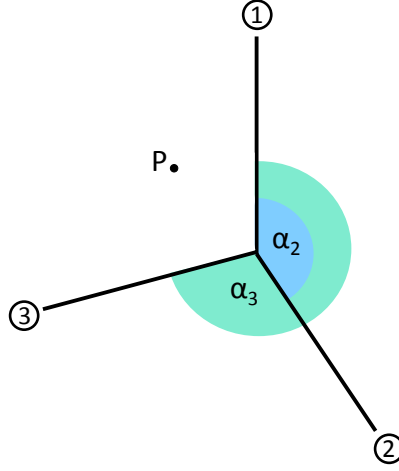


FIGURE 6.1: Three glenses arranged such that they share a common edge. If the intersection behaves like a transformation optics device, the point  $\mathbf{P}$  will be mapped back to itself on being imaged through each of the glenses in order.

to be met

$$\mathbf{N}_1 = \mathbf{N}_2 = \mathbf{N}_3 \quad (6.3)$$

$$\sin \alpha_2 \neq 0, \quad \sin \alpha_3 \neq 0, \quad \sin(\alpha_2 - \alpha_3) \neq 0, \quad (6.4)$$

$$\frac{g_2}{f_3} = \frac{\sin \alpha_2}{\sin \alpha_3}, \quad \frac{g_1}{f_2} = -\frac{\sin \alpha_3}{\sin(\alpha_2 - \alpha_3)}, \quad g_1 g_2 g_3 \sin(\alpha_2 - \alpha_3) \neq f_2^2 f_3 \sin \alpha_3, \quad (6.5)$$

$$f_1 f_2 f_3 = -g_1 g_2 g_3. \quad (6.6)$$

Recall, that in the limit when the focal length of a glens goes to infinity, a glens becomes a homogeneous gCLA. Hence we know that in that limit, the above expressions automatically hold for gCLAs. Other systems of glenses will produce different equations which have to be satisfied with it being obvious that the more interfaces intersecting the closed loop, the more complicated the expressions will be. Again these expressions will also hold for homogeneous gCLAs in the limit when the focal lengths tend to infinity. What this result tells us is that as long as the expressions produced by applying this loop calculation are met, a system of glenses or gCLAs which intersect at a single point will have zero “curvature”. If these conditions are not met, then the final coordinate system we end up with must be a generalised rotation of the original coordinate system, and hence the loop spans a “curved” space.

### 6.2.2 Insulation window

Our gCLAs could in principle be used to create transformation optics devices which may be of commercial value. Specifically, sheets which image like gCLAs could be used to create a type of domestic window which hides insulation. It is well known that modern buildings lose a large proportion of their heat through their windows, hence improving window design is one simple way of improving the thermal efficiency of buildings. We will show how such a window can be designed using gCLAs. The coordinate transformation involves mapping a “downwards” pointing triangle into a compressed version of itself. We now explain in detail how this is achieved. Consider light rays which originally intersect the point  $\mathbf{E}$  in Fig. 6.2. If our device is to image the point  $\mathbf{E}$  to  $\mathbf{E}'$  then it is clear that in the new space our device has created, these rays must now intersect at the point  $\mathbf{E}'$ . This means that gCLA **1** has to image  $\mathbf{E}$  to  $\mathbf{E}'$ . To find the parameters for gCLA **1** one simply uses Eq.(4.12) using  $\mathbf{E}$  and  $\mathbf{E}'$  as the object and image positions respectively. GCLA **1** will also map  $\mathbf{C}$  to the position  $\mathbf{C}_{int}$ . On its own this is a problem as the piecewise mapping we employ should ensure that all positions on the outer edge of the device image back to themselves. As such we must also map  $\mathbf{C}_{int}$  through gCLA **2**. Again, in order to find the parameters of gCLA **2** we use Eq.(4.12) with  $\mathbf{C}_{int}$  as the object position and  $\mathbf{C}$  as the image position. Note that due to the form of Eq.(4.12) we must always ensure the interface in question is positioned in the local  $z = 0$  plane and that our object and image positions are for this local coordinate system. Due to the symmetry of the design shown in Fig.6.3, the parameters for gCLAs **3** and **4** are identical to those of gCLAs **2** and **1** respectively. If  $\mathbf{E} = (0, 0, 1)$  and we wish  $\mathbf{E}' = (0, 2, 1)$ , (i.e. shifted vertically by two units of distance) on performing the calculation outlined, one finds the following parameters for gCLAs **1** and **2**:

$$\delta_{1_x} = 0, \delta_{1_y} = -2, \eta_1 = 1, \quad (6.7)$$

$$\delta_{2_x} = 0, \delta_{2_y} = 1, \eta_2 = 0.5 \quad (6.8)$$

where again the  $x$  and  $y$  refer to that particular gCLAs local coordinate system and again the parameters for gCLAs **3** and **4** are the same as for **2** and **1**.

The effect of the transformation is shown in Fig. 6.3. The left hand image shows a cross section of how light should travel through an empty window frame. The right hand image shows how, with the use of idealised gCLAs, one can perform a piecewise



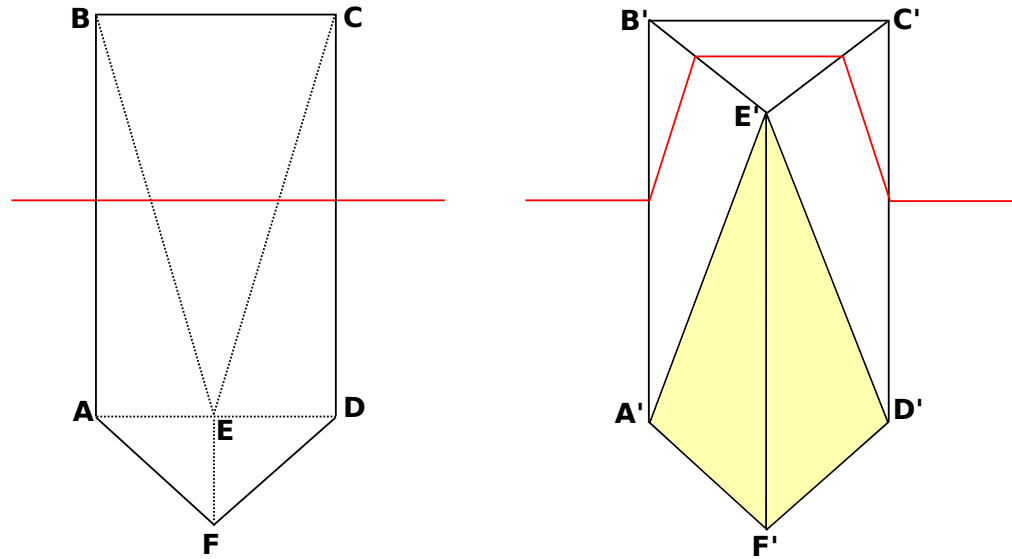


FIGURE 6.3: Left: View of a light ray (red) passing through a rectangle of empty space. Right: The same space after a piecewise coordinate transformation using gCLA interfaces. The point  $E$  has been mapped to the point  $E'$ . A new region spanning  $A'E'D'F'$  has been created. This region can in principle be used to conceal an object. For architectural purposes this could hide insulation, thus rendering the above device into an insulation window.

However in practice there would be problems with the view through such a window. First of all, as mentioned previously, gCLAs suffer from a limited field of view [35, 36]. as such, those light-rays which do not refract properly will be absorbed by the insulation region and thus the outgoing image will lose intensity. But even putting aside field of view issues, there would still be the issue of seeing the internal sheets when looking through the structure. Figure 6.4 shows a simulated view through an insulation window when viewed from a direction which is normal to the window plane. In this instance the internal structure of the window is visible, but not significantly so. However, this changes when viewed from an angle. Consider the top image in Fig.6.5. We see that when viewed from an angle, the internal structure is far more visible within the window. When the window is made thinner, as in the bottom image in Fig. 6.5, the internal structure intrudes far less. However when the window is made thinner, it limits the size of the region in which insulation can be placed and also requires more extreme sheet parameters. If insulation windows are to be used in the real world, a compromise between thermal efficiency and visual performance will have to be found.

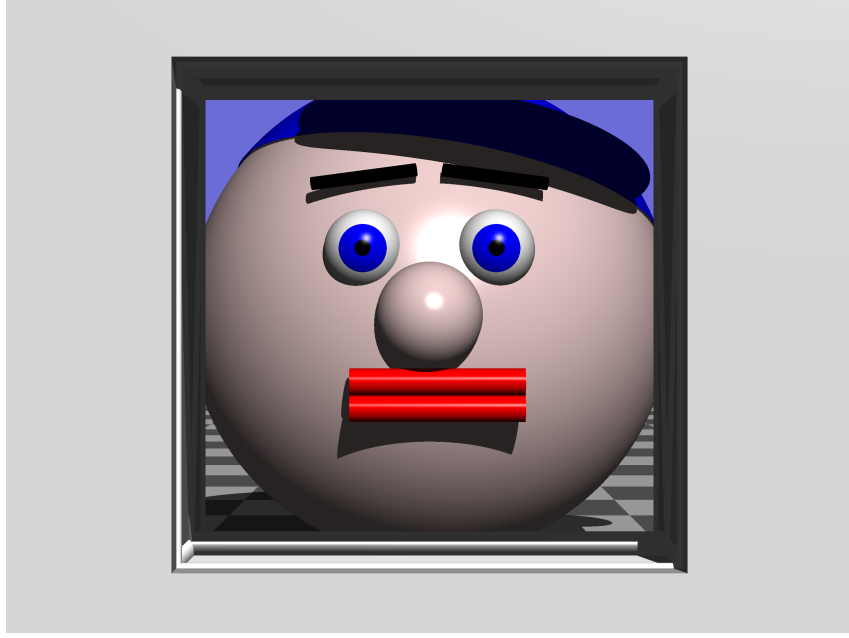


FIGURE 6.4: The simulated view through an insulation window when the viewing direction is orthogonal to the normal of the plane of the window.

## 6.3 Piecewise cloaking using CLAs

### 6.3.1 Initial cloaking design

Motivated by the hexagonal cloak described in the introduction of this chapter [31] and our discovery of the very general imaging possibilities with gCLAs, we attempted to simulate a similar effect using a device constructed from imaging gCLAs. Unlike the hexagonal device described previously, our device has four sides, and is constructed of gCLAs and empty space rather than of solid prisms. The gCLAs change light-ray direction like the interface between two solid prisms.

Recall previously we showed that a subset of gCLAs are imaging [25, 33] and that, for a homogeneous gCLA placed in the  $z = 0$  plane, a point  $\mathbf{P}$  in object space was mapped to a point  $\mathbf{P}'$  in image space according to the equation

$$\mathbf{P}' = \mathbf{P} - z \begin{pmatrix} \delta_x \\ \delta_y \\ 1 - \eta \end{pmatrix}, \quad (6.9)$$

where  $\delta_x$ ,  $\delta_y$  and  $\eta$  are parameters of the sheet. Following the thinking used to design the hexagonal cloak described above, our design was for a cloak with four sides (as

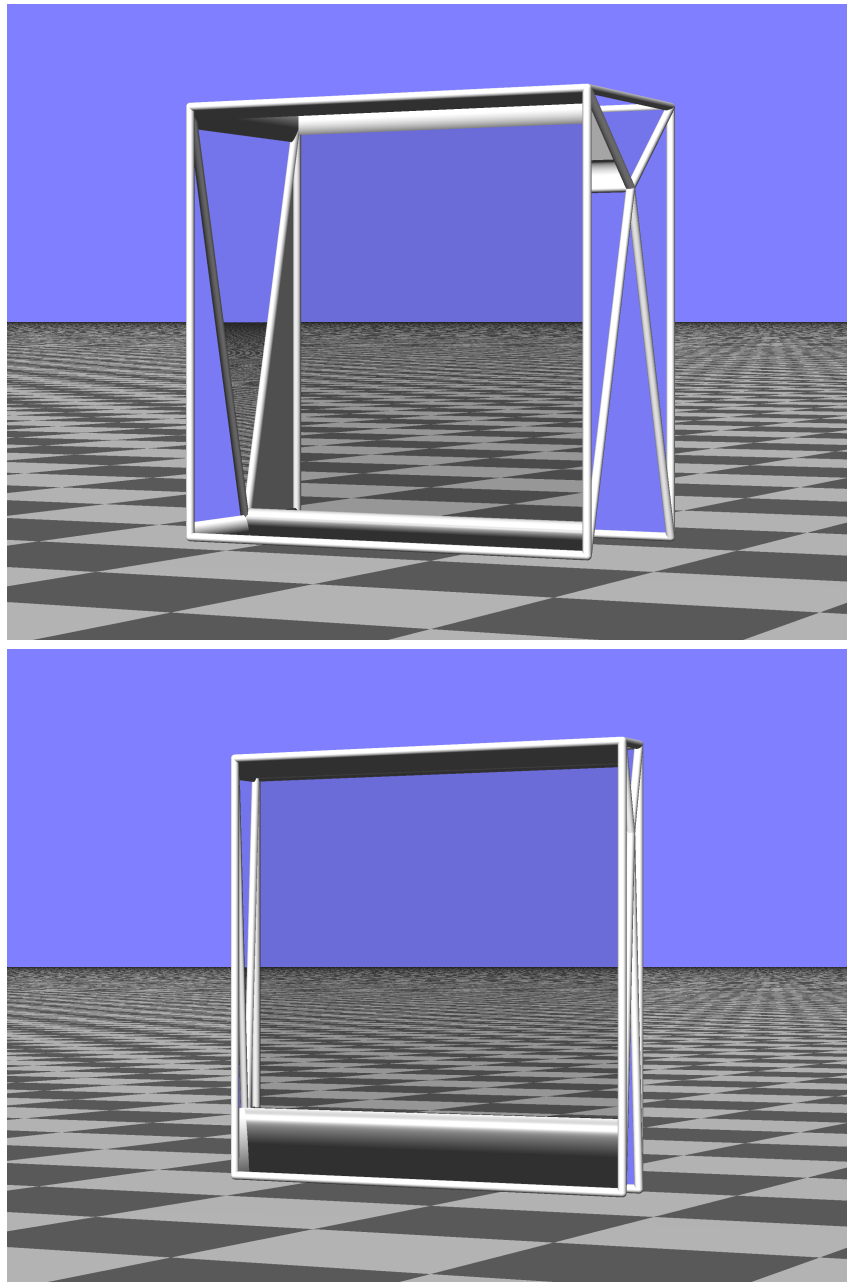


FIGURE 6.5: When viewed from an angle the thickness of the insulated region becomes an issue. When the insulation window is thick (top) the view through the window is heavily distorted where the window meets the wall. When the insulation window is thin (bottom), the distortion is reduced, however the insulation then begins to block the image through the window.

opposed to six). As a result, the device consisted of twelve gCLAs in total as seen in the top image in Fig. 6.6. The gCLA parameters were found by applying the loop imaging theorem introduced in section 6.2.1. First we took an object position outside the cloak  $\mathbf{P}$ , and mapped it consecutively through the four individual sheets in our cloak - the two outer sheets and the two inner sheets between them - and ensured that the final image position  $\mathbf{P}'$  after passing completely through the cloak matched the original object position. For this to be true it has to be the case that  $\mathbf{P}' - \mathbf{P} = \mathbf{0}$ . This equation represents three polynomials - one for each of the components of the object position  $\mathbf{P}$  - and is a function of the parameters for each sheet. In order for this polynomial to be zero for all object positions  $\mathbf{P}$ , it must be true that the coefficients for each term in the polynomial are individually zero. Hence by setting each of these coefficients to zero and solving them simultaneously, one can find the sheet parameters which are, unsurprisingly, a function of the cloak geometry. Specifically when the cloak is situated in the  $x - z$  plane and the angles between the sheets is  $\pi/6$ , the values for the interior sheet parameters are  $\eta_2 = -1/\sqrt{3}$ ,  $\eta_3 = -\sqrt{3}$ ,  $\delta_{x_2} = 1 - 1/\sqrt{3}$ ,  $\delta_{x_3} = 1 - \sqrt{3}$ ,  $\delta_{y_2} = 0$ ,  $\delta_{y_3} = 0$  while the outer sheets share the same parameters as one another and can take any values as long as  $\eta_1 \neq 0$ . This design worked perfectly for four different light-ray directions (at least from a geometric perspective) and we show a “bird’s eye” view of the design in Fig. 6.6 and also a ray tracing simulation of the view through the cloak from one of the “working” directions. It is clear that the face which is placed in the background is unaltered when viewed through the cloak.

### 6.3.2 Subsequent cloaking designs

Clearly, the above cloak works extremely well for the four directions for which it was designed, however it is known that from any other viewing direction, this design does not work. Proper transformation cloaks are able to work from all viewing directions, hence our second approach strived to emulate transformation optics as closely as possible. Note that the mapping homogeneous gCLAs perform is affine, that is to say, the sheet parameters are not dependent on position. As such, if we are to attempt to design transformation optics devices (which generally use mappings with parameters which vary with position) using gCLAs, we will have to do it in a piecewise fashion where we use a number of sheets configured in a specific orientation. We shall explain how this is achieved for a simple example - the square-prismatic cloak.

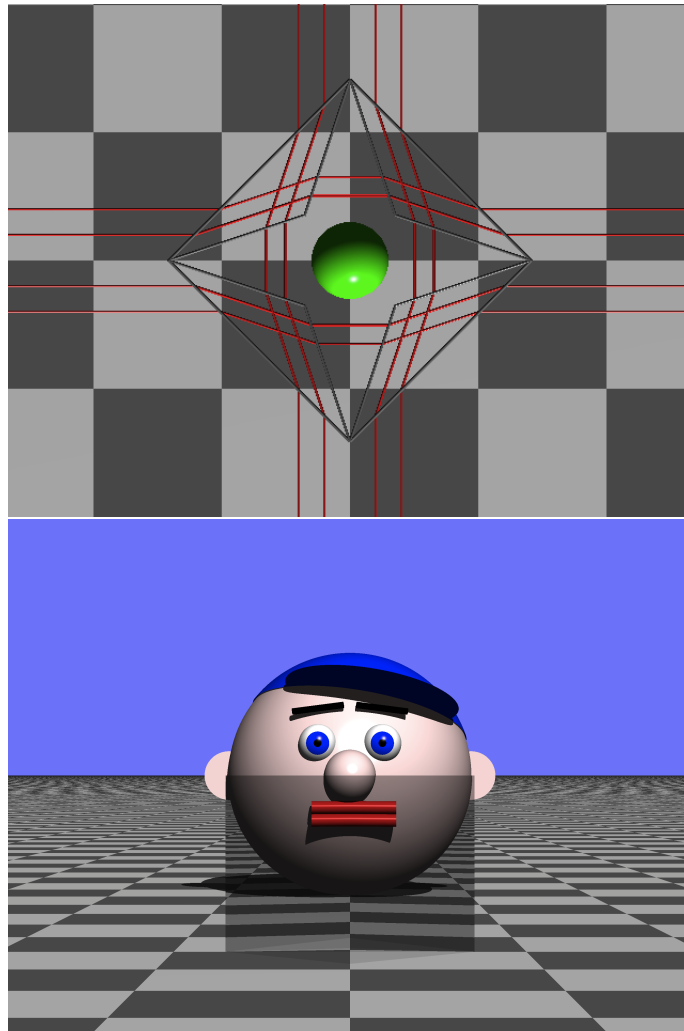


FIGURE 6.6: Top: A bird's eye view of our first attempt at a cylindrical cloak. A green ball is what is being cloaked. The red lines represent light rays which are being refracted at each of the gCLAs, which are represented by grey lines. Bottom: The view through the cloak when viewed from one of the correct viewing angles.

In the conventional transformation optics cylindrical cloak we take a coordinate system and blow it up at a point. We see in Fig. 6.7 that when blowing up a point in the middle, the coordinate system immediately surrounding the point is also distorted. We can replicate this effect using a piecewise transformation in the following way [34]. Consider two concentric squares of different sizes with an angular displacement of  $\pi/4$  between the two. By connecting the corners of one of the squares to the nearest-neighbour corners of the other square, we can segment the space between the two squares into discrete triangles. Suppose now we change the size of the interior square and make it larger without changing its orientation. The triangles that surround the interior square will now be of a different shape. This is analogous to what we observe in transformation optics when we blow up a point and the surrounding

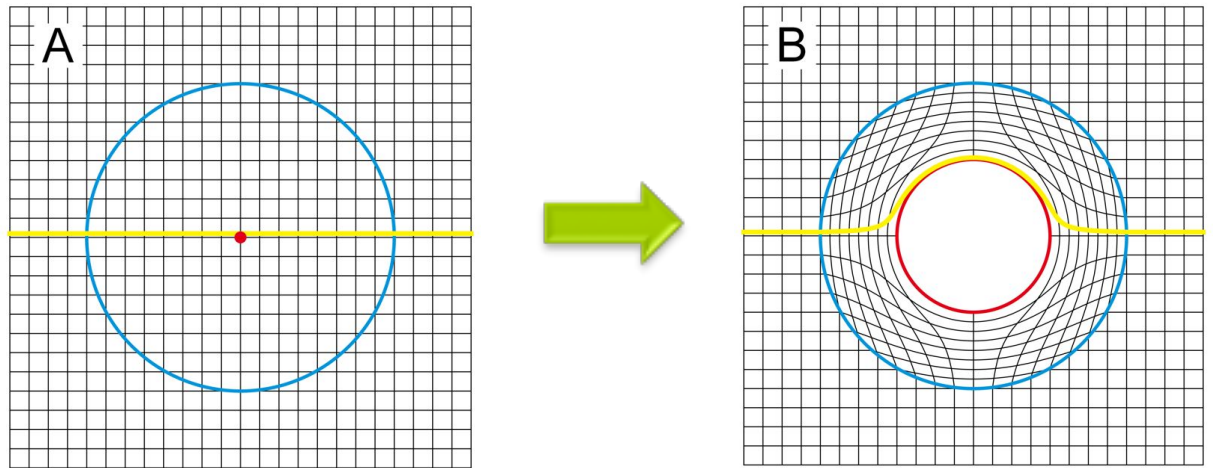


FIGURE 6.7: Graphical representation of a cylindrical coordinate transformation. Left: before the cylindrical transformation. Right: after the cylindrical transformation, light rays are directed around the central region and then redirected along their original trajectories.

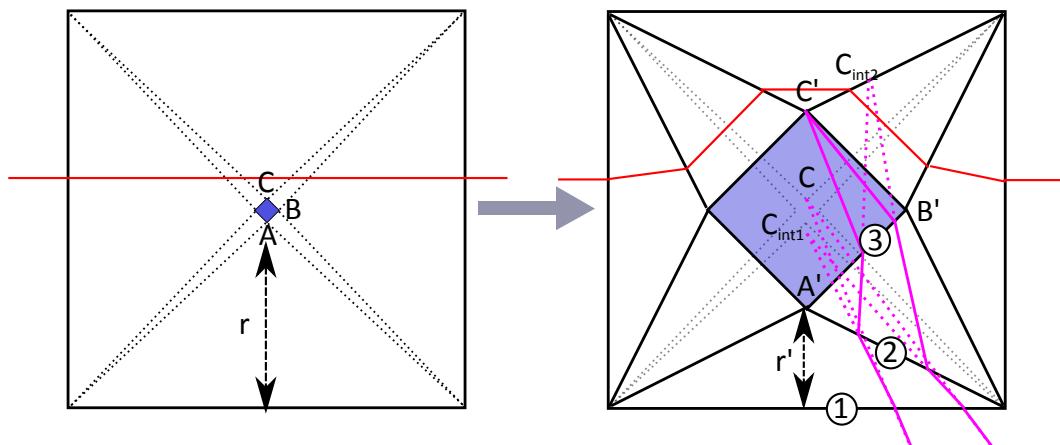


FIGURE 6.8: gCLA equivalent transformation for square prismatic cloaks. In this case, instead of a point being blown up to a circle, a smaller square is blown up to a larger one. This is an example of piecewise transformation optics.

space is altered. Specifically what we have done is we have mapped the corners of the interior square to new positions using the imaging equations that describe gCLAs.

The procedure used to design this type of cloak is identical to the procedure outlined in section 6.2.2, but as this is a new approach to transformation optics we shall once again outline how this is achieved. First we shall consider the Point **A** in Fig. 6.8. The point **A** gets mapped to the point **A'** which clearly involves simply moving the point **A** closer to the  $z = 0$  plane, which sheet **1** lies on, i.e. the  $x$  and  $y$  components of **A** do not change. Using Eq.(6.9) we see then that the  $z$ -component of **A** gets

mapped as follows

$$A'_z = \eta_1 A_z, \quad (6.10)$$

which means that

$$\eta_1 = \frac{A'_z}{A_z} = \frac{r'}{r}, \quad (6.11)$$

as the  $z$ -components of  $\mathbf{A}$  and  $\mathbf{A}'$  are  $r$  and  $r'$  respectively. We see that because  $r' < r$ , the optical space within the device after sheet **1** is compressed. This is why despite the inner region now being larger than it was, it actually appears no bigger. We now have the sheet parameters for sheet **1**.

It would be tedious to go through the entire procedure for all three types of sheet that are used to construct the cloak, so we shall simply outline the general procedure that must be followed in order to fully define all the sheet parameters. In order to understand the mappings that will take place, consider a pair of rays originating outside our region that enter the cloak through sheet **1** and, before transformation, intersect at the point  $\mathbf{B}$ . In our new “transformed” region, these light rays would first intersect sheet **1** and be refracted to the point  $\mathbf{B}_{int_1}$ . However before they can reach this new intersection point, they encounter sheet **2** which in turn refracts them. Sheet **2** therefore has the role of imaging the virtual intersection point  $\mathbf{B}_{int_1}$  to the new transformed point  $\mathbf{B}'$ . To perform this mapping between  $\mathbf{B}_{int_1}$  and  $\mathbf{B}'$ ,  $\mathbf{B}_{int_1}$  must first be rotated into the local coordinate system of sheet **2** (for all sheets in the cloak, the “local”  $z$ -axis is always in the direction of the sheet normal and the sheet itself sits in the “local”  $z = 0$  plane). Once this is done, the rotated version of  $\mathbf{B}_{int_1}$  is mapped using Eq.(6.9) (with  $\delta_{x_2}$ ,  $\delta_{y_2}$  and  $\eta_2$  as the sheet parameters) to  $\mathbf{B}_{int_2}$ , and the resulting point is equated to  $\mathbf{B}'$ . Using the three components of

$$\mathbf{B}_{int_2}(\delta_{x_2}, \delta_{y_2}, \eta_2) - \mathbf{B}' = 0, \quad (6.12)$$

as equations, one then solves for  $\delta_{x_2}$ ,  $\delta_{y_2}$  and  $\eta_2$ . A similar procedure (as shown in Fig. 6.8 can then be followed for the point  $\mathbf{C}$  to find the sheet parameters for sheet **3**. When all the parameters are found, one has then fully defined the cloak. The parameters for this cloak are shown in Table 6.1 while Fig. 6.9 shows a simulation of our square prismatic cloak.

One can see that this cloak works from all horizontal viewing directions (one cannot look through the top or bottom of the device), however it does not quite work exactly, as the green ball which we are cloaking is still seen in the form of a thin vertical slit. This is a consequence of trying to cloak in the “real world”. In pure transformation

Side length	2
$r$	0.9
$r'$	0.1
<b>Sheet 1</b>	
$\eta_1$	0.111
<b>Sheet 2</b>	
$\eta_2$	46.895
$\delta_{x_2}$	-33.684
<b>Sheet 3</b>	
$\eta_3$	15.545
$\delta_{x_3}$	0

TABLE 6.1: Parameters for a square prismatic cloak as simulated in Fig. 6.9.

optics theory, one blows up a point to a sphere (by a factor  $\infty$ ) and the cloak works perfectly because a hidden region has been created where before there was nothing. However in reality, one cannot blow up a point into a finite volume as material parameters diverge, one can only blow up a smaller region to become a larger one. This is why we can see the green vertical strip in our simulation; the inner region we are blowing up was already finite in size, so we are not creating a hidden region that was not there before, we are making the sphere appear smaller in the horizontal direction.

The above procedure can also be applied to create a cubic cloak. The cubic cloak is obviously more complicated to construct and as such the sheet parameters are also able to take non-zero values for  $\delta_y$ . The parameters for such a cloak are shown in Table 9.1 of the Appendix. We see in Fig. 6.10 that again an artefact of the real world remains, this time however the green ball appears as a much smaller green ball.

In practice all these cloaks will suffer from a limited field of view [35, 36] due to the fact that they are constructed from sheets comprising lenslets. The outgoing image will also be pixellated and so we are now looking at trying to improve our sheets so as to erase this pixellation effect. In order to do this we will have to examine the wave-optical properties of sheets that perform generalised refraction in more detail. This will briefly be mentioned in the final chapter when we introduce future projects worth exploring.

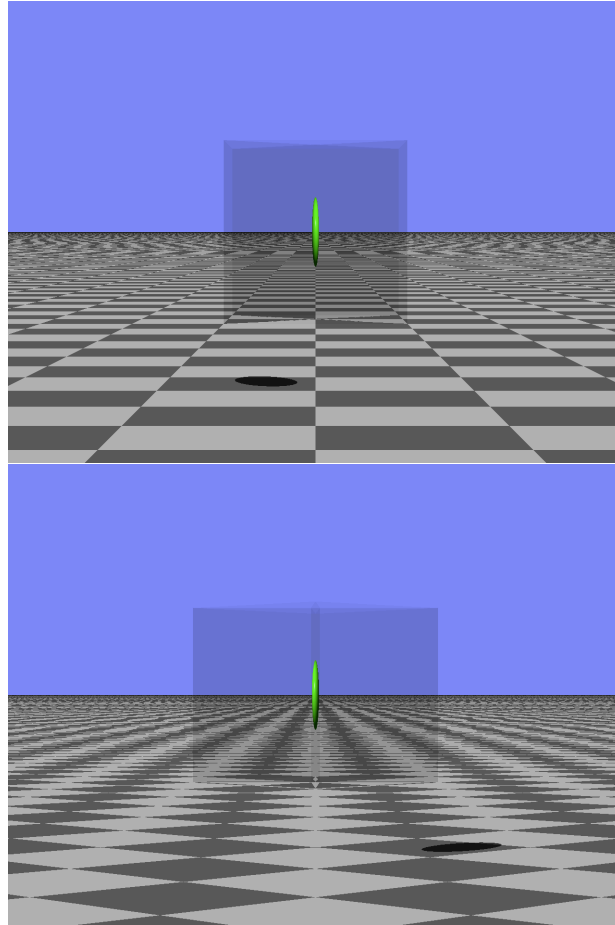


FIGURE 6.9: View through the square prismatic cloak from a view orthogonal to one of the outer faces (top) and a view looking directly at one of the edges (bottom).

### 6.3.3 Carpet Cloak

Another cloak which is of interest is the carpet cloak. Unlike other cloak designs, carpet cloaks do not ensure that all light rays continue along their original trajectory after passing through the device. Instead, carpet cloaks ensure that ingoing light rays which are intending to intersect the plane on which the cloak rests are redirected such that they appear as reflections off this plane after passing through the cloak [39], while all other light rays reemerge along their original trajectories. There have been several attempts at carpet cloaking [40–42]. These devices have all been designed using transformation optics and executed using metamaterials with spatially varying optical properties, however other designs have been suggested which require discrete coordinate transformations [43]. We proceed in the similar way, though of course we use gCLAs to achieve our discrete coordinate transformations and as such our

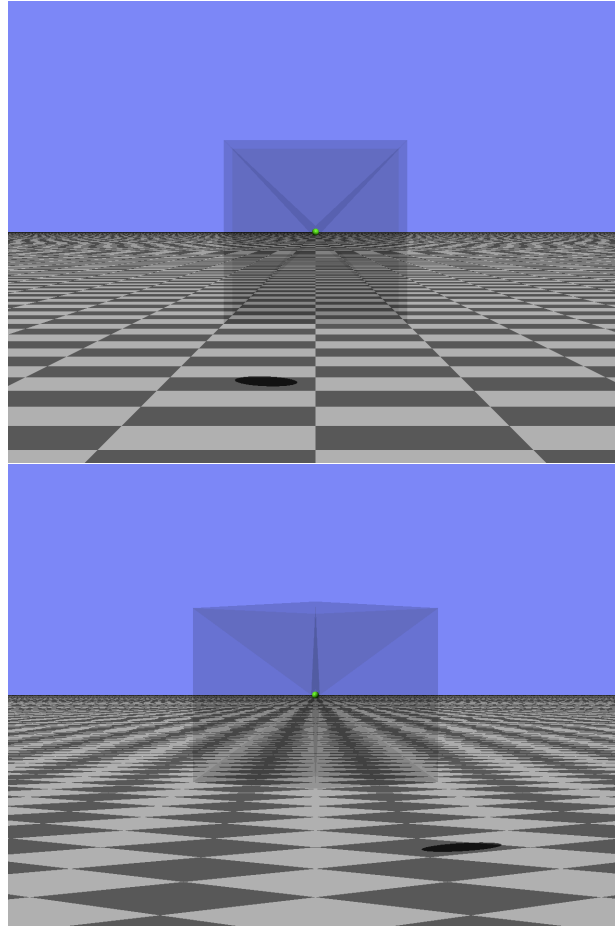


FIGURE 6.10: View through the cubic cloak from a view orthogonal to one of the outer faces (top) and a view looking directly at one of the edges (bottom).

device will only work geometrically and not wave-optically. For example, consider Fig.6.11. Here the rays are being “reflected” off the plane at the bottom of the device. This device can be understood in terms of transformation optics, however it is more complicated than the devices which we have described thus far as there are mirrors involved. As such, the device has to image any position outside of itself to one of two different image positions depending on the viewing direction of an observer. Hence, any light rays passing through the carpet cloak will be redirected around the central region and leave the cloak along their original trajectory. However, if the ingoing light rays are heading towards the lower plane of the device, then a different process takes place. The purpose of the carpet cloak is to give the illusion that these ingoing rays are being reflected off the lower plane of the device. As a result, when an observer looks towards the lower plane of the device, the carpet cloak must image object positions so that they appear as reflections across the lower plane of the device. This is easily shown algebraically. Consider a point lying on the lower ray on the left hand

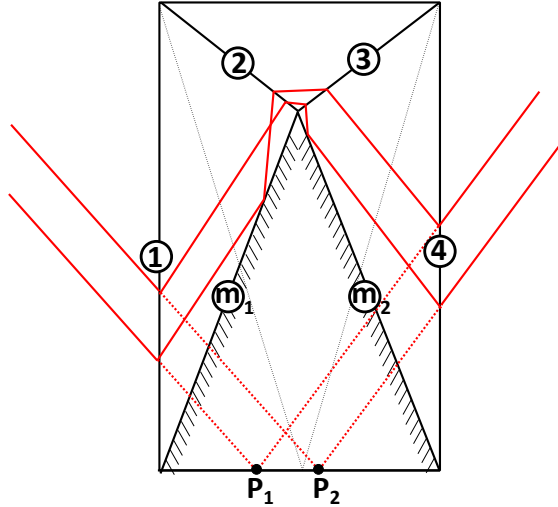


FIGURE 6.11: A carpet cloak could in principle be built using gCLAs and exotic mirrors. If the gCLAs have the same properties as they do for an insulation window, then the mirrors have to have inhomogenous reflection properties.

side of the carpet cloak. This point will first be imaged by gCLA **1**. After imaging by gCLA **1**, according to the transformation required, the imaged point must then be reflected by mirror  $m_1$ . After reflection by  $m_1$ , the resulting point must then be imaged through gCLA **2**, then gCLA **3** and finally gCLA **4**, such that the final image point is a reflection of the original object point across the lower plane of the device. We see that the region bounded by gCLA **1**, mirror  $m_1$  and gCLA **2** plays host to two coordinate systems, the first corresponding to the coordinate system introduced by gCLA **1** and the second corresponding to this same coordinate system after it has been reflected in mirror  $m_1$ . The overall transformation is given by

$$\Lambda_4 \Lambda_3 \Lambda_2 \Lambda_{m_1} \Lambda_1. \quad (6.13)$$

So we see that any given point in object space can be imaged in two different ways by a carpet cloak. In this sense the carpet cloak is more like two devices merged together than a true transformation optics device, as the imaging observed depends upon the viewing direction of the observer. While a carpet cloak, as shown in Fig.6.11, is more complicated than other devices presented thus far, it is in principle possible to create one. One aspect of this design which would be hard to create would be the mirrors  $m_1$  and  $m_2$ . Clearly these have to be flat mirrors performing coordinate transformations much more complicated than conventional component flipping. How these mirrors could be built is not clear, but it is not unreasonable to assume they could become a reality in the future.

## 6.4 Recent developments

In recent months our work on piecewise transformation optics has been expanded. We are now able to consider devices not just comprised of homogeneous gCLAs, but glenses and lenses as well [44]. For example, a simpler cloaking design has been achieved, as shown in Fig. 6.12. Here we have two concentric cubes joined by diagonal

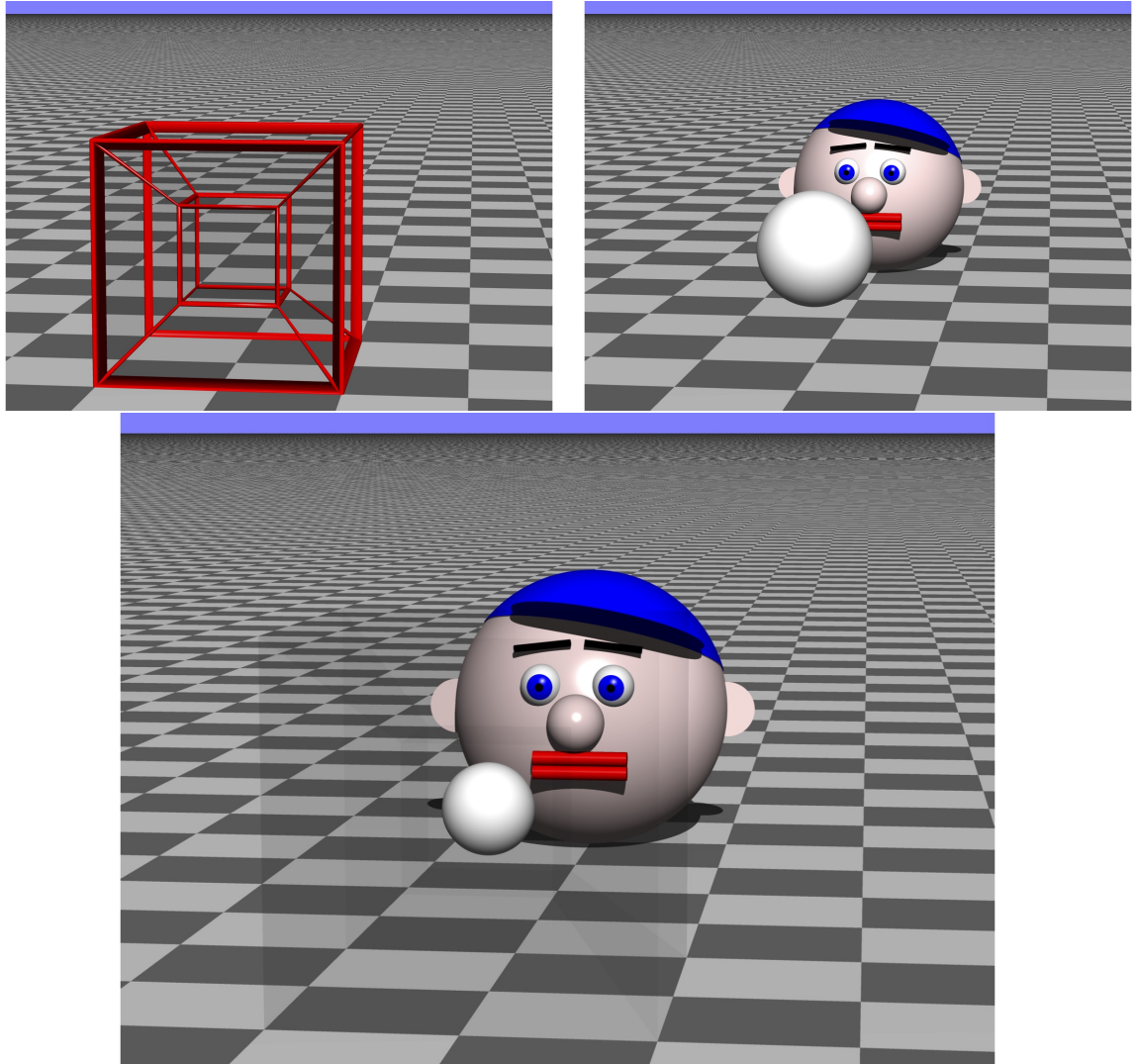


FIGURE 6.12: A cloak designed using glenses and lenses. The cloak is constructed from two concentric cubes joined together by diagonal interfaces (top left). The faces of the inner and outer cube are spanned by glenses, while the diagonal faces are traditional lenses. For sample glens parameters see Table 9.2 in the Appendix. The cloak suffers the same flaw that all cloaks have; the object can never be completely cloaked, only shrunk.

interfaces. The faces of the cubes are spanned by glenses, while the diagonal faces

are lenses. This design has the benefit of being, in principle, easier to assemble, but more importantly, because some of the interfaces are lenses, the image quality should be superior to a cloak constructed entirely from gCLAs, as the light passing through the cloak will not be further pixellated when passing through the lenses.

We have also started looking at whether or not it is possible to construct transformation optics devices purely using lenses. We have, thus far, managed to show that such a device can be created. Whilst not a cloak, the device shown in Fig.6.13 is an exciting discovery as this device will not pixellate the image it produces. It is a triangular based pyramid with two smaller pyramids located inside, much like a Russian doll system. The peaks of the three pyramids are connected at their bottom corners as they share a common base, and also at their peaks by interconnecting lenses. As can be seen from the ray tracing simulation, the device produces the correct background image. For sample lens parameters for simulation purposes see Table 9.3 in the Appendix. Surprisingly, two of these pyramid structures, can be used to create a completely omnidirectional cloak. We explain this now.

### 6.4.1 Omnidirectional cloak constructed from lenses

In order to show how the previously mentioned device can be used to create a cloaking device, at least in the sense we have discussed previously where the object is only shrunk rather than truly cloaked, we first have to understand how the device works. In order to do this we place an object, in this case a green ball, inside the device. Specifically we place the ball in the space bounded by the smallest inner pyramid of the device. As can be seen in Fig.6.14, the green ball appears to be compressed, predominantly in the vertical direction, when compared to the green ball of the same size which is positioned outside the device. Recall we observed a similar effect with the square prismatic cloak in Fig.6.9. The effect here is of the same kind which suggests that by placing inside the ball inside two tetrahedra whose bases are at right angles to one another, one can compress in both the horizontal and the vertical directions. Of course in order to achieve this one of the tetrahedra has to fit inside the smallest inner pyramid of the other. A possible set up achieving this is given in Fig.6.15. We see in the upper image the outline of the structure of the two tetrahedra. The lower image shows the simulated through such a device. As expected, the combined effect of both the tetrahedra has compressed the ball hidden inside in both the horizontal and vertical directions. If this device could be built this

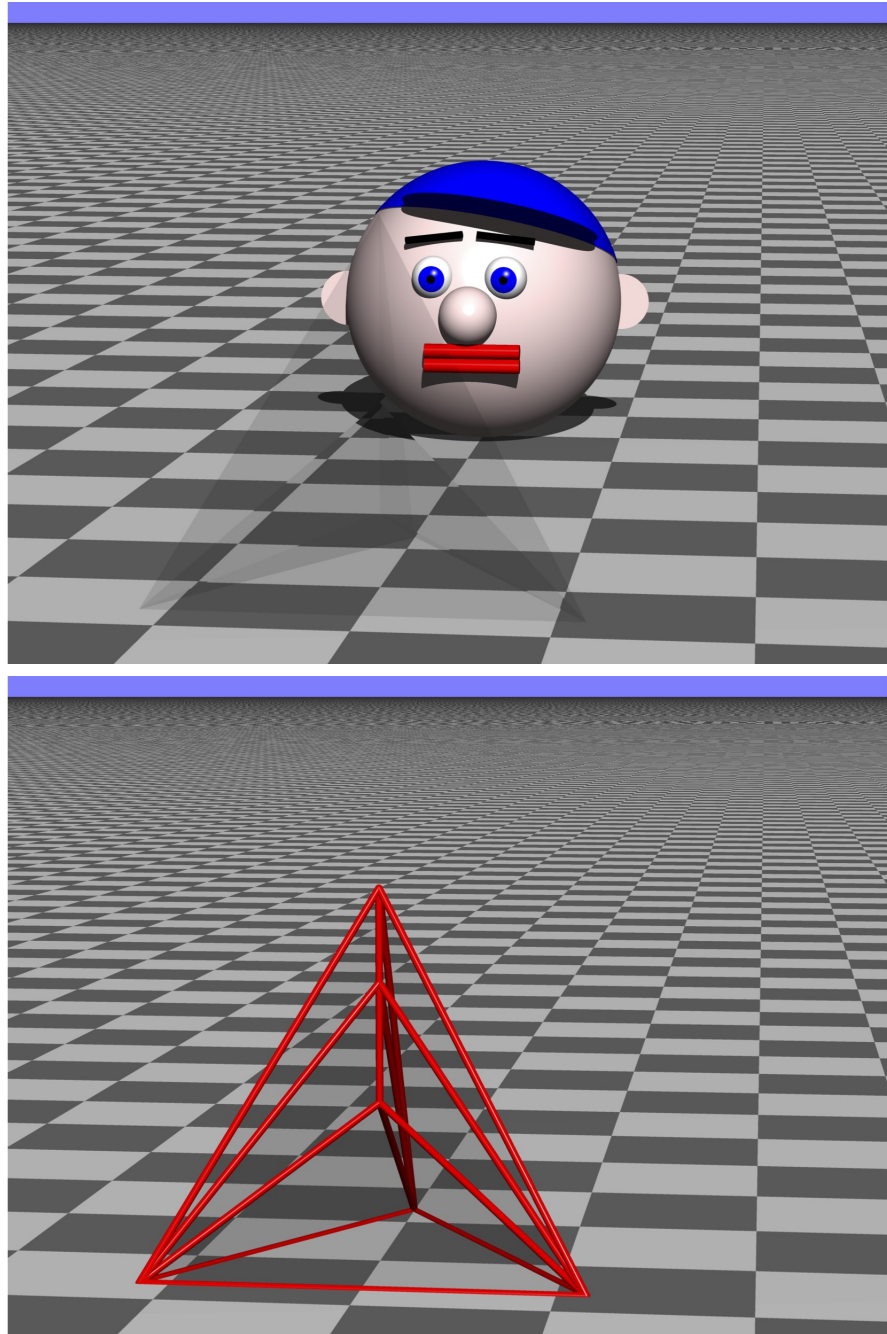


FIGURE 6.13: A ray tracing simulation of a transformation optics device constructed entirely from lenses. The upper image shows the view through the device, whilst the lower image shows, using red lines, the lines where the constituent lenses intersect.

would be the world first “honest” visible spectrum, omnidirectional cloak. But can we make it any better? It is clear that the inner tetrahedron is floating inside the larger tetrahedron. In practice this is impossible and so the smaller tetrahedron would have to be supported in some way. This suggests we try and construct a new device where

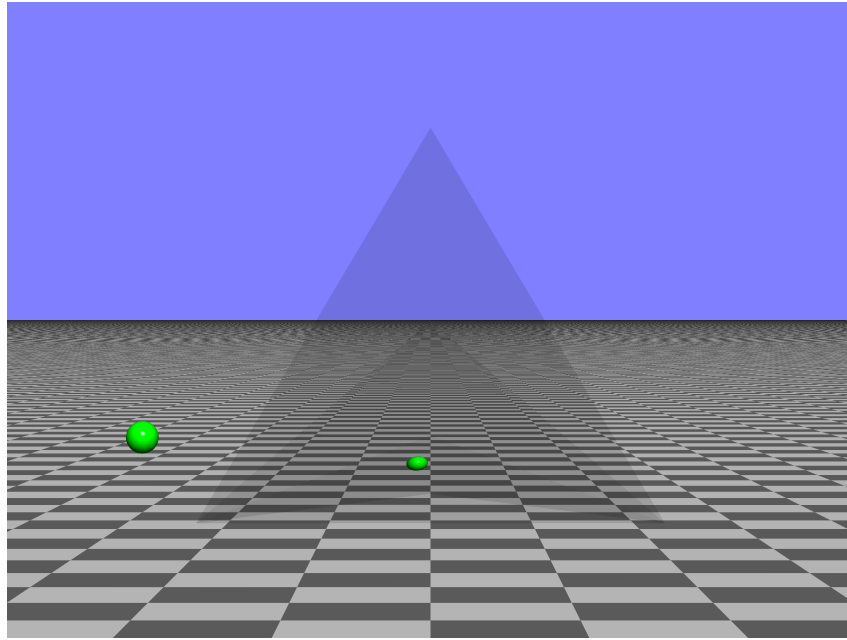


FIGURE 6.14: A raytracing simulation of a green ball set inside a tetrahedral transformation-optics device made entirely from lenses. In comparison to the green ball positioned outside the device, we see that the green ball positioned within the smallest internal pyramid of the device has been compressed significantly in the vertical direction.

the two tetrahedron are, by construction, connected. What follows is speculation - no detailed analysis of this composite device has been performed to date.

One possible idea to achieve the required structure is to transform the smaller of the two tetrahedra such that it completely fills the volume of the smallest pyramid in the larger tetrahedron. This in principle should be possible, but it is not guaranteed that the overall device would still act like a cloak. The reasons are as follows. Notice in Fig.6.14 that while the ball is compressed in the vertical direction, it has also, to a lesser extent, been compressed in the horizontal direction. Intuitively we can think of the vertical compression as being aligned with the “axis” of the pyramid, i.e. the axis which runs down the centre of the device through the peaks of all the pyramids inside it. If we transform our interior tetrahedron, it stands to reason that its compression axis would change also. This in turn would mean that the ball would not be compressed in the correct way, as the compression would be a combination of vertical compression from the larger tetrahedron and compression along some diagonal line due to the smaller tetrahedron. Detailed calculations and simulations would need to be performed to see how such a device would compress and if we have any control over the axis of compression for it. Assuming that it

was possible to construct the device such that it fit the required volume and also compressed in the correct direction, the next question would be to see if the inner tetrahedron's surfaces could be chosen such that its outer surfaces had the same properties as the surfaces of the smallest pyramid inside the larger tetrahedron. If this was possible, the two tetrahedra would be seamlessly joined.

## 6.5 Conclusion

In this chapter we have shown how gCLAs which are perfectly imaging can be used to build piecewise transformation optics devices such as invisibility cloaks. These devices have the advantage over conventional transformation optics devices that they are, in principle, much cheaper to construct and do not suffer from the same bandwidth restrictions. Indeed, because gCLAs are constructed from lenslets made of conventional dielectrics, they can refract light from across the entire visible spectrum and of any polarisation. However, because gCLAs themselves are pixellated, the outgoing image will also be pixellated. Further to this, even if the same devices could be made using interfaces which behave like gCLAs, but without pixellation, the ingoing phase would still, in general, be broken up on passing through the device, as the law of refraction for the interfaces would still be wave-optically forbidden. As such whilst bypassing most of the limitations of conventional transformation optics devices, piecewise transformation optics devices designed using gCLAs introduce their own compromises.

We also presented some preliminary theoretical results showing cloaks constructed from glenses and lenses and finally a possible design for cloaking completely using lenses. Our work on transformation optics is still ongoing, and our work with lenses in particular is still in its infancy. In future more work will have to be done to understand how lenses can be used to create general transformation optics devices. A part of this will involve expanding our ideas on transformation around loops. Currently all our devices are zero-curvature devices. However, it may be possible to arrange gCLAs, glenses and lenses in such a way as to create new, more exotic devices which mimic curved spaces.

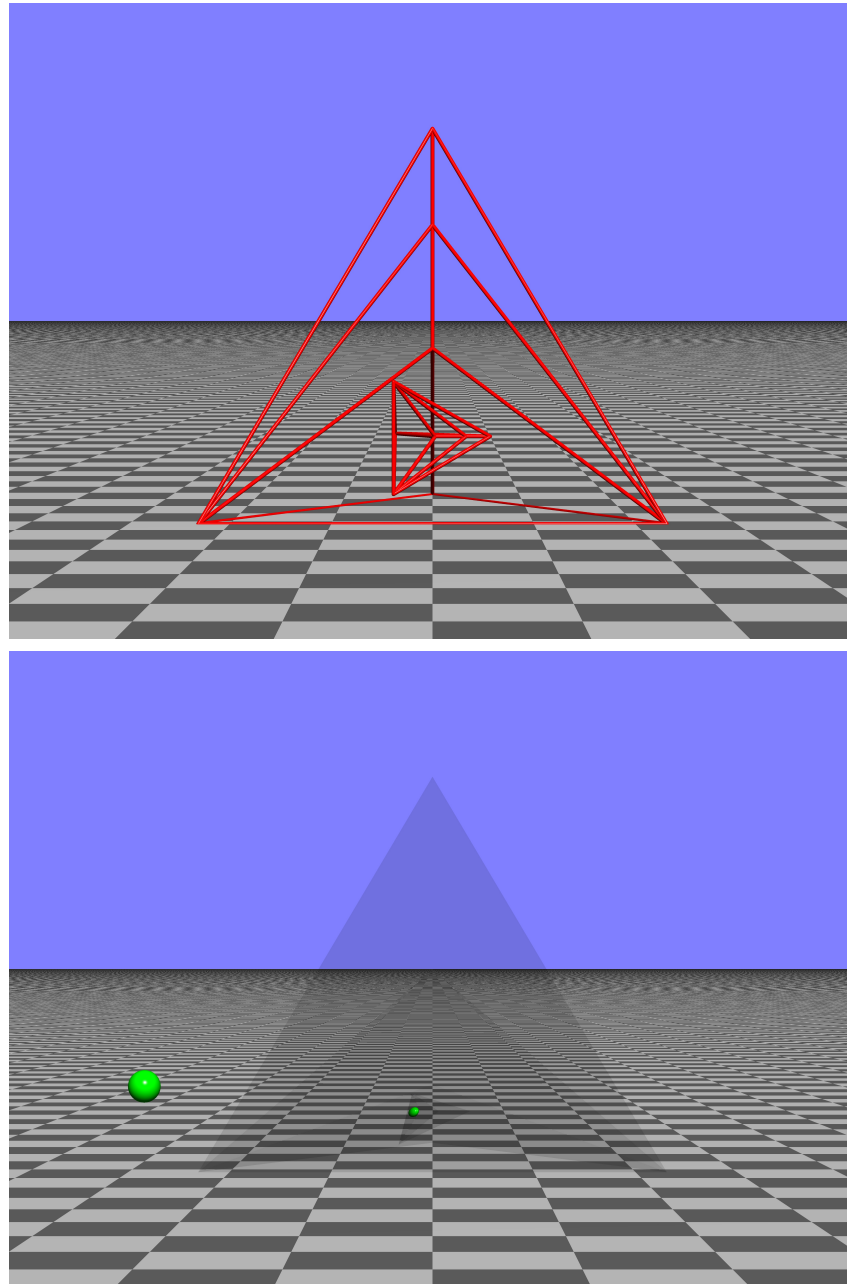


FIGURE 6.15: One possible configuration to achieve cloaking using two transformation-optics tetrahedra. Upper image: using red lines to show where the lenses intersect, we can outline the structure of a possible omnidirectional cloak. In this case we have positioned a smaller transformation-optics tetrahedron inside the smallest internal pyramid of a larger transformation-optics such that the bases of the two tetrahedra are at right angles. Lower image: The simulated view through such a device. As can be seen the ball placed inside the composite device has been compressed in both the vertical and horizontal directions.

# Chapter 7

## Geometrical imaging into abstract spaces

### 7.1 Introduction

We have seen in previous chapters that a sophisticated mathematical approach can be implemented when describing the refraction and imaging performed by gCLAs, and that this implementation leads in a straight forward way towards the realisation of pixellated transformation optics. In this chapter we attempt to do the same for our second type of metarefracting sheets: ray-rotation sheets. Ray-rotation sheets are, as the name suggests, sheets which rotate light rays. In the simplest case, which we consider here, they rotate light rays around the sheet normal. Previously it was shown that ray-rotation sheets can be modelled as the interface between two isotropic materials which have a complex refractive-index ratio [18]. It is known that for paraxial rays, crossing a planar interface, Snell's law is imaging. This suggests that an interface which behaves according to Snell's law, even if one of the refractive indices is complex, must also be imaging, at least paraxially, and that the resulting image becomes complex. This indeed was shown in [18] where it was found that for a ray-rotation sheet placed in the  $z = 0$  plane the  $x$ -component and  $y$ -component of the original object point were unchanged, but the  $z$ -component was transformed as

$$z' = -\exp(-i\alpha)z, \quad (7.1)$$

where  $\alpha$  is the angle of rotation. Motivated by this result we attempted to derive a general imaging equation for complex positions across an interface using the same approach used to find the imaging equation for a real position across an interface [24]. This approach immediately runs into problems however as while the object positions are complex, the positions on the interface have to be real. However, the method used for deriving the real imaging equations would lead to the positions on the interface to be complex. Consequently, a new approach has to be adopted which deals with the complex positions indirectly.

In what follows we will define how a complex position is related to a real position and using this definition derive a number of results which highlight the difference between real space and complex space. We will then use these results to attempt to derive a general imaging equation for complex positions across a planar interface as well as applying them to other systems of interest.

### 7.1.1 Contributions

The ideas in this chapter concerning light rays and how they intersect positions in complex space is the result of collaboration between myself and Johannes Courtial. The work on the equivalence between gCLA imaging and ray-rotation was undertaken by myself, as was the group theory discussion at the end of the chapter.

## 7.2 Definition of a complex position and the light rays which pass through it

We start by defining a complex position  $\mathbf{P} = \mathbf{P}_r + i\mathbf{P}_i$ , and state that a light ray with direction  $\hat{\mathbf{a}}$  passes through  $\mathbf{P}$  if and only if the ray also passes through the corresponding real position

$$\mathbf{C} = \mathbf{P}_r + \mathbf{P}_i \times \hat{\mathbf{a}}. \quad (7.2)$$

We call  $\mathbf{C}$  the contact point;  $\mathbf{C}$  is, the closest position in real space to the real part of the complex position that the light ray intersects.

We can qualitatively justify this definition by the following reasoning. A ray-rotation sheet will refract a cone of light rays into a hyperboloid as shown in Fig.7.1. The

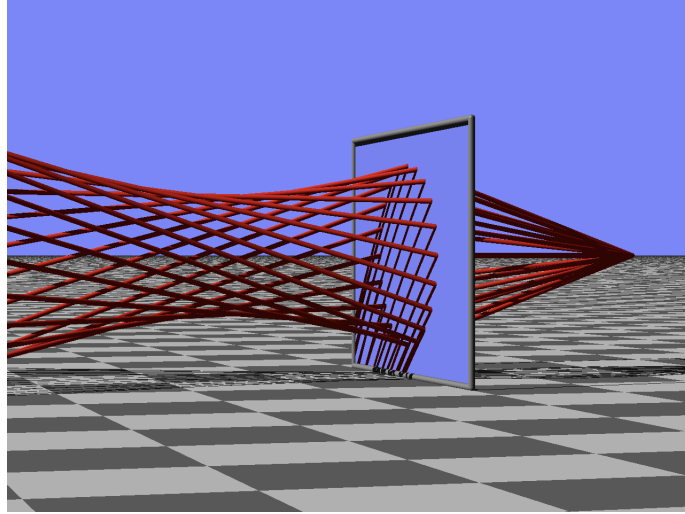


FIGURE 7.1: A ray-rotation sheet which rotates light rays by  $140^\circ$ . A cone of light rays is transformed into a hyperboloid of light rays. Before rotation, the light rays share a common intersection point whilst after rotation the light rays share a common hyperboloid waist. We can think of the ray-rotation sheet as mapping the intersection point before the sheet to a complex position after the sheet, which is physically manifested as a hyperboloid, via our definition of the contact point defined in Eq.(7.2).

light rays in our cone are refracted such that they intersect a ring which encircles the central point of the hyperboloid. If the position before the sheet where the rays intersect is imaged into a complex position then it would appear that the central point of the hyperboloid is somehow related to the complex position. Intuitively we assume this must be true, as before the sheet the light rays shared an intersection point and after refraction through the sheet they share proximity to the hyperboloid centre. So whilst we cannot explicitly see this new complex position, we can see the ring of positions where the light rays pass through. Because the points on this ring where the light rays intersect are surrounding the central position at the hyperboloid waist, we say that this is the closest contact that the real light rays can make with the complex position and hence we call them contact points.

The contact point  $\mathbf{C}$  always lies on a disc of radius  $|\mathbf{P}_i|$  which is orthogonal to  $\mathbf{P}_i$  and centred on  $\mathbf{P}_r$ . Precisely where the contact point lies on the disc depends on the light-ray direction  $\hat{\mathbf{a}}$ . The contact point is a distance  $|\mathbf{P}_i \times \hat{\mathbf{a}}|$  from the centre and clearly  $|\mathbf{P}_i \times \hat{\mathbf{a}}|$  is a maximum when  $\mathbf{P}_i$  and  $\hat{\mathbf{a}}$  are orthogonal and  $|\mathbf{P}_i \times \hat{\mathbf{a}}| = |\mathbf{P}_i|$ . If  $\mathbf{P}_i = 0$  then the contact point coincides with  $\mathbf{P}_r$ , and we are once again dealing with positions in conventional space.

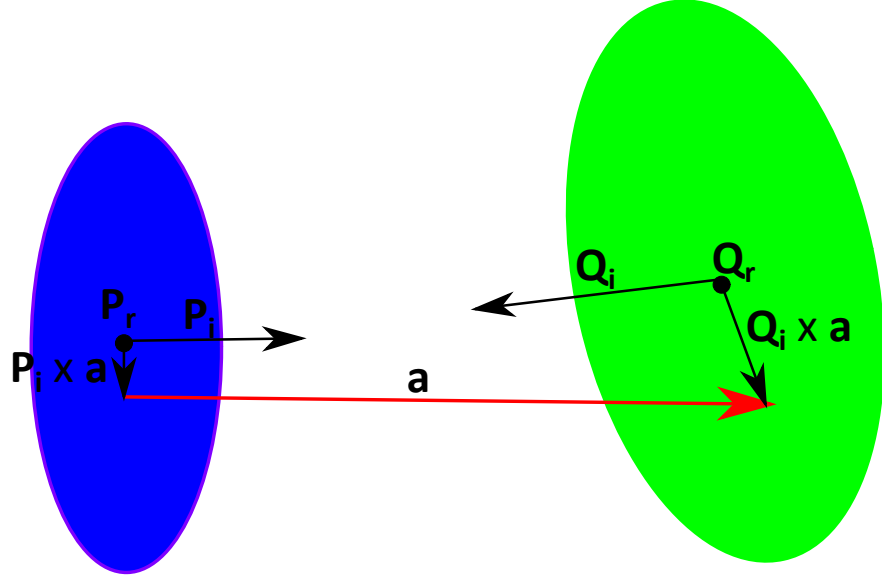


FIGURE 7.2: A visual representation of a light ray passes between two complex positions in real space. The light ray with direction  $\hat{\mathbf{a}}$  passes between the two contact points  $|\mathbf{P}_i \times \hat{\mathbf{a}}|$  and  $|\mathbf{Q}_i \times \hat{\mathbf{a}}|$ . For the case of the complex position  $\mathbf{P}$ , the contact point lies on a disc of radius  $|\mathbf{P}_i|$  and is a distance  $|\mathbf{P}_i \times \hat{\mathbf{a}}|$  from  $\mathbf{P}_r$ , the centre of the disc. Similarly expressions hold for the complex position  $\mathbf{Q}$ .

We can use our definition of the contact point to learn about how complex positions differ from their real counterparts. What follows are a number of intriguing properties concerning light rays in complex space which arise from our definition of the contact point.

### 7.2.1 Uniqueness of complex positions

If a light ray with direction  $\hat{\mathbf{a}}$  intersects two complex positions,  $\mathbf{P}$  and  $\mathbf{Q}$ , then  $\mathbf{P}$  and  $\mathbf{Q}$  are related by the following relation

$$\Delta_r + \Delta_i \times \hat{\mathbf{a}} - \alpha \hat{\mathbf{a}} = 0, \quad (7.3)$$

where  $\Delta_r = \mathbf{Q}_r - \mathbf{P}_r$  and  $\Delta_i = \mathbf{Q}_i - \mathbf{P}_i$ . This is because the contact positions for  $\mathbf{P}$  and  $\mathbf{Q}$ ,  $\mathbf{C}$  and  $\mathbf{D}$  respectively, lie on the light ray and so it must be true that  $\mathbf{D} = \mathbf{C} + \alpha \hat{\mathbf{a}}$ .

We now wish to see whether or not all light rays passing through  $\mathbf{P}$  also pass through  $\mathbf{Q}$ . Let us assume in the first instance that any light ray intersecting  $\mathbf{P}$  also intersects  $\mathbf{Q}$ . It must then follow that Eq.(7.3) holds for any light ray direction  $\hat{\mathbf{a}}$  when used

in conjunction with the complex positions  $\mathbf{P}$  and  $\mathbf{Q}$ . Consider the light ray which is perpendicular to  $\Delta_i$ , that is where  $\hat{\mathbf{a}} \perp \Delta_i$ . The second term in Eq.(7.3) is always perpendicular to both  $\Delta_i$  and  $\hat{\mathbf{a}}$ . We know also that  $\hat{\mathbf{a}}$  is perpendicular to  $\Delta_i$ , hence it must be true that the first term in Eq.(7.3),  $\Delta_r$ , is perpendicular to  $\Delta_i$ , that is  $\Delta_r \perp \Delta_i$ . We now consider a light ray which is parallel to  $\Delta_r$ , i.e.  $\hat{\mathbf{a}} \parallel \Delta_r$ . In this case clearly the first and third terms of Eq.(7.3) are parallel to  $\Delta_r$ . This implies that the second term is also parallel to  $\Delta_r$ , however the second term must be perpendicular to the light ray and hence  $\Delta_r$ . The only way around this issue is if the second term is zero and hence  $\Delta_i \parallel \Delta_r$ . We have considered only two light rays and have already seen that the conditions they require the complex positions to meet cannot be reconciled. Clearly then arbitrary light rays will not, in general pass through the same two complex positions.

### 7.2.2 Choosing light rays which pass through two complex positions

We know that if a light ray passes through two complex positions that it automatically satisfies Eq.(7.3) for those two positions. Hence, given two complex positions  $\mathbf{P}$  and  $\mathbf{Q}$  we can, using Eq.(7.3), find the light ray which passes between them.

We start by noting that the cross product term in Eq.(7.3) can be written in matrix form:

$$\Delta_i \times \hat{\mathbf{a}} = \mathbf{M} \cdot \hat{\mathbf{a}} = \begin{pmatrix} 0 & -\Delta_{iz} & \Delta_{iy} \\ \Delta_{iz} & 0 & -\Delta_{ix} \\ -\Delta_{iy} & \Delta_{ix} & 0 \end{pmatrix} \cdot \begin{pmatrix} a_x \\ a_y \\ a_z \end{pmatrix}, \quad (7.4)$$

and so too can the  $\alpha \hat{\mathbf{a}}$  term

$$\alpha \hat{\mathbf{a}} = \alpha \mathbf{I} \cdot \hat{\mathbf{a}} = \begin{pmatrix} \alpha & 0 & 0 \\ 0 & \alpha & 0 \\ 0 & 0 & \alpha \end{pmatrix} \cdot \begin{pmatrix} a_x \\ a_y \\ a_z \end{pmatrix}. \quad (7.5)$$

We can therefore re-write Eq.(7.3) as

$$\Delta_r - \mathbf{K} \cdot \hat{\mathbf{a}} = 0, \quad (7.6)$$

where  $\mathbf{K} = \alpha \mathbf{I} - \mathbf{M}$ . It is then simply a matter of multiplying Eq.(7.6) by the inverse matrix for  $\mathbf{K}$  to find the light-ray direction  $\hat{\mathbf{a}}$ . On performing this calculation, we

find that the light-ray direction is given by

$$\mathbf{a} = \frac{\Delta_i(\Delta_i \cdot \Delta_r) + \alpha^2 \Delta_r + \alpha \Delta_i \times \Delta_r}{\alpha(\alpha^2 + \Delta_i^2)}. \quad (7.7)$$

We see that this is a function of  $\alpha$ , which is a problem, as the light-ray direction should not depend on the distance between the two complex positions. However by insisting that the light-ray direction is normalised, we can solve for  $\alpha$ . On doing so it is found that  $\alpha$  is given by

$$\alpha = \pm \frac{\sqrt{\Delta_r^2 - \Delta_i^2 \pm \sqrt{(\Delta_r^2 - \Delta_i^2)^2 + 4(\Delta_i \cdot \Delta_r)^2}}}{\sqrt{2}}. \quad (7.8)$$

On substituting Eq.(7.8) into Eq.(7.7) the normalised light-ray direction is found. We see in Eq.(7.8) that there are four mathematically possible solutions for  $\hat{\mathbf{a}}$  as there are  $\pm$  symbols both before and under the square root. However on closer examination we see that some of these solutions can be ignored. Consider the  $\pm$  under the square root in the numerator of Eq.(7.8). If the  $-$  symbol is used we see that the number under the square root is negative, which in turn means that  $\alpha$  and therefore  $\hat{\mathbf{a}}$  is complex. We can therefore ignore the solutions for  $\alpha$  which use the  $-$  symbol under the square root, as these result in unphysical light-ray directions. We are therefore only able to consider solutions which use the  $+$  under the square root. This then leaves us with two choices of  $\alpha$  as we are still free to choose whether or not the overall expression is positive or negative. We will now examine these two cases as it will show clearly the unusual nature of our complex space. First of all we consider the case where the imaginary parts of  $\mathbf{P}$  and  $\mathbf{Q}$  are zero. In this case we see that  $\alpha = \pm \|\Delta_r\|$  and subsequently that  $\hat{\mathbf{a}} = \pm \Delta_r / \|\Delta_r\|$ . This is exactly what we expect when dealing with real positions, as if the  $\alpha$  is chosen which uses the  $+$  symbol we see that this corresponds to the ray passing from  $\mathbf{P}$  to  $\mathbf{Q}$  while if the  $\alpha$  which uses the  $-$  symbol is chosen it corresponds to the ray passing from  $\mathbf{Q}$  to  $\mathbf{P}$ . In summary, the two light rays which pass between  $\mathbf{P}$  and  $\mathbf{Q}$  are simply the reverse of one another. We now compare this to the general complex case. First we consider the case where  $\hat{\mathbf{a}}$  is constructed with the  $\alpha$  which uses the  $-$  symbol. In this case we see that the first and second terms in Eq.(7.7) will be negative, while the third term will be positive. In the case where  $\hat{\mathbf{a}}$  is constructed with the  $\alpha$  which uses the  $+$  symbol, all three terms are positive. So we see that in complex space that switching the sign of  $\alpha$  does not simply correspond to reversing the light ray. Thus we can say that for any two complex positions, there are two unique light rays which pass through them both.

In trying to decide which light ray to choose when performing a calculation, one has to consider the system at hand. This will be shown when we look at applications of these results.

### 7.2.3 Finding the intersection point of two light rays in complex space

In real space, two light rays can always be shown to intersect at a unique real position (or at  $\pm\infty$ ) if they lie in a common plane. It is reasonable to assume that these same two light rays will also intersect at a unique complex position in complex space. We will show however, that this is not the case, and that two light rays can intersect at an infinite number of complex positions.

Consider the two light rays which we assume pass through the complex position  $\mathbf{P}$ :

$$\begin{aligned} \mathbf{A}_1 + \alpha_1 \hat{\mathbf{a}}_1 - \mathbf{P}_r - \mathbf{P}_i \times \hat{\mathbf{a}}_1 &= 0, \\ \mathbf{A}_2 + \alpha_2 \hat{\mathbf{a}}_2 - \mathbf{P}_r - \mathbf{P}_i \times \hat{\mathbf{a}}_2 &= 0. \end{aligned} \tag{7.9}$$

We wish to find  $\mathbf{P}_r$  and  $\mathbf{P}_i$ . Trying to solve directly for  $\mathbf{P}_r$  and  $\mathbf{P}_i$  using Eq.(7.9) results in a system of linear equations which is singular. As such it is therefore impossible to get linearly independent expressions for the components of  $\mathbf{P}_r$  and  $\mathbf{P}_i$ . However we can find a region of possible positions where the two rays intersect. First of all we note that while we cannot find a solution where all the components of the complex position are linearly independent, if some of the components are set to zero we can find a solution where the remaining components are linearly independent. This would then give us one possible intersection position in complex space, however it does not give us all of them. We know that the components of Eq.(7.9) each have to simultaneously equal zero, as such they must all be equal along some line of complex positions. By considering each of the components of Eq.(7.9) to be a hyperplane in a six dimensional real space (where the six dimensional space arises because we have combined the three real and the three imaginary components of complex space), we can find the gradients of each of the components and then construct a nullspace for the gradients. The basis vectors of the null space are by definition orthogonal to all the gradients of the hyperplanes corresponding to the components, and as such must lie on the intersection of the hyperplanes. In practice one is left with only one basis

vector which spans the null space, and so one can find a subspace of points, all of which are possible intersection points for the two rays, by using an initial intersection point and a vector proportional to the basis vector which passes through it.

### 7.2.4 Finding the intersection point of three light rays in complex space

In real space light rays are one-dimensional and so have codimension 2 (as real space is three dimensional and the light rays are one-dimensional, hence the codimension is  $3 - 1 = 2$ ). We now show that in complex space light rays also have codimension 2. We start with Eq.(7.2) and write  $\mathbf{C} = \mathbf{A} + \alpha \hat{\mathbf{a}}$ :

$$\mathbf{C} = \mathbf{P}_r + \mathbf{P}_i \times \hat{\mathbf{a}} = \mathbf{A} + \alpha \hat{\mathbf{a}}. \quad (7.10)$$

We then rearrange for  $\mathbf{P}_r$ :

$$\mathbf{P}_r = \mathbf{A} + \alpha \hat{\mathbf{a}} - \mathbf{P}_i \times \hat{\mathbf{a}}. \quad (7.11)$$

Using this we can then write our complex position  $\mathbf{P}$  as a six dimensional vector,

$$\begin{pmatrix} P_{r,x} \\ P_{r,y} \\ P_{r,z} \\ P_{i,x} \\ P_{i,y} \\ P_{i,z} \end{pmatrix} = \begin{pmatrix} A_x \\ A_y \\ A_z \\ 0 \\ 0 \\ 0 \end{pmatrix} + \alpha \begin{pmatrix} \hat{a}_x \\ \hat{a}_y \\ \hat{a}_z \\ 0 \\ 0 \\ 0 \end{pmatrix} + P_{i,x} \begin{pmatrix} 0 \\ \hat{a}_z \\ -\hat{a}_y \\ 1 \\ 0 \\ 0 \end{pmatrix} + P_{i,y} \begin{pmatrix} -\hat{a}_z \\ 0 \\ \hat{a}_x \\ 0 \\ 1 \\ 0 \end{pmatrix} + P_{i,z} \begin{pmatrix} \hat{a}_y \\ -\hat{a}_x \\ 0 \\ 0 \\ 0 \\ 1 \end{pmatrix}, \quad (7.12)$$

where the vectors multiplied by  $\alpha$ ,  $P_{i,x}$ ,  $P_{i,y}$  and  $P_{i,z}$  are linearly independent basis vectors in our new six-dimensional complex space. As the points  $\mathbf{P}$  lie along the trajectory of the light ray, we can say that in our six dimensional space, light rays

are four-dimensional objects, as they lie on a four-dimensional subspace of the six-dimensional space. As such, light rays in complex space also have codimension 2.

Because of this we can state that we require three light rays to uniquely determine a complex position in complex space. The reason for this is easily understood by comparing with an analogy in three dimensional real space. Consider a plane of constant  $z$  in three dimensional space. The  $z$ -component of all points lying in this plane is fixed while we are free to choose the  $x$  and  $y$  components. If we now intersect the plane of constant  $z$  with a plane of constant  $y$ , the points on the line where these planes intersect have both their  $y$  and  $z$  components fixed. Finally if we intersect these two planes with a plane of constant  $x$ , the  $x$  component is fixed and we see that the three planes intersect at a single point. Hence the two dimensional planes, which have co-dimension 1, each fix one component of the intersection point. By analogy, in our six dimensional complex space, our four dimensional light rays in complex space which have co-dimension 2, each fix two components of an intersection point, and since our space is six dimensional, we therefore have to use three light rays to find the unique intersection point. This is backed up by the result of the previous section which stated that two light rays in complex space intersected at an infinite number of potential positions in a subspace of complex space. In order to find a unique position for the intersection, we would require a third light ray.

The intersection point is calculated as follows. We take three light rays which we assume all pass through the complex position  $\mathbf{P} = \mathbf{P}_r + i\mathbf{P}_i$  and hence satisfy

$$\begin{aligned}\mathbf{A}_1 + \alpha_1 \hat{\mathbf{a}}_1 &= \mathbf{P}_r + \mathbf{P}_i \times \hat{\mathbf{a}}_1, \\ \mathbf{A}_2 + \alpha_2 \hat{\mathbf{a}}_2 &= \mathbf{P}_r + \mathbf{P}_i \times \hat{\mathbf{a}}_2, \\ \mathbf{A}_3 + \alpha_3 \hat{\mathbf{a}}_3 &= \mathbf{P}_r + \mathbf{P}_i \times \hat{\mathbf{a}}_3,\end{aligned}\tag{7.13}$$

and we combine their components into a nine-dimensional vector equation. Specifically in our example, the first, second and third equations in Eq.(7.13) will provide the first three components, the second three components and the third three components respectively. The nine-dimensional vector equation

$$\mathbf{A} - \mathbf{M} \cdot \mathbf{V} = 0,\tag{7.14}$$

is constructed as follows: the first part,  $\mathbf{A}$ , contains the components of  $\mathbf{A}_1$ ,  $\mathbf{A}_2$  and  $\mathbf{A}_3$ :

$$\mathbf{A} = (A_{1,x}, A_{1,y}, A_{1,z}, A_{2,x}, A_{2,y}, A_{2,z}, A_{3,x}, A_{3,y}, A_{3,z})^T, \quad (7.15)$$

while the second part is composed of a nine by nine square matrix,  $\mathbf{M}$ , multiplying the vector  $\mathbf{V}$ , where

$$\mathbf{V} = (P_{r,x}, P_{r,y}, P_{r,z}, P_{i,x}, P_{i,y}, P_{i,z}, \alpha_1, \alpha_2, \alpha_3)^T, \quad (7.16)$$

$$\mathbf{M} = \begin{pmatrix} 1 & 0 & 0 & 0 & a_{1,z} & -a_{1,y} & -a_{1,x} & 0 & 0 \\ 0 & 1 & 0 & -a_{1,z} & 0 & a_{1,x} & -a_{1,y} & 0 & 0 \\ 0 & 0 & 1 & a_{1,y} & -a_{1,x} & 0 & -a_{1,z} & 0 & 0 \\ 1 & 0 & 0 & 0 & a_{2,z} & -a_{2,y} & 0 & -a_{2,x} & 0 \\ 0 & 1 & 0 & -a_{2,z} & 0 & a_{2,x} & 0 & -a_{2,y} & 0 \\ 0 & 0 & 1 & a_{2,y} & -a_{2,x} & 0 & 0 & -a_{2,z} & 0 \\ 1 & 0 & 0 & 0 & a_{3,z} & -a_{3,y} & 0 & 0 & -a_{3,x} \\ 0 & 1 & 0 & -a_{3,z} & 0 & a_{3,x} & 0 & 0 & -a_{3,y} \\ 0 & 0 & 1 & a_{3,y} & -a_{3,x} & 0 & 0 & 0 & -a_{3,z} \end{pmatrix}.$$

By multiplying Eq.(7.14) by  $\mathbf{M}^{-1}$ ,  $\mathbf{V}$ , and hence the intersection point which is the first six components of  $\mathbf{V}$ , can be found.

## 7.3 Applications of complex imaging

### 7.3.1 Complex imaging calculation

When working in ray optics, one often has to calculate ray trajectories and points of intersection when trying to predict the outcome of a system. The results derived above can therefore in principle be utilised to perform similar calculations for complex space. Indeed the motivation for deriving the previous results was the dream of finding the most general imaging system possible using a thin interface. We are now in a position to attempt to derive such an imaging equation. Keeping with the theme of this thesis, we shall outline the steps involved in deriving an imaging equation for complex positions using our definitions. We draw inspiration from the imaging equation derived previously in [24] which assumed that the interface was infinitesimally thin and did not offset light rays. In theory applying the same logic

to our complex imaging calculation, but this time using our results found for light rays in complex space, an imaging equation will present itself.

As with the case of our homogenous imaging equation we derived in a previous chapter, we consider a plane which lies in the  $z = 0$  plane. We will concern ourselves

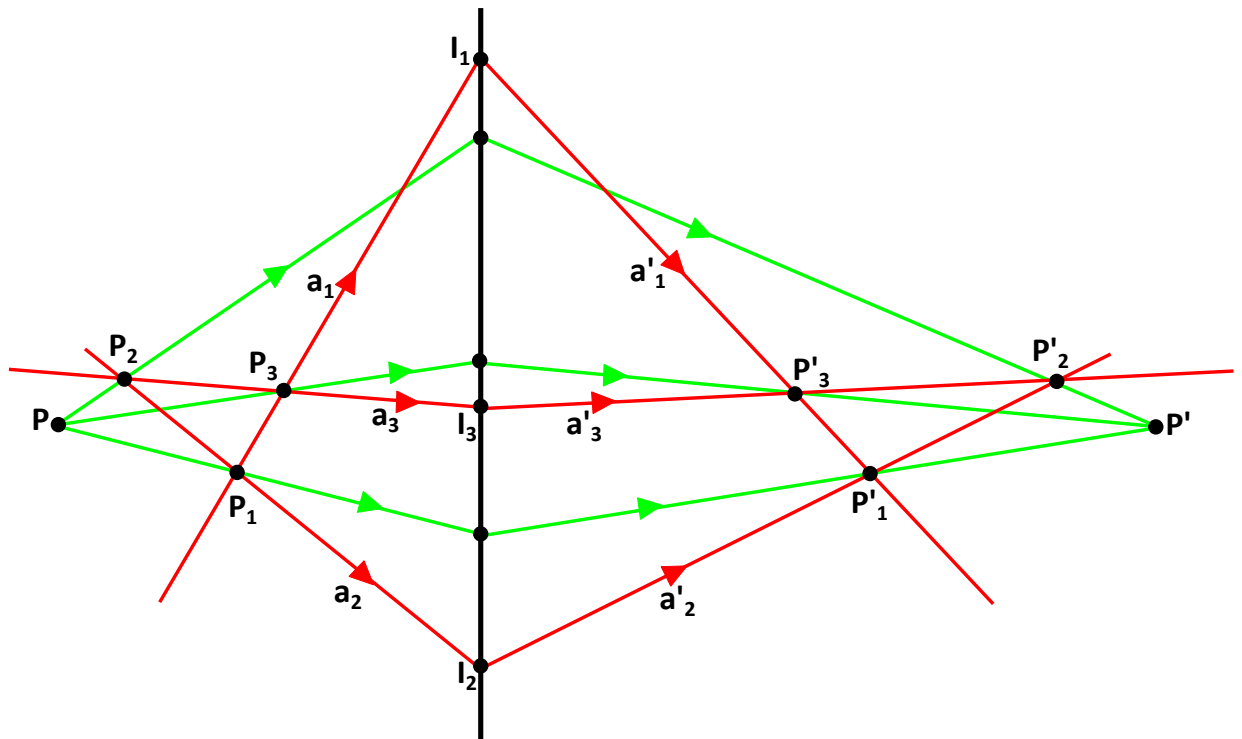


FIGURE 7.3: A two-dimensional representation of our complex imaging system. Primary rays (green) emanate from the object point  $\mathbf{P}$  and refract across the real sheet situated in the  $z = 0$  plane before intersecting again at the image point  $\mathbf{P}'$ . Consistency rays (red) intersect the primary rays before the sheet and on refraction intersect the refracted primary rays.

with two classes of light rays, those we call primary rays, and those we call consistency rays. The primary rays are those which emanate from our object point and then intersect, after refraction, at our image point. The consistency rays are those rays which intersect the primary rays before refraction and which also intersect the corresponding refracted primary rays after refraction. Clearly, we cannot draw rays passing through a complex space, however we can draw a diagram in real space which can help visualise the system we are working with. For simplicity our diagram will be constrained to two dimensions, though our system is in fact six dimensional, as there are three real dimensions and three imaginary dimensions. Figure 7.3 shows a representation of our system.

### 7.3.1.1 Consistency Rays

We begin our derivation by calculating the positions where the consistency rays before the sheet intersect. We know from earlier theorems that we require three light rays to completely find a position in complex space, hence we will require three rays (which we will now refer to as primary rays) which emanate from our object point  $\mathbf{P}$  and therefore three consistency rays intersecting these rays, as shown in Fig. 7.3. We first define three points on the sheet,  $\mathbf{I}_1$ ,  $\mathbf{I}_2$  and  $\mathbf{I}_3$  and the three consistency light rays,  $\hat{\mathbf{a}}_1$ ,  $\hat{\mathbf{a}}_2$  and  $\hat{\mathbf{a}}_3$ , which intersect these points. We use the procedure from section 7.2.3 to find each of the positions where our consistency rays intersect in complex space. We name these positions  $\mathbf{P}_1$ ,  $\mathbf{P}_2$  and  $\mathbf{P}_3$ . Recall that this procedure results in an infinite number of positions where each of these rays can intersect, however we need only choose one of them for each intersection, as the information we require is, by construction, intrinsic to all the possible intersection points. Using the same points on the sheet,  $\mathbf{I}_1$ ,  $\mathbf{I}_2$  and  $\mathbf{I}_3$ , and the same procedure, we can calculate the intersection points of the refracted consistency rays,  $\mathbf{P}'_1$ ,  $\mathbf{P}'_2$  and  $\mathbf{P}'_3$ . In this case however, we clearly have to use the refracted consistency rays  $\hat{\mathbf{a}}'_1$ ,  $\hat{\mathbf{a}}'_2$  and  $\hat{\mathbf{a}}'_3$ .

### 7.3.1.2 Primary Rays

We now have all of the points where the consistency rays intersect, both before and after the sheet. We know from [24] and Fig. 7.3 that these intersection points also lie on the primary rays. We now need to define these primary rays. Given that we have  $\mathbf{P}$  and also the intersection points  $\mathbf{P}_1$ ,  $\mathbf{P}_2$  and  $\mathbf{P}_3$ , we can calculate the direction of the light rays between  $\mathbf{P}$  and  $\mathbf{P}_1$ ,  $\mathbf{P}_2$  and  $\mathbf{P}_3$  using Eq.(7.7). The points on the sheet where these rays intersect is easily calculated. For example, consider the light ray passing between  $\mathbf{P}$  and  $\mathbf{P}_2$ . Using this light ray, we construct the corresponding contact position of  $\mathbf{P}$

$$\mathbf{P}_{\text{contact},\hat{\mathbf{a}}_{\mathbf{P}_2\mathbf{P}}} = \mathbf{P}_r + \mathbf{P}_i \times \hat{\mathbf{a}}_{\mathbf{P}_2\mathbf{P}}. \quad (7.17)$$

We know that all the points on the sheet are real, hence we can state that the point on the sheet  $\mathbf{Q}_2$  lies along the real trajectory of  $\hat{\mathbf{a}}_{\mathbf{P}_2\mathbf{P}}$ . Thus  $\mathbf{Q}_2$  can be written as

$$\mathbf{Q}_2 = \mathbf{P}_{\text{contact},\hat{\mathbf{a}}_{\mathbf{P}_2\mathbf{P}}} + \beta \hat{\mathbf{a}}_{\mathbf{P}_2\mathbf{P}}, \quad (7.18)$$

and since the interface lies in the  $z = 0$  plane, we know that the  $z$ -component of this equation must be zero. Therefore we can solve the third component of this equation

for  $\beta$ , and once  $\beta$  is found, it can be substituted back into the expressions for the other two components to find the  $x$  and  $y$  components of the point where the ray  $\hat{\mathbf{a}}_{\mathbf{P}_2\mathbf{P}}$  strikes the sheet. The other points where the primary rays intersect the sheet,  $\mathbf{Q}_1$  and  $\mathbf{Q}_3$  are calculated in the same way. Once these intersection points are found, it is then a matter of finding the light rays which pass between them and the points  $\mathbf{P}'_1$ ,  $\mathbf{P}'_2$  and  $\mathbf{P}'_3$ . Once these light rays are obtained, the final image point  $\mathbf{P}'$ , is found by intersecting these rays, using the points on the sheet  $\mathbf{Q}_1$ ,  $\mathbf{Q}_2$  and  $\mathbf{Q}_3$ , and Eqn.(7.13).

The procedure outlined above is in principle completely consistent as all equations are completely satisfied with nothing left undefined. However in practice, despite numerous attempts to perform this calculation, we were unable to find the image position. This suggests something is wrong with our calculation, or that the final calculation at the end to calculate the image position is too complicated to be calculated by a conventional computer and mathematics software (the software used was Mathematica). It is also possible that the procedure outlined above is incorrect. As we stated at the beginning, our calculation simply takes the process which we know works for real imaging and generalises it so that it can be applied to complex imaging. It is an assumption that this will work. We have no proof that this is the correct method to follow. However it could be, as stated, that the computers we used (everyday laptops) are simply not powerful enough to calculate the final image point. All the intersection positions and light rays were calculated with no issues, however these quantities are represented by complicated expressions with many variables, and the final imaging calculation relies on all of these quantities. As such this topic will require further work in future to see if it might be simplified and results obtained.

### 7.3.2 Reflection in a planar mirror

Whilst the imaging equation derivation above has proven too complicated to solve at present, we can still apply our results to other systems. In contrast to above, we now apply our results to the simplest, non-trivial situation we can think of: examining the image point of a complex position after it is reflected in a planar mirror. Consider a complex position  $\mathbf{P} = (P_{r,x} + iP_{i,x}, P_{r,y} + iP_{i,y}, P_{r,z} + iP_{i,z})$  and a mirror situated in the  $z = 0$  plane. We define three rays passing through  $\mathbf{P}$  and use Eqn.(7.2) and the fact that the  $z$ -components of all points on the sheet are zero to solve for the three positions where these rays intersect the mirror (this is the same procedure

carried out in Eqn.(7.18)). We then use these three positions along with the reflected light rays, whose components differ to the incident light rays only with regards to the  $z$ -component, which is the negative of what it was for the incident ray, and then compute the complex position where these reflected rays intersect using the procedure outlined in Eqns.(7.13)-(7.14). On doing this one is faced with an extremely long and complicated expression for each component of the image position for  $\mathbf{P}$ . However, one can see more clearly as to where  $\mathbf{P}$  gets reflected when one examines the solutions in the limit where the rays are paraxial. This is easily achieved when we take a ray passing through  $\mathbf{P}$  which is orthogonal to the mirror (i.e. the ray is travelling along the  $z$ -axis) and then define the other two rays passing through  $\mathbf{P}$  to be a rotation of this ray either around the  $x$ -axis, by an angle  $\theta_1$ , or around the  $y$ -axis by an angle  $\theta_2$ . To ensure that this will give paraxial results, we take a Taylor series of the trigonometric functions in the components of these two light rays around  $\theta_{1,2} = 0$ , and then only use the first few terms of the series for each function. If we then follow the procedure for finding the reflected point as before, this results in a much shorter expression for the intersection point of the three reflected rays and on substituting small angles in for  $\theta_1$  and  $\theta_2$  we are able to see that the expression produces a result which is, almost but not quite, of the form

$$\mathbf{P}' = \begin{pmatrix} P_x^* \\ P_y^* \\ -P_z^* \end{pmatrix}, \quad (7.19)$$

where  $P_x = P_{r,x} + iP_{i,x}$ ,  $P_y = P_{r,y} + iP_{i,y}$  and  $P_z = P_{r,z} + iP_{i,z}$ . We are then able to take this mapping as a guess for the true, non-paraxial relationship between a complex position and its reflection and test whether or not it is correct. To test this guess solution we simply calculate the direction of three ingoing light rays which pass through  $\mathbf{P}$  and intersect the sheet at the points  $\mathbf{I}_1$ ,  $\mathbf{I}_2$  and  $\mathbf{I}_3$  respectively using Eqn.(7.7) and then likewise calculate the light-ray directions of the reflected rays in the same way, using the three points on the sheet and our guess for the reflected point  $\mathbf{P}'$  as given in Eqn.(7.19). We know that for a planar mirror in the  $z = 0$  plane that any incident light ray with direction  $\hat{\mathbf{a}} = (a_x, a_y, a_z)$  gets reflected off the mirror and leaves with direction  $\hat{\mathbf{a}}' = (a_x, a_y, -a_z)$ . Hence by comparing the components we should be able to tell whether or not our guess for the image position is correct. On doing so one can see that indeed the components of the ray passing through  $\mathbf{P}'$  are correct, in that the  $x$  and  $y$  components are the same as for the incident ray, but the  $z$ -component changes sign. Specifically when calculating the light rays between

the object point and the points on the sheet, we must use the positive solution of  $\alpha$  when calculating  $\hat{\mathbf{a}}$ . The reason for this is that if one uses the negative version of  $\alpha$ , one ends up with both the ingoing and reflected light rays pointing away from the surface of the mirror.

## 7.4 On the equivalence between ray-rotation sheets and CLAs

### 7.4.1 The equivalence between confocal lenslet array imaging and ray-rotation imaging

In the previous section we discussed a procedure that could be used to find an imaging equation which imaged complex positions across an interface. Ultimately we were unable to solve the final equations necessary to calculate the image position. Our starting point for such a system depended upon the relationship between real and complex positions as defined in Eq.(7.2). But this expression in turn was motivated by the effect of ray-rotation on light rays, which, if the sheet is placed in the  $z = 0$  plane, we stated to image according to

$$\begin{aligned}x' &= x, \\y' &= y, \\z' &= -\exp(-i\alpha)z.\end{aligned}\tag{7.20}$$

This equation describes imaging a real or complex position to a complex position, hence we might have expected our previous, failed derivation to be a generalisation of this equation for complex to complex imaging. Note that Eq.(7.20) can be written in the same form as the gCLA imaging equations

$$\mathbf{P}' = \mathbf{P} - z \begin{pmatrix} 0 \\ 0 \\ 1 - \eta_c \end{pmatrix}.\tag{7.21}$$

where  $\eta_c = -\exp(-i\alpha)$ . Written in this way, we can consider ray-rotation sheets to be complex confocal lenslet arrays. However it is also clear to see that when the angle of rotation is imaginary, the expression becomes that for an imaging confocal

lenslet array (recall that a CLA is a gCLA where  $\delta_x = \delta_y = 0$  and the rotation angle of the lenslets is zero). In this sense we can state that CLAs and ray-rotation sheets are related to one another.

### 7.4.2 The non-equivalence between confocal lenslet array refraction and ray-rotation

As we know, the imaging equation describing gCLAs allows us to perform pixellated coordinate transformations. As the imaging performed by ray-rotation sheets is of the same form we can therefore also consider ray rotation sheets as performing complex, pixellated coordinate transformations, though clearly of a much simpler (but more abstract) form as they perform no shearing. However there is a problem. If the imaging performed in Eq.(7.21) is correct then we would expect that the law of refraction would have the same form as the law of refraction for CLAs, i.e. the law of refraction would be given by

$$\mathbf{d}' = \left( \frac{d_x}{\eta_c}, \frac{d_y}{\eta_c}, d_z \right). \quad (7.22)$$

However this clearly results in complex light-ray directions which are not observed. The correct law of refraction is given by

$$\mathbf{d}'_{real} = (d_x \cos \alpha - d_y \sin \alpha, d_y \cos \alpha + d_x \sin \alpha, d_z). \quad (7.23)$$

We can arrive at Eq.(7.23) from Eq.(7.22) via the following equation

$$\mathbf{d}'_{real} = -Re [ \mathbf{d}' \cdot (\hat{\mathbf{x}} + i\hat{\mathbf{y}})(\hat{\mathbf{x}} - i\hat{\mathbf{y}}) ] + (\mathbf{d}' \cdot \hat{\mathbf{z}}) \cdot \hat{\mathbf{z}}. \quad (7.24)$$

The transformation in Eq.(7.24) is a serious problem for our mathematical equivalence because there is no explanation for why it is necessary to perform this transformation to go from the complex light-ray direction of Eq.(7.22) to the correct real one of Eq.(7.23). The transformation was derived on an ad hoc basis. Currently there is no concrete understanding of why this intermediate step is necessary.

The notion of distance also raises concerns. We know from Eq.(5.33) that if a coordinate transformation can be used to describe the imaging performed by our sheets then this coordinate transformation can be used to find a metric. The metric itself can then be used to measure distances in our system. The metric for our ray-rotation

sheet using a euclidean object-sided metric and Eq.(5.33) is given by

$$h = \begin{pmatrix} 1 & 0 & 0 \\ 0 & 1 & 0 \\ 0 & 0 & 1/\eta_c^2 \end{pmatrix}, \quad (7.25)$$

and so the distance between two complex positions in this space is given by

$$|\mathbf{Q} - \mathbf{P}| = \sqrt{(\mathbf{Q} - \mathbf{P}) \cdot h \cdot (\mathbf{Q} - \mathbf{P})}. \quad (7.26)$$

Recall however that with gCLAs we did not use the gCLA metric to calculate optical distance as the space before and after the interface is actually air. The same applies here, hence the actual distance between  $\mathbf{Q}$  and  $\mathbf{P}$  is

$$\begin{aligned} |\mathbf{Q} - \mathbf{P}| &= \sqrt{(\mathbf{Q} - \mathbf{P}) \cdot (\mathbf{Q} - \mathbf{P})}, \\ &= \sqrt{(\Delta_r + i\Delta_i) \cdot (\Delta_r + i\Delta_i)}. \end{aligned} \quad (7.27)$$

If we assume that light travels at the speed of light in both real space and complex space, and that time flows at the same rate, then it must be true that the time taken for a light ray to pass from  $\mathbf{P}$  to  $\mathbf{Q}$  is the same as the time taken for light passing from the corresponding contact points  $\mathbf{C}$  to  $\mathbf{D}$ , and hence that the distances  $|\mathbf{Q} - \mathbf{P}|$  and  $|\mathbf{D} - \mathbf{C}|$  must be the same. However they are not. The distance between  $\mathbf{C}$  to  $\mathbf{D}$  is

$$\begin{aligned} |\mathbf{D} - \mathbf{C}| &= \sqrt{(\mathbf{D} - \mathbf{C}) \cdot (\mathbf{D} - \mathbf{C})}, \\ &= \sqrt{(\Delta_r + \Delta_i \times \hat{\mathbf{a}}) \cdot (\Delta_r + \Delta_i \times \hat{\mathbf{a}})}. \end{aligned} \quad (7.28)$$

Instantly we see two problems. First of all we see that the distance calculated using the complex positions is (unsurprisingly) complex while the distance calculated using the real positions is real. The second problem is that the real distance is dependent on the light-ray direction, while the complex distance is not. It makes no sense that the distance between two positions should depend on the light-ray direction. The issue of the distances not being equal does not affect the usefulness of the previously derived results concerning light rays in complex space, nor does it stop us considering ray-rotation sheets as complex gCLAs, as the refraction and therefore the imaging effected by ray-rotation sheets has no wave-optical description and as such does not need to satisfy theorems from wave optics such as those concerning optical path length. However it does mar the interpretation somewhat and so it would be nice to remove this flaw.

Finally we note that, even if the above problem regarding the law of refraction can be resolved, the resulting equivalence can only ever be geometrical. Previously when studying the wave-optical limit of ray-rotated light-ray fields we showed that it was possible for a certain class of optical fields which were a function of the angle of rotation to be refracted such that the curl of the outgoing light-ray field was zero. Based on the equivalence between the imaging equations for CLAs and ray-rotation sheets it would be sensible to assume that the same class of fields, constructed with imaginary angles, will also produce outgoing light-ray fields with zero curl for CLAs. However, on inspection, the equations never produce the required results, and so we can conclude that if our equivalence is correct, it only applies when one considers the system ray-optically.

## 7.5 An analysis of the structure of complex space

Clearly complex space, as we define it, is fundamentally different, so far as rays are concerned, to real space. This stems from the fact that three dimensional complex space can, in principle, be considered as a six dimensional real space. The fundamental difference between three dimensional real space and the six dimensional real space we construct to represent complex space is that the two spaces are not homomorphic. We can show this by considering the points that lie along a light ray in three dimensional real space and those that lie along the same light ray in the corresponding six dimensional real space which represents the complex space.

The group structure of the points that lie on a light ray which passes through the origin in three dimensional real space is trivial and well known, and in itself is of no interest. What is of interest however is whether or not this structure survives on transitioning to our complex space framework. We shall see that even though both spaces share the same group properties, they do not share the same group structure. In order to show this we must first state clearly the properties and structure of the group representing three dimensional real space and then show that this structure does not carry over to the six dimensional space of complex positions.

Our definitions of the group representing three dimensional real space are as follows: The group consists of two types of element - three dimensional positions which lie along on the light ray and the light-ray direction itself. The group multiplication is addition and consequently the identity element of the group is the zero-vector, while

the inverse of a specific element is simply the negative of that element. Our group therefore consists of elements as follows:

$$\{\mathbf{P}_r + \mathbf{P}_i \times \hat{\mathbf{a}}, \alpha \hat{\mathbf{a}} + (\alpha \mathbf{0} \times \hat{\mathbf{a}}), \mathbf{Q}_r + \mathbf{Q}_i \times \hat{\mathbf{a}}, \dots\}, \quad (7.29)$$

where  $\hat{\mathbf{a}}$  is the light-ray direction and  $\mathbf{P}_r + \mathbf{P}_i \times \hat{\mathbf{a}}$  and  $\mathbf{Q}_r + \mathbf{Q}_i \times \hat{\mathbf{a}}$  are points that lie on the light ray. On mapping to our six dimensional space, the group (which has the same group properties as the three dimensional group) becomes

$$\{(\mathbf{P}_r, \mathbf{P}_i), \alpha(\hat{\mathbf{a}}, \mathbf{0}), (\mathbf{Q}_r, \mathbf{Q}_i), \dots\}. \quad (7.30)$$

We now show that this mapping, denoted by  $\phi$ , is not homomorphic. Recall that a mapping,  $\phi$ , between two groups is homomorphic if it preserves the group structure. That is to say

$$\phi(a \cdot b) = \phi(a) \cdot \phi(b). \quad (7.31)$$

Following Eqn.(7.31) we see that for our real group the left hand side gives

$$\phi((\mathbf{P}_r + \mathbf{P}_i \times \hat{\mathbf{a}}) + \alpha \hat{\mathbf{a}}) = \phi(\mathbf{Q}_r + \mathbf{Q}_i \times \hat{\mathbf{a}}) = (\mathbf{Q}_r, \mathbf{Q}_i), \quad (7.32)$$

while the right hand side gives

$$\phi(\mathbf{P}_r + \mathbf{P}_i \times \hat{\mathbf{a}}) + \phi(\alpha \hat{\mathbf{a}}) = (\mathbf{P}_r, \mathbf{P}_i) + (\alpha \hat{\mathbf{a}}, \mathbf{0}) = (\mathbf{P}_r + \alpha \hat{\mathbf{a}}, \mathbf{P}_i). \quad (7.33)$$

If our mapping is indeed homomorphic then the above implies that  $\mathbf{Q}_r = \mathbf{P}_r + \alpha \hat{\mathbf{a}}$  and  $\mathbf{Q}_i = \mathbf{P}_i$ . This is however untrue in general as  $\mathbf{Q}_i$  and  $\mathbf{Q}_r$  need only be chosen such that they satisfy

$$\mathbf{P}_r + \mathbf{P}_i \times \hat{\mathbf{a}} + \alpha \hat{\mathbf{a}} = \mathbf{Q}_r + \mathbf{Q}_i \times \hat{\mathbf{a}}, \quad (7.34)$$

At face value the above discussion of the group structure appears to be sensible. However on closer scrutiny it transpires that this is not the case. We now show this. Consider a light ray with direction  $\hat{\mathbf{a}}$  which passes through two complex positions  $\mathbf{P}$  and  $\mathbf{Q}$ . Does this light ray also pass through a complex position  $\mathbf{W} = \mathbf{P} + \mathbf{Q}$ ? According to our group as defined above, if the light ray does pass through  $\mathbf{W}$ , then it must also pass through the point  $\mathbf{W}_r + \mathbf{W}_i \times \hat{\mathbf{a}}$  in real space. Hence it would be true that

$$\mathbf{W}_r + \mathbf{W}_i \times \hat{\mathbf{a}} = \mathbf{P}_r + \mathbf{P}_i \times \hat{\mathbf{a}} + \alpha \hat{\mathbf{a}}, \quad (7.35)$$

and since  $\mathbf{W} = \mathbf{P} + \mathbf{Q}$  that

$$\mathbf{Q}_r + \mathbf{Q}_i \times \hat{\mathbf{a}} = \alpha \hat{\mathbf{a}}. \quad (7.36)$$

If Eq.(7.36) is to hold, then either  $\mathbf{Q}_r = \hat{\mathbf{a}} = 0$  or  $\mathbf{Q}_i = 0$  and  $\mathbf{Q}_r = \alpha \hat{\mathbf{a}}$  or more generally that  $\alpha$  is not a constant. If  $\alpha$  is not constant, then solving for  $\alpha$  using the three components of Eq.(7.36) leads to three different solutions for  $\alpha$  which are not compatible. Hence it must therefore be the case that if a light ray passes through  $\mathbf{P}$  and  $\mathbf{Q}$  that it does not, in general, pass through  $\mathbf{W}$  as  $\hat{\mathbf{a}}$  can never equal zero and in general  $\mathbf{Q}_i \neq 0$  and  $\mathbf{Q}_r \neq \alpha \hat{\mathbf{a}}$ . Hence the group structure we have defined for our complex space is not correct as we see that under addition of  $\mathbf{P}$  and  $\mathbf{Q}$  we cannot always arrive at  $\mathbf{W}$  as one would have expected.

## 7.6 Conclusion

We have shown that ray-rotation sheets can be considered as interfaces which perform imaging from real space to complex space. Using the further definition which related points in complex space to contact points in real space, we derived expressions which describe how real light rays pass between different complex positions. We then showed that up to a point the imaging performed by ray-rotation sheets and CLAs are related to one another, but that this relationship does not seem to hold directly for their law of refractions and that distances in complex space do not match the corresponding distances in real space. We also noted that the equivalence itself does not hold wave-optically. Finally, we studied the group structure of complex space and found that our original definition relating complex positions to their corresponding contact points in real space is inadequate if complex space is to have the same group structure as real space.

# Chapter 8

## Future work

### 8.1 Introduction

This thesis has focussed purely on the mathematical interpretation and application of metarefraction. We have seen that a subset of gCLAs are capable of performing unique imaging, but that other, more generalised, gCLAs cannot. We also showed that ray-rotation sheets appear to image into an abstract complex space, and that this can, to an extent, be considered as a complex equivalent of gCLA imaging.

I briefly outline a few areas which have the potential to be developed further.

### 8.2 Continued exploration of imaging into abstract spaces

It would be worth revisiting ray-rotation, to see if the mathematical differences between ray-rotation sheets and gCLA refraction can be reconciled. Further to this, and in keeping with the theme of abstract imaging, if ray-rotation sheets can be described as imaging into an abstract space, then perhaps non-imaging gCLAs can also. This area will be explored in the future. One possible approach to studying this would be to apply the same logic as shown in section **6.3.3**, but instead of following a position around a closed loop, follow light-ray direction instead. The reason for this is as follows.

Consider an imaging gCLA. The points  $\mathbf{A}$  and  $\mathbf{B}$  are separated by a vector  $\mathbf{d}$  and will be imaged to  $\mathbf{A}'$  and  $\mathbf{B}'$ . It is straight forward to show that the vector separating  $\mathbf{A}'$  and  $\mathbf{B}'$  is simply a vector with the same direction as  $\mathbf{d}$  after refraction through the gCLA. In other words, the information contained in the imaging equations encapsulates the law of refraction. Hence, if it is possible for imaging gCLAs to find conditions which must be satisfied if a position is to be mapped back to itself after circumnavigating a closed loop, it may also be possible to find a similar set of conditions which must be satisfied if the light-ray direction is to be unchanged after circumnavigating a loop (indeed, one would expect the conditions to be identical to those found when mapping a position around the closed loop). Now suppose we take the same idea, but this time attempt to find conditions using the non-imaging gCLA law of refraction. If conditions can be found using the law of refraction, it may then be possible to use the analogous loop calculations for the imaging case as a template to find a corresponding set of imaging equations (albeit abstract equations) for the non-imaging gCLAs.

### 8.3 Investigating metarefraction as a means of achieving a classical optical analogue of a black hole

In chapter 6 we stated that an intersection of refractive interfaces acts like a transformation optics device if, on circumnavigating a closed loop where we map any starting position sequentially through all the interfaces crossing the loop, one arrives back at the original position. Because the imaging and refraction of metarefracting interfaces is closely linked, we suspect that if the position is mapped back to itself, then the light-ray direction of all the rays passing through the position must also be mapped back to themselves after traversing the loop. However, what if on mapping round a closed loop, the light-ray direction is not preserved? In this case the light-ray direction has changed. This also occurs when the loop is placed on a curved manifold. Returning to our piecewise equivalent, if we perform a loop calculation for light-ray direction and find sheet parameters which satisfy the conditions which are required for light-ray direction to change on traversing a closed loop, we would be able to mimic the effects of a curved manifold, albeit in a discrete form. This in turn would open up the possibility of investigating whether or not it is possible to mimic exotic spaces such as black holes. Of course, our black hole would be purely spatial, our

interfaces have no effect or dependence on time and as such we would be unable to detect Hawking radiation.

## 8.4 Improving pixellated refraction

We have seen in this thesis that gCLAs have the potential to perform refraction which can be utilised to construct piecewise transformation optics devices but that because gCLAs are pixellated surfaces they suffer from imperfections such as a limited field of view and an outgoing image which is pixellated. One possible way of eliminating the limited field of view is to construct a similar device where the lenslet arrays are constructed using transformed Luneburg lenses which are touching instead of conventional lenses separated by the sum of their focal lengths. For example consider two Luneburg lenses touching as in Fig.8.1. We see that for normal incidence, shown by

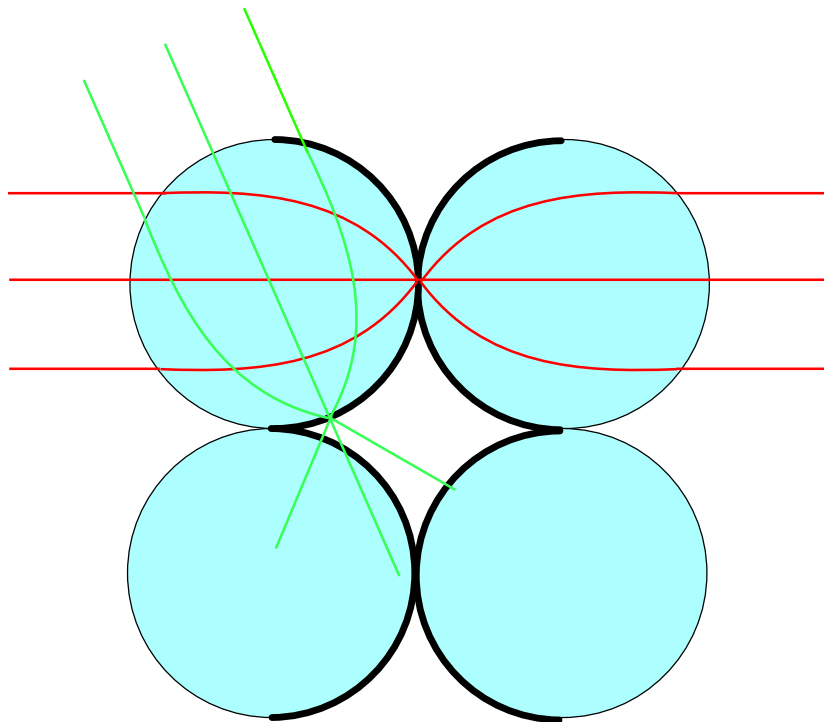


FIGURE 8.1: An array of Luneburg lenses in contact with one another. We see that light rays entering the array at normal incidence (red rays) are refracted in a uniform way as they pass through the point where the lenses touch. Ray bundles going in at any other angle (green rays) get redirected in different ways directions. By transforming the Luneburg lenses such that their surfaces on the interior of the array are touching at all points, one could in effect create a gCLA whilst removing field of view issues.

red light rays, that the rays reemerge one the other side of the interface parallel. This

is because the rays have passed through the correct two Luneburg lenses. However, we see that for any other incidence direction, such as that shown by the green rays, that these rays will not pass through and reemerge parallel. The reason for this is because the red rays are focussed onto a point which is shared by both Luneburg lenses. A Luneburg lens essentially has its focal plane coupled to its surface, and so rays of normal incidence pass through a system where two lenses share a focal plane - this is what happens with a gCLA, light is refracted according to the gCLA law of refraction because it passes through the focal planes of both lenslets simultaneously. The green rays however are not passing through two of the focal planes simultaneously, and so will not be refracted in the way we would like. Clearly then Luneburg lenses in and of themselves do not help at all. Indeed we see that this system clearly results in a severely limited field of view, which is in fact worse than that suffered by gCLAs, as only normal incidence ensures parallel light rays are refracted such that they reemerge parallel. However, if we transform the Luneburg lenses such that the inner surfaces (highlighted in thick black) of both lenses in the pair are touching, then it might be possible to get a perfect field of view as in this case both focal planes coincide at all points on the inner surfaces of the lens.

Further to this it is in principle possible to design interfaces which perform new laws of generalised refraction using Luneburg lenses. When we discussed using Luneburg lenses to achieve gCLA refraction, we stated that the Luneburg lenses had to be transformed in an appropriate way. This suggests that if a different transformation was used different laws of refraction could be realised. This in turn may have implications for our research into abstract imaging.

## 8.5 Designing wave-optically perfect refracting interfaces

Redesigning gCLAs using Luneburg lenses goes some way to producing a better quality image after refraction. However, the outgoing image is still pixellated. To get the best image possible, the device performing the refraction must produce non-pixellated light-ray fields with zero curl. This is a very challenging problem and it is not altogether obvious how this can be achieved. It is clear by now that only certain light-ray fields can be refracted to produce light-ray fields which are curl free. In order to make this idea a reality we first have to understand what the outgoing fields

---

will look like. The work presented previously in section **3.4.3** would be a good place to start, though, of course, we really want to achieve wave-optical gCLAs rather than wave-optical ray-rotation sheets. Once the outgoing phase has been determined, the problem is in making the outgoing field non-pixellated. To do this the ingoing phase has to somehow be manipulated such that the phase discontinuities between pixels never arises in the first place. Resonators may be of help here, as somehow causing certain parts of the incident field to make multiple trips within a resonator while others do not could allow the outgoing phase to be constructed properly. This is a reasonable idea, but the details have not been looked at, and so it may in fact not be possible to do this.



## Chapter 9

### Appendix

#### 9.1 Sheet parameters for cubic gCLA cloak

Side length	2
Inner volume* - EM space	0.1
Inner volume* - physical space	0.9
* as a fraction of side length	
<b>Outer surfaces</b>	
$\eta_o$	0.111
$\delta_{x_o}$	0
$\delta_{y_o}$	0
<b>Inner pyramid surfaces</b>	
$\eta_{pyr}$	46.895
$\delta_{x_{pyr}}$	-33.684
$\delta_{y_{pyr}}$	0
<b>Inner octahedral surfaces</b>	
$\eta_{octa}$	12.429
$\delta_{x_{octa}}$	0
$\delta_{y_{octa}}$	0
<b>Inner corner surfaces</b>	
$\eta_c$	11.257
$\delta_{x_c}$	0
$\delta_{y_c}$	-2.837

TABLE 9.1: Parameters for a cubic gCLA cloak as simulated in Fig. 6.10.

## 9.2 Glens parameters for cubic glens cloak

Side length	2
Inner volume* - EM space	0.4
Inner volume* - physical space	0.8
* as a fraction of side length	
<b>Outer cube glenses</b>	
$f_-$	0.2
$f_+$	-1.2
<b>Inner cube glenses</b>	
$f_-$	-1.2
$f_+$	0.4
<b>Diagonal lenses</b>	
$f_-$	-0.849
$f_+$	0.849

TABLE 9.2: Parameters for a cubic glens cloak as simulated in Fig. 6.12.

### 9.3 Lens parameters for lens tetrahedron

Base radius	2.666
Height	4
Height of lower inner vertex (physical space)	1
Height of upper inner vertex (physical space)	2.5
Height of lower inner vertex (EM space)	0.8
<b>Base lens</b>	
$f_-$	4
$f_+$	-4
<b>Outer pyramid lenses</b>	
$f_-$	-3.035
$f_+$	3.035
<b>Lower inner pyramid lenses</b>	
$f_-$	-1.92
$f_+$	1.92
<b>Upper inner pyramid lenses</b>	
$f_-$	1.059
$f_+$	-1.059
<b>Lower inner vertical lenses</b>	
$f_-$	-1.847
$f_+$	1.847
<b>Upper inner vertical lenses</b>	
$f_-$	1.847
$f_+$	-1.847

TABLE 9.3: Parameters for a lens tetrahedron device as simulated in Fig. 6.13.

# Bibliography

- [1] Francesco Aieta, Patrice Genevet, Nanfang Yu, Mikhail A. Kats, Zeno Gaburro, and Federico Capasso. Out-of-plane reflection and refraction of light by anisotropic optical antenna metasurfaces with phase discontinuities. *Nano Letters*, 12(3):1702–1706, March 2012. doi: DOI10.1021/nl300204s.
- [2] Nanfang Yu, Patrice Genevet, Mikhail A. Kats, Francesco Aieta, Jean-Philippe Tetienne, Federico Capasso, and Zeno Gaburro. Light propagation with phase discontinuities: Generalized laws of reflection and refraction. *Science*, 334:333–337, 2011. doi: 10.1126/science.1210713.
- [3] M. Born and E. Wolf. *Principles of Optics*, chapter 3.3.2. Pergamon Press, Oxford, 1980.
- [4] M. Born and E. Wolf. *Principles of Optics*, chapter 4.2. Pergamon Press, Oxford, 1980.
- [5] Luis Martín-Moreno Paloma A. Huidobro, Maxim L. Nesterov and Francisco J. García-Vidal. Transformation optics for plasmonics. *Nano Letters*, 10(6):1985–1990, May 2010.
- [6] M. Kadic et al. Transformation plasmonics. *Nanophotonics*, 1:51–64, 2012.
- [7] Thomas G. Philbin, Chris Kuklewicz, Scott Robertson, Stephen Hill, Friedrich König, and Ulf Leonhardt. Fiber-optical analog of the event horizon. *Science*, 319(5868):1367–1370, 2008. URL <http://www.sciencemag.org/cgi/content/abstract/319/5868/1367>.
- [8] Stephen Hawking. Particle creation by black holes. *Communications in Mathematical Physics*, 43(3):199–220, 1975.
- [9] C. King S. Horsley and T. Philbin. Wave propagation in complex coordinates. *Journal of Optics*, 18(4), April 2016.

- [10] G. Castaldi S. Savoia and V. Galdi. Complex-coordinate non-hermitian transformation optics complex-coordinate non-hermitian transformation optics complex-coordinate non-hermitian transformation optics. *Journal of Optics*, 18(4), April 2016.
- [11] J. B. Pendry et al. Magnetism from conductors and enhanced nonlinear phenomena. *IEEE Trans. Microwave Theory Tech.*, 47(11):2075–2084, November 1999.
- [12] D. Schurig, J. J. Mock, B. J. Justice, S. A. Cummer, J. B. Pendry, A. F. Starr, and D. R. Smith. Metamaterial Electromagnetic Cloak at Microwave Frequencies. *Science*, 314(5801):977–980, 2006.
- [13] David R. Smith Nathan Landy. A full parameter unidirectional metamaterial cloak for microwaves. *Nature Materials*, 12:25–28, October 2013.
- [14] Alasdair C. Hamilton, Bhuvanesh Sundar, and Johannes Courtial. Local light-ray rotation around arbitrary axes. *J. Opt.*, 12:095101, 2010. doi: 10.1088/2040-8978/12/9/095101.
- [15] Alasdair C. Hamilton, Bhuvanesh Sundar, John Nelson, and Johannes Courtial. Local light-ray rotation. *J. Opt. A: Pure Appl. Opt.*, 11:085705, 2009. doi: 10.1088/1464-4258/11/8/085705.
- [16] L. Allen, M. W. Beijersbergen, R. J. C. Spreeuw, and J. P. Woerdman. Orbital angular momentum of light and the transformation of Laguerre-Gaussian modes. *Phys. Rev. A*, 45:8185–8189, 1992.
- [17] Johannes Courtial and Tomáš Tyc. Generalised laws of refraction that can lead to wave-optically forbidden light-ray fields. *J. Opt. Soc. Am. A*, 29:1407–1411, 2012. doi: 10.1364/JOSAA.29.001407.
- [18] Johannes Courtial, Blair C. Kirkpatrick, and Miguel A. Alonso. Imaging with complex ray-optical refractive-index interfaces between complex object and image distances. *Opt. Lett.*, 37:701–703, 2012. doi: 10.1364/OL.37.000701. URL <http://www.opticsinfobase.org/ol/abstract.cfm?URI=ol-37-4-701>.
- [19] Robert W Boyd reuben S Aspden, Daniel S Tasca and Miles J. Padgett. Epr-based ghost imaging using a single-photon-sensitive camera. *New J. Phys.*, 15(073032):11, July 2013.

- [20] Ulf Leonhardt. Optical conformal mapping. *Science*, 312:1777–1780, 2006.
- [21] J. B. Pendry, D. Schurig, and D. R. Smith. Controlling electromagnetic fields. *Science*, 312:1780–1782, 2006. doi: 10.1126/science.1125907.
- [22] D. Gabor. Improvements in or relating to optical systems composed of lenticules. UK Patent 541,753, 1940.
- [23] C. Hembd-Sölner, R. F. Stevens, and M. C. Hutley. Imaging properties of the gabor superlens. *J. Opt. A: Pure Appl. Opt.*, 1:94–102, 1999. doi: 10.1088/1464-4258/1/1/013.
- [24] Johannes Courtial. Geometric limits to geometric optical imaging with infinite, planar, non-absorbing sheets. *Opt. Commun.*, 282:2480–2483, 2009. doi: 10.1016/j.optcom.2009.03.036.
- [25] Georgios Antoniou Stephen Oxburgh, Chris D. White and Johannes Courtial. Law of refraction for generalised confocal lenslet arrays. *Optics Communications*, 313:118–122, February 2014.
- [26] Max Born and Emil Wolf. *Principles of Optics*. Pergamon Press, Oxford, 1993.
- [27] Stephen Oxburgh, Tomáš Tyc, and Johannes Courtial. Dr TIM: Ray-tracer TIM, with additional specialist capabilities. in preparation, 2013.
- [28] Dean Lambert, Alasdair C. Hamilton, George Constable, Harsh Snehanshu, Sharvil Talati, and Johannes Courtial. TIM, a ray-tracing program for META-TOY research and its dissemination. *Comp. Phys. Commun.*, 183:711–732, 2012. doi: 10.1016/j.cpc.2011.11.011.
- [29] Ulf Leonhardt and Thomas G. Philbin. Transformation optics and the geometry of light. *Progr. Opt.*, 53:69–152, 2009. URL <http://arxiv.org/abs/0805.4778v2>.
- [30] Ulf Leonhardt and Tomáš Tyc. Broadband Invisibility by Non-Euclidean Cloaking. *Science*, 323(5910):110–112, 2009. doi: 10.1126/science.1166332. URL <http://www.sciencemag.org/cgi/content/abstract/323/5910/110>.
- [31] Hongsheng Chen, Bin Zheng, Lian Shen, Huaping Wang, Xianmin Zhang, Nikolay I. Zheludev, and Baile Zhang. Ray-optics cloaking devices for large objects in incoherent natural light. *Nature Communications*, 4(2652), October 2013.

- [32] Horsley et al. Removing singular refractive indices with sculpted surfaces. *Scientific Reports*, 4(4876), May 2014.
- [33] Stephen Oxburgh and Johannes Courtial. Perfect imaging with planar interfaces. *Journal of the Optical Society of America A*, 30(11):2334–2338, October 2013.
- [34] Oxburgh et al. Transformation optics with windows. *Proc. SPIE 9193, Novel Optical Systems Design and Optimization XVII, 91931E*, 9193, September 2014.
- [35] Johannes Courtial. Standard and non-standard metarefraction with confocal lenslet arrays. *Opt. Commun.*, 282:2634–2641, 2009. doi: 10.1016/j.optcom.2009.03.046.
- [36] Tautvydas Maceina, Gediminas Juzeliūnas, and Johannes Courtial. Quantifying metarefraction with confocal lenslet arrays. *Opt. Commun.*, 284:5008–5019, 2011. doi: 10.1016/j.optcom.2011.06.058.
- [37] S. Oxburgh et al. Large-scale, white-light, transformation optics using integral imaging. *Journal of Optics*, 18, 2016.
- [38] M. Schumann et al. Cloaked contact grids on solar cells by coordinate transformations: designs and prototypes. *Optica*, 2(10):850–853, 2015.
- [39] Jensen Li and J. B. Pendry. Hiding under the carpet: A new strategy for cloaking. *Phys. Rev. Lett.*, 101:203901, 2008. doi: 10.1103/PhysRevLett.101.203901.
- [40] X.Zhang et al. An optical cloak made of dielectrics. *Nature Materials*, 8:568–571, April 2009.
- [41] R. Liu, C. Ji, J. J. Mock, J. Y. Chin, T. J. Cui, and D. R. Smith. Broadband Ground-Plane Cloak. *Science*, 323(5912):366–369, 2009. doi: 10.1126/science.1166949. URL <http://www.sciencemag.org/cgi/content/abstract/323/5912/366>.
- [42] Tie Jun Cui Hui Feng Ma. Three-dimensional broadband ground-plane cloak made of metamaterials. *Nature Communications*, 1(21), June 2010.
- [43] B.Zhang et al. Electromagnetic detection of a perfect carpet cloak. *Scientific Reports*, 5(10401), May 2015.
- [44] Johannes Courtial et al. Omni-directional transformation-optics cloak made from lenses and glenses. *JOSA A*, 33(6):1032–1040, 2016.